

University of Windsor

Scholarship at UWindor

Electronic Theses and Dissertations

Theses, Dissertations, and Major Papers

2001

Load distribution in curved composite concrete deck-steel multiple-spine box girder bridges.

Said Ibrahim. Nour
University of Windsor

Follow this and additional works at: <https://scholar.uwindsor.ca/etd>

Recommended Citation

Nour, Said Ibrahim., "Load distribution in curved composite concrete deck-steel multiple-spine box girder bridges." (2001). *Electronic Theses and Dissertations*. 2629.
<https://scholar.uwindsor.ca/etd/2629>

This online database contains the full-text of PhD dissertations and Masters' theses of University of Windsor students from 1954 forward. These documents are made available for personal study and research purposes only, in accordance with the Canadian Copyright Act and the Creative Commons license—CC BY-NC-ND (Attribution, Non-Commercial, No Derivative Works). Under this license, works must always be attributed to the copyright holder (original author), cannot be used for any commercial purposes, and may not be altered. Any other use would require the permission of the copyright holder. Students may inquire about withdrawing their dissertation and/or thesis from this database. For additional inquiries, please contact the repository administrator via email (scholarship@uwindsor.ca) or by telephone at 519-253-3000ext. 3208.

INFORMATION TO USERS

This manuscript has been reproduced from the microfilm master. UMI films the text directly from the original or copy submitted. Thus, some thesis and dissertation copies are in typewriter face, while others may be from any type of computer printer.

The quality of this reproduction is dependent upon the quality of the copy submitted. Broken or indistinct print, colored or poor quality illustrations and photographs, print bleedthrough, substandard margins, and improper alignment can adversely affect reproduction.

In the unlikely event that the author did not send UMI a complete manuscript and there are missing pages, these will be noted. Also, if unauthorized copyright material had to be removed, a note will indicate the deletion.

Oversize materials (e.g., maps, drawings, charts) are reproduced by sectioning the original, beginning at the upper left-hand corner and continuing from left to right in equal sections with small overlaps.

Photographs included in the original manuscript have been reproduced xerographically in this copy. Higher quality 6" x 9" black and white photographic prints are available for any photographs or illustrations appearing in this copy for an additional charge. Contact UMI directly to order.

ProQuest Information and Learning
300 North Zeeb Road, Ann Arbor, MI 48106-1346 USA
800-521-0600

UMI[®]

NOTE TO USERS

This reproduction is the best copy available.

UMI[®]

LOAD DISTRIBUTION IN CURVED COMPOSITE CONCRETE DECK-STEEL MULTIPLE-SPINE BOX GIRDER BRIDGES

BY

SAID IBRAHIM NOUR, B. Eng.

A Thesis submitted to Faculty of Graduate Studies and Research through
Civil and Environmental Engineering Program in partial fulfillment of the requirements
for the degree of Master of Applied Science at the
University of Windsor

Windsor, Ontario, Canada
December 2000



National Library
of Canada

Acquisitions and
Bibliographic Services

395 Wellington Street
Ottawa ON K1A 0N4
Canada

Bibliothèque nationale
du Canada

Acquisitions et
services bibliographiques

395, rue Wellington
Ottawa ON K1A 0N4
Canada

Your file Votre référence

Our file Notre référence

The author has granted a non-exclusive licence allowing the National Library of Canada to reproduce, loan, distribute or sell copies of this thesis in microform, paper or electronic formats.

The author retains ownership of the copyright in this thesis. Neither the thesis nor substantial extracts from it may be printed or otherwise reproduced without the author's permission.

L'auteur a accordé une licence non exclusive permettant à la Bibliothèque nationale du Canada de reproduire, prêter, distribuer ou vendre des copies de cette thèse sous la forme de microfiche/film, de reproduction sur papier ou sur format électronique.

L'auteur conserve la propriété du droit d'auteur qui protège cette thèse. Ni la thèse ni des extraits substantiels de celle-ci ne doivent être imprimés ou autrement reproduits sans son autorisation.

0-612-62260-6

Canada

928778

© ————— 2000
Said Ibrahim Nour
All Rights Reserved

I hereby declare that I am the sole author of this document.

I authorize the University of Windsor to 'lend this document to other institutions or individuals for the purpose of scholarly research.

Said Ibrahim Nour

I further authorize the University of Windsor to reproduce the document by photocopying or by other means, in total or part, at the request of other institutions or individuals for the purpose of scholarly research.

Said Ibrahim Nour

THE UNIVERSITY OF WINDSOR requires the signatures of all persons using or photocopying this document.

Please sign below, and give address and date.

ABSTRACT

Horizontally curved composite box girder bridges are used in interchanges of modern highway systems. They have become increasingly popular for economic as well as aesthetic reasons. A multiple-spine steel box section composite with a concrete deck is one of the most suitable in resisting torsional, distortional, and warping effects induced by highway curvature. This type of structure has created new design problems for bridge engineers in estimating its lateral load distribution when subjected to concentric or eccentric truck loadings. North American Codes of Practice have recommended some analytical methods for the design of curved multiple-spine bridges, providing a geometrically defined criterion to establish when a horizontally curved bridge may be treated as a straight one. However, practical requirements arising during the design process necessitate a simple design method for curved composite multiple-spine bridges in the form of load distribution factors for flexural stresses and shear. On the basis of literature review on curved multiple-spine bridges, such load distribution factors for curved multiple-spine steel box girders, composite with a concrete deck, are not available yet for shear. However, those for flexural stresses were based on bridges without intermediate diaphragms or based on analytical methods other than a finite-element method.

This study consisted of a theoretical investigation. An analytical modelling was performed using the finite-element method with the commercially available “ABAQUS”

software. A shell element was used to model the concrete deck, steel webs, bottom flanges, and end-diaphragms. A three-dimensional beam element was adopted to model the top flanges, cross-bracings, and top chords. The multi-point-constraint option in the ABAQUS software was used between the shell nodes of the concrete deck and the beam element nodes of the steel top flanges, thus modelling the presence of shear connectors.

Extensive parametric study, using the finite-element modelling, was conducted, in which 50 prototype bridges were analyzed to evaluate their load distribution factors for bending stress and shear under dead load and truck loading conditions. The span length of prototype bridges ranged from 20 to 100 meters, with two to four lanes. The number of steel boxes ranged from 2 to 4 in the case of two lanes, 3 to 5 in the case of three lanes, and 3 to 6 in the case of four lanes. The span-to-radius ratio was taken as 0, 0.4, 1, 1.4, and 2 for selected prototype bridges. The key parameters considered in the study were: number and stiffness of cross-bracings and top-chord systems, number of steel boxes, number of traffic lanes, bridge aspect ratio, and degree of curvature. Although X-type bracings as well as top-chords were normally used in the radial direction inside the boxes during the construction phase to minimize distortional, longitudinal warping, and transverse bending encountered in an open-box cross-section, their usefulness at service load was investigated herein. Also, the beneficial effects of similar bracings between the boxes were evaluated.

Based on the data generated from the parametric study, recommendations for the minimum number of internal and external X-type cross-bracings were made. Moreover,

empirical expressions for load distribution factors for flexural stress, deflection at mid-span, maximum force in bracings, and shear force carried by the webs were deduced for this type of bridge. It is hoped that the results from this research will be made available to bridge engineers in North America for the design of curved steel multiple-spine bridges.

**TO MY MOTHER,
HAWA HASSAN GALEB**

ACKNOWLEDGEMENTS

My sincere thanks and gratitude are due to His Almighty ALLAH, who helped and blessed me during the days of my study.

The author wishes to express his deep appreciation to his advisors Dr. J. B. Kennedy, University Distinguished Professor, and Dr. Khaled M. Sennah for their constant support and valuable supervision during the development of this research. Dr. Kennedy and Dr. Sennah devoted their time and effort to make this study a success. Their most helpful supervision is greatly appreciated.

The author wishes to acknowledge the financial support provided by the Natural Sciences and Engineering Research Council of Canada.

The author is also very grateful to his brothers and sisters for their great support, understanding, and patience throughout the course of this study.

TABLE OF CONTENTS

ABSTRACT.....	vi
ACKNOWLEDGEMENTS.....	x
List of Tables.....	xv
List of Figures.....	xvi
Notation.....	xix
CHAPTER	
I-INTRODUCTION.....	1
1.1 General.....	1
1.2 The Problem.....	3
1.3 Objectives and Scope.....	4
1.4 Contents and Arrangement of the Thesis.....	5
II- LITERATURE REVIEW.....	7
2.1 General.....	7
2.2 Elastic Analysis of Box Girder Bridges.....	7
2.2.1 Orthotropic Plate Theory Method.....	8
2.2.2 Grillage Analogy Method.....	8
2.2.3 Folded Plate Method.....	8
2.2.4 Finite-Strip Method.....	9
2.2.5 Finite-Element Method.....	10
2.2.6 Thin-Walled Curved Beam Theory.....	13
2.3 Load Distribution and Codes of Practice for Box Girder Bridges.....	15
III- FINITE-ELEMENT ANALYSIS.....	22
3.1 General.....	22
3.2 Finite-Element Approach.....	23
3.3 Description of the Finite-Element Program ‘ABAQUS’.....	25

3.4 Finite-Element Modelling of Curved Composite Multiple-Spine Bridges..	26
3.4.1 Geometric Modelling.....	26
(a) Modelling of Deck Slab, Webs, Bottom Flange, and End- Diaphragms.....	26
(b) Modelling of Steel Top-Flanges, Top-Chord, and Cross-Bracings.....	27
3.4.2 Boundary Conditions.....	27
3.4.3 Material Modelling.....	28
3.5 Finite-Element Analysis of the prototype bridges.....	29
 IV-PARAMETRIC STUDIES.....	 31
4.1 General.....	31
4.2 Description of the Bridge Prototypes Used in the Parametric Studies.....	31
4.3 Loading Conditions of Composite Multiple-Spine Bridges at Service.....	35
4.3.1 Dead Load.....	35
4.3.2 Live Load.....	35
4.4 Parametric Studies.....	37
4.4.1 Stress Distribution in Simply-Supported straight and Curved Composite Multiple-Spine Bridges.....	37
4.4.2 Deflection Distribution in Simply-Supported straight and Curved Composite Multiple-Spine Bridges.....	39
4.4.3 Axial Forces in Bracing System in Simply-Supported straight and Curved Composite Multiple-Spine Bridges.....	39
4.4.4 Shear Distribution in Simply-Supported Straight and Curved Composite Multiple-Spine Bridges.....	40
 V-RESULTS FROM THE PARAMETRIC STUDY.....	 41
5.1 General.....	41
5.2 Stress Distribution in Simply-Supported Straight and Curved Composite Multiple-Spine Bridges.....	41
5.2.1 Effect of Cross-Bracing System.....	43

5.2.2 Effect of Curvature.....	45
5.2.3 Effect of Bridge Aspect Ratio.....	46
5.2.4 Effect of Number of Boxes and Number of Traffic Lanes.....	46
5.2.5 Empirical Formulas for Bottom Stress Distribution Factor, D_{σ} ..	47
5.3 Deflection in Simply-Supported Straight and Curved Composite	
Multiple-Spine Bridges.....	50
5.3.1 Cross-Bracing Versus Degree of Curvature.....	50
5.3.2 Number of Boxes and Number of Lanes versus Curvature.....	51
5.3.3 Aspect Ratio versus Curvature.....	52
5.3.4 Empirical Expressions for Curved/Straight Bridge Deflection...	52
5.4 Axial Forces in Bracing Members.....	53
5.5 Shear Distribution in Simply-Supported Straight and Curved Composite	
Multiple-Spine Bridges.....	55
5.5.1 Effect of Cross-Bracing.....	56
5.5.2 Effect of Curvature.....	58
5.5.3 Effect of Aspect Ratio.....	59
5.5.4 Effect of Number of Boxes and Number of Lanes.....	60
5.5.5 Empirical Formula for Shear Distribution Factor, D_s	60
5.5.6 AASHTO and Proposed Equations: Comparison for Shear.....	65
5.6 Illustrative Design Examples.....	65
5.6.1 Design Example No. 1.....	65
5.6.2 Design Example No. 2.....	67
VI-SUMMARY AND CONCLUSIONS.....	69
6.1 Summary.....	69
6.2 Conclusions.....	70
6.3 Recommendations.....	71
REFERENCES.....	72
TABLES.....	80
FIGURES.....	90

APPENDIX.....	131
A.1 Geometries of Bridge Prototypes Used in the Parametric Study.....	131
A.2 ‘ABAQUS’ Input Data.....	134
VITA AUCTORIS.....	146

LIST OF TABLES

<u>Table</u>		<u>Page</u>
4.1	Geometries of the prototypes bridges in the parametric study.....	80
4.2	Ranges for the parameters considered in the sensitivity and parametric studies...	81
4.3	Material properties for concrete and steel in the parametric study.....	81
5.1	Finite Element Analysis (FEA) versus Straight Simple Beam Analysis (SBA)...	82
5.2	Effect of number of inner cross-bracing systems on stress distribution of straight and curved bridges.....	83
5.3	Effect of number of inner cross-bracing systems on deflection of curved bridges.....	84
5.4	Effect of number of inner cross-bracing systems on maximum bracing axial force.....	85
5.5	Effect of the area of cross-bracings on structural response of curved Multiple- spine bridge.....	86
5.6	Effect of span-to-depth ratio on shear distribution factor of 31-3b-60 straight bridges under AASHTO truck loading.....	87
5.7	Effect of number of cross-bracing systems on shear distribution factor of two-lane, two-box bridges of 60 m span under AASHTO truck loading....	88
5.8	Effect of cross-bracing area on the shear distribution factor of two-lane, two-box straight bridges of 60 m span under AASHTO truck loading.....	89

LIST OF FIGURES

<u>Figure</u>	<u>Page</u>
1.1 Box girder cross-sections.....	90
1.2 Jacques Cartier, I-girder bridge in Montreal, Quebec.....	91
1.3 Box girder bridge in Downtown Toronto.....	91
1.4 Two-Box bridge Cross-Section.....	92
3.1 Shell element “S4R” used for plate modelling.....	93
3.2 Beam element “B31H” for modelling beam in space.....	94
3.3 Finite-element discretization of cross-section of the bridge.....	95
3.4 Typical finite-element mesh for a composite bridge prototype.....	96
4.1 Basic cross-section configurations and symbols.....	97
4.2 Cross-section configurations used in the parametric studies.....	98
4.3 Truck loading configuration according to ‘AASHTO’ specifications.....	99
4.4 Loading cases considered in the parametric study.....	100
4.5 Idealized cross-section for stress distribution.....	101
5.1 Effect of number of cross-bracing systems on stress distribution of outer girder of two-lane, two-box bridge of 60 m under dead load.....	102
5.2 Effect of number of cross-bracing system on stress distribution of inner girder of two-lane, two-box bridge of 60 m under dead load.....	103
5.3 Effect of curvature on stress distribution factor of two-lane, four-box and 40 m bridge under dead load.....	104
5.4 Effect of curvature on stress distribution of two-lane, four-box and 40 m bridge under Full AASHTO truck loading.....	105
5.5 Effect of curvature on stress distribution factor for the inner girder of four-lane bridges of 100 m span under dead load.....	106

5.6	Effect of curvature on stress distribution for the outer girder of four-lane bridges of 100 m span under dead load.....	107
5.7	Effect of curvature on stress distribution for the outer girder of four-lane bridges of 100 m span under full AASHTO truck loading.....	108
5.8	Effect of span length on the stress distribution factor for the central girders of four-lane, five-box bridges under full AASHTO truck loading.....	109
5.9	Effect of number of boxes on stress distribution factor for the outer girder of straight bridges of 60 m span due to full AASHTO truck loading.....	110
5.10	Effect of number of traffic lanes on stress distribution factor for the central girders of bridges of 100 m span and $L/R=1$, under full AASHTO truck loading.....	111
5.11	Effect of curvature on stress distribution factor for the inner girder of two-lane bridges of 60 m span under full AASHTO truck loading.....	112
5.12	Effect of curvature on stress distribution factor for the internal girders of two-lane bridges of 60 m span under full AASHTO truck loading.....	113
5.13	Effect of number of cross-bracings on the deflection of the outer girder of two-lane, two-box bridges of 60 m span under full AASHTO truck load....	114
5.14	Effect of number of cross-bracings on mid-span web deflection of straight two-lane, two-box bridges of 60 m span.....	115
5.15	Effect of number of boxes on the average mid-span deflection of four-lane bridges of 100 m span under dead load.....	116
5.16	Effect of number of traffic lanes on the average mid-span deflection for four-box bridges of 40 m span under full AASHTO truck loading.....	117
5.17	Effect of span length on the mid-span average deflection of four-lane, five-box bridges under full AASHTO truck loading.....	118
5.18	Effect of the number of cross-bracing systems on the maximum axial force in bracings of two-lane, two-box bridges of 60 m span under full AASHTO truck loading.....	119
5.19	Effect of span on the maximum compressive force in bracings of two-lane, two-box bridges under full AASHTO truck loading.....	120
5.20	Effect of number of boxes on maximum compressive force in bracings of four-lane bridges of 100 m span under dead load.....	121

5.21	Effect of number of traffic lanes on maximum compressive force in bracings of four-box bridges of 40 m span under dead load.....	122
5.22	Effect of number of cross Bracings on shear forces carried by the outer web of two-lane, two-box and 60 m span bridges under dead load.....	123
5.23	Effect of cross-bracing area on the shear force carried by the webs of two-lane, two-box curved bridges of 60 m and $L/R=1$ under full AASHTO truck loading.....	124
5.24	Effect of curvature on shear distribution factor for the outer web of two-lane, two-box bridges due to dead load.....	125
5.25	Effect of curvature on shear distribution factor for the inner web of two-lane, two-box bridges due to dead load.....	126
5.26	Effect of span length on shear distribution of two-lane, two-box curved bridge, with $L/R=1.0$, under partial AASHTO truck loading.....	127
5.27	Effect of span length on shear distribution for the outer web of two-lane, four-box bridges under AASHTO truck loading.....	128
5.28	Effect of number of boxes on the shear distribution factor for the outer web of curved bridges of 60 m span , with $L/R = 2$, under dead load.....	129
5.29	Effect of number of boxes on shear distribution factor of inner webs in curved bridges of 100 m span, with $L/R=1$, due to full AASHTO truck loading.....	129
5.30	Effect of number boxes on shear force carried by the central webs of straight bridges having 60 meter span and 100 mm X 100 mm cross-bracing and top-chord systems subjected to full AASHTO truck loading.....	130
5.31	Effect of number boxes on shear force carried by the central webs of straight bridges having 20 meter span and 100 mm X 100 mm cross-bracing and top-chord systems subjected to full AASHTO truck loading.....	130

NOTATION

A	Bridge Width
A_b	Cross-sectional area of top-chords and cross-bracing system
[A]	The transformation matrix from local to global coordinates at the nodes
[B(x,y)]	The strain-displacement matrix at the nodes
b	Symbol of boxes in designation of bridge types, half bridge width
C	Steel top flange width
c	Symbol of curvature in designation of bridge types
D	Total depth of the steel boxes
D_σ	Flexural stress distribution factor
D_s	Shear distribution factor
D_{SS}	Shear distribution factor for straight bridges
D_{SC}	Shear distribution factor for curved bridges
[D]	The constitutive matrix or the elasticity matrix
E	Modulus of elasticity of steel
E_C	Modulus of elasticity of concrete deck slab
F	Total depth of composite bridge
$(F_C)_s$	Maximum compressive force in the bracing system of straight bridges
$(F_C)_c$	Maximum compressive force in the bracing system of curved bridges
I	Second moment of inertia
[K]	Structure stiffness matrix
L	Centre line span of simply supported bridges

l	Symbol of lanes in the designation of bridge types
M	Maximum moment in straight simply supported bridge
M_{DL}	Dead load moment for a straight bridge
M_{LL}	Maximum live load moment for a straight bridge under a line of wheel loads or half the equivalent lane loading
N_B	Number of boxes
N_L	Number of traffic lanes
n	Modular ratio
$[P]$	Applied loads vector at the nodes
R	Radius of curvature measured from the centre of curvature to bridge centre line
sc	Symbol of simply supported and curved bridge in the designation of bridge types
ss	Symbol of simply supported and straight bridge in the designation of bridge types
t_1	Thickness of steel top flange
t_2	Thickness of steel web
t_3	Thickness of steel bottom flange
t_4	Thickness of concrete deck slab
$[U]$	Displacement vector at the nodes
V	Maximum reaction of simply supported straight girder
V_{DL}	Maximum reaction due to dead load
V_{LL}	Maximum reaction due to live (truck) load
V_{max}	Maximum reaction at a bridge web from finite element analysis
W_1, W_2, \dots, W_i	Bridge webs starting from the inner side of curvature

W_E	The external virtual work
W_I	The internal virtual work
y_b	Distance of the neutral axis of the idealized girder from the bottom of the bridge
y_t	Distance of the neutral axis of the idealized girder from the surface of the concrete deck slab
Δ_s	Mid-span deflection of straight bridges
Δ_c	Mid-span deflection of curved bridges
$[\varepsilon(x,y)]$	The strain matrix in the finite element structure
σ	Maximum stress of simply supported straight girder due to dead load or live (truck) load
σ_b	Maximum tensile stress at the bottom flange of simply supported girder due to dead load or live (truck) load
$(\sigma)_{\max}$	Maximum tensile stress at the bottom flange from finite element analysis
$[\sigma]$	Stress matrix in the finite element solution
ν_s	Poisson ratio of steel
ν_c	Poisson's ratio of concrete deck slab

CHAPTER I

INTRODUCTION

1.1 General

Modern highway bridges are often subject to tight geometric restrictions and, in many cases, must be built in curved alignment. Horizontally curved bridges have become important component in highway bridges, especially in densely populated cities where elevated freeways and multi-level interchange structures are necessary.

Curved bridges may be entirely of reinforced concrete, prestressed concrete, steel, or composite concrete deck-steel girders. Moreover, these curved bridges may take the form of a deck slab on I-girders or box girders. Concrete box girders are usually cast in-situ or precast in segments erected on falsework or launching frame and then prestressed. Steel box girders are frequently constructed as segmented cantilevers. In some cases, they are prefabricated in long lengths and lifted into position by climbing jacks and connected together. The decks could be of steel or reinforced concrete. For the case of curved steel plate girders, two methods of fabrications have been employed. One method involves prefabrication of straight webs followed by either cold-bending or heat-curving to achieve the required curvature. In the second method, the curved flanges are cut from straight plates and welded to the webs which are curved. This actual curving of girders has allowed greater

span lengths, fewer piers, and more aesthetically pleasing structures than straight girders used as chords in forming a curved alignment.

A typical curved box girder bridge consists of top and bottom flange plates connected together by cylindrical webs to form the closed structure. Box girder cross-sections may be composed of one or more cells which are either contiguous or separated. Usually interior cell shape is rectangular while edge cells often have vertical, inclined, or rounded outside webs. As shown in Fig. 1.1, a box girder cross-section may take the form of single box (one cell), multiple-spine (separate boxes), or multi-cell with a common bottom flange (contiguous cells or cellular shape).

On horizontally curved alignment of highways in rural and urban areas, where curvature is small, open-section bridges such as beam-slab structures have been used. However, as the curvature of the highway increases due to space limitation, bridges of multiple-spine cross-section become more suitable. In addition to their light weight, shallower depth of cross-section, and significant longitudinal bending stiffness, multiple-spine bridges are favoured for their considerable torsional stiffness to resist applied loads when compared to open sections, thus rendering an efficient transverse load distribution. Such structures are aesthetically pleasing and relatively inexpensive to maintain since the surface area vulnerable to environmental conditions is small compared to open-sections. In addition, the steel boxes can be used to carry the required utilities.

The ramp shown in Fig. 1.2 is a sharply curved part of the Jacques Cartier Bridge crossing St. Lawrence River between Montreal Island and Longueuil in Quebec. It is made of curved composite I-girder with small spans and massive vertical, horizontal, and diagonal bracings to increase its torsional stiffness to resist the applied loads. Also, Fig. 1.3 shows a four-span continuous, twin-spine, box girder bridge crossing the railway in downtown Toronto. Composite multiple-spine cross-sections could provide considerable savings in the material content due to their excellent transverse distribution of loads which is nearly uniform in straight bridges. Proper design of straight and curved composite concrete deck-steel multiple-spine bridges requires good understanding of their overall structural behaviour. A study of their load distribution is also necessary.

1.2 The Problem

The multiple-spine bridge cross-section, shown in Fig. 1.4, consists of composite construction of a concrete deck and steel boxes. The steel box consists of two top flanges and a bottom flange connected to the top flanges by webs. Shear connectors connecting the steel top flanges with the concrete deck slab ensure full interaction between them. Solid end-diaphragms are used at the support lines of such bridges to seal off the end of the steel box with an opening to access or lay the utility cables inside the box. Cross-bracings and top chords (lateral ties to the steel top flanges) made of steel are used between the support lines inside and/or outside the boxes along the span, and also at the support lines between the boxes.

While the current design practices in North America recommend few analytical methods for the design of straight composite multiple-spine girder bridges, practical considerations in the design process require a need for a simplified design method in the form of expressions for bending stress and shear distribution factors. The Canadian Highway Bridge Design Code, CHBDC 1998, (59) recognized plan curvature as one of the factors that affect the structural response of bridges and therefore must be accounted for in the design process. While the North American codes provide a geometrically defined criterion to establish when a horizontally curved bridge may be treated as a straight one, it is not clear how bridge curvature affects the structural response and the extent of the conservatism employed in defining this criterion. A simplified design method is therefore required for curved multiple-spine bridges of composite construction.

1.3 Objectives and Scope

The main objectives of the present research work are:

- 1- Investigate the key geometric parameters of the bridge superstructure that affect its behaviour at the service load.
- 2- Develop a simplified design method for straight and curved composite multiple-spine bridges in the form of load distribution factors for longitudinal bending stress and shear force, and empirical equations for deflection at mid-span and maximum compressive force in the bracings.

In this practical-design-oriented thesis, a detailed analytical study on straight and

curved composite multiple-spine bridges is presented. The analysis is based on the finite-element method that seems to be the only approach capable of including all the important factors influencing the structural behaviour. The main parameters examined in the current research are: number and stiffness of bracing systems, bridge span length, number of traffic lanes, number of steel boxes, degree of curvature, and loading conditions.

The scope of this study thus includes the following:

- 1- A literature review of previous theoretical research work, and codes of practice for straight and curved box girder bridges.
- 2- A parametric study on the key parameters that may affect the (a) longitudinal flexural stress distribution characteristics; (b) shear distribution characteristics; (c) deflection at mid-span; and (d) maximum axial force in bracing members. The study applies to both straight and curved simply supported bridges.

1.4 Contents and Arrangement of the Thesis

The literature review and previous work on box girder bridges are presented in Chapter II. Chapter III describes the finite-element program used in the analytical study. This includes the linear static, and idealization and modelling of the composite bridge components. Chapter IV deals with a description of the prototype bridges used in the parametric study as well as the loading cases considered in the study. Chapter V presents the results of the parametric studies performed on the prototype bridges. Chapter VI gives a

summary of this research, the conclusions reached, and recommendations for further research.

CHAPTER II

LITERATURE REVIEW

2.1 General

The curvilinear nature of box girder bridges along with the complex deformation patterns and stress fields developed for different boundary conditions and loading cases have encouraged designers to adopt approximate and conservative methods for static analysis. Recent literatures on straight and curved box girder bridges dealt with analytical formulations. The literature survey presented herein deals with: (i) elastic analysis of box girder bridges; and (ii) load distribution and codes of practice for box girder bridges.

2.2 Elastic Analysis of Box Girder Bridges

In the design of bridges, analysis is usually simplified by means of assumptions that establish the relationship between the behaviour of single elements in the integrated structure. The combined response of these single elements is assumed to represent the response of the whole structure. The accuracy of such solutions depends on the validity of the assumptions made. The Canadian Highway Bridge Design Code, CHBDC 1998, (59) has recommended several method of analysis for only straight box girder bridges. These methods include: Orthotropic Plate Theory, Grillage Analogy, Folded Plate, Finite-Strip, and Finite-Element technique. Several authors have applied these methods along with the

thin-walled beam theory to the analysis of straight and curved box girder bridges. In the following sections, these different approaches to box girder bridge idealizations and their limitations will be discussed.

2.2.1 Orthotropic Plate Theory Method

In the equivalent orthotropic plate theory method, the stiffness of the flanges and girders are lumped into an orthotropic plate of equivalent stiffness and the stiffness of diaphragms is distributed over the girder length. This method is suggested mainly for multi-girder straight and curved bridges. The 1998 CHBDC code (59) has recommended using this method for the analysis of only straight box girder bridges of multi-spine cross-section.

2.2.2 Grillage Analogy Method

The Canadian Highway Bridge Design Code of 1998 (59) limits the applicability of this method to voided slab and box girder bridges in which the number of cells or boxes is greater than two. In this method, the multi-cellular superstructure was idealized as a grid assembly by Hambly and Pennells (33). One difficulty of the grillage analogy method lies in the representation of torsional stiffness of the closed cells. Satisfactory, but approximate representation can be achieved in modelling the torsional stiffness of a single closed cell by an equivalent I-beam torsional stiffness (Evans and Shanmugam, 25).

2.2.3 Folded Plate Method

The folded plate method utilises the plane stress elasticity theory and the classical

two-way plate bending theory to determine the membrane stresses and slab moments in each folded plate member. The folded plate system consists of an assemblage of longitudinal annular plate elements interconnected at joints along their longitudinal edges and simply-supported at the ends. No intermediate diaphragms are assumed. Solution of simply-supported straight or curved box girder bridges is obtained for any arbitrary longitudinal load function by using direct stiffness harmonic analysis. The method has been applied to box girder bridges by Al-Rifaie and Evans (1), and, Meyer and Scordelis (50). In 1982, Evans (24) applied also this method to cellular structures. However, it was evident that the method is complicated and time-consuming. Furthermore, the 1998 CHBDC code (59) restricted this method to bridges with support conditions closely equivalent to line supports at both ends of the bridge.

2.2.4 Finite-Strip Method

The finite-strip method may be regarded as a special form of the displacement formulation of the finite-element method. In principle, it employs the minimum total potential energy theorem to develop the relationship between unknown nodal displacement parameters and the applied load. In this method, the box girders and plates are discretized into annular finite-strips running from one end-support to the other and connected transversely along their edges by longitudinal nodal lines. The displacement functions of the finite-strips are assumed as a combination of harmonics varying longitudinally and polynomials varying in the transverse direction. In 1971, Cheung and Cheung (16) applied the finite-strip method to curved box girder bridges. In 1974, Kabir and Scordelis (43)

developed a finite-strip computer program to analyse curved continuous span cellular bridges, with interior radial diaphragms, on supporting planar frame bents. In 1978, Cheung and Chan (15) used the finite-strip method to determine the effective width of the compression flange of straight multi-spine and multi-cell box girder bridges. In 1984, Cheung (14) used a numerical technique based on the finite-strip method and the force method for the analysis of continuous curved multi-cell box girder bridges. In 1988, Li et al. (46) presented the application of spline finite-strip method to the elasto-static analysis of circular and non-circular multi-cell box girder bridges. In 1992, Bradford and Wong (8) used the finite-strip method to study the local buckling of straight composite concrete deck-steel box section in negative bending. Compared to the finite-element method, the finite-strip method yields considerable savings in both computer time and effort, since only a small number of unknowns are generally required in the analysis. However, the drawback of the finite-strip method is that the method is limited to simply-supported prismatic structures with simple line support (59).

2.2.5 Finite-Element Method

During the past two decades, the finite-element method of analysis has rapidly become a very popular technique for the computer solution of complex problems in engineering. In structural analysis, the method can be regarded as an extension of earlier established analytical techniques, in which a structure is represented as an assemblage of discrete elements interconnected at a finite number of nodal points (80). In 1971, Chapman et al. (13) conducted a finite-element analysis on steel and concrete box girder bridges to

investigate the effect of intermediate diaphragms on the warping and distortional stresses. In 1970, Sisodiya et al. (67) approximated the curvilinear boundaries of finite elements used to model the curved box girder bridges by a series of straight boundaries using parallelogram elements. This approximation would require a large number of elements enough to achieve a satisfactory solution. Such an approach is impractical especially for highly curved box bridges. In 1974, Bazant and El Nimeiri (7) attributed the problems associated with the neglect of curvilinear boundaries in elements used to model curved box beams by the loss of continuity at the end cross-sections of two adjunct elements meeting at an angle. They developed a skew-ended finite-element with shear deformation using straight elements and adopted a more accurate theory that allows for transverse shear deformations.

In 1972, Willam and Scordelis (76) presented an elastic analysis of cellular structures of constant depth with arbitrary geometry in plan using quadrilateral elements. In 1975, Fam and Turkstra (27), Fam (26), and Turkstra and Fam (28) described a finite-element scheme for static and free-vibration analysis of box girders with orthogonal boundaries and arbitrary combinations of straight and horizontally curved sections using a four-node plate bending annular element with two straight radial boundaries, for the top and bottom flanges, and conical elements for the inclined web members. They (70) also demonstrated the importance of warping stresses in single-box curved bridge, in relation to the longitudinal normal bending stresses obtained from curved beam theory.

Malcolm and Redwood (48) and Moffatt and Dowling (53) investigated the shear

lag phenomena in steel box girder bridges. In 1979, Sargious et al. (65) studied the behaviour of end-diaphragm with opening in single-cell concrete box girder bridges supported by a central pier. In 1985, Ishac and Smith (41) presented simple design approximations for determining the transverse moments in single-span single-cell concrete box girder bridges. In 1988, Dilger et al. (22) studied the effect of presence and orientation of diaphragms on the reaction, internal forces, and the behaviour of skew, single cell, concrete box girder bridges. In 1995, Galuta and Cheung (32) developed a hybrid analytical solution that combines the boundary element method (BEM) with the finite-element method (FEM) to analyse box girder bridges. The finite-element method was used to model the webs and bottom slab of the bridge, while the boundary element method was employed to model the top slab.

Recently, few authors have dealt with temperature effects on box girder bridges. In 1990, Chan et al. (12) presented temperature data collected continuously in three composite box-girder bridges over a one-to-two year period. The first bridge was the Portage Bridge spanning the Ottawa River between Hull, Quebec, and Ottawa, Ontario. This bridge is a three-lane, three-span continuous, composite concrete deck-steel five-box girder with a total length of 158.5 m. The second bridge was the St. Leonard bridge, International bridge over the St. John River connecting St. Leonard, New Brunswick and Van Buren, Maine. This bridge is a continuous, five-span, composite concrete deck-steel two-box girder with a total length of 222.5 m. The third bridge was the Robert Campbell Bridge spanning the Yukon River in the city of Whitehorse. It is a continuous two-span composite concrete deck-steel

three-box girders with a total span of 109.7 m. Thermal stresses induced in these bridges were determined using the finite-element method, with input being the measured extreme temperature profiles. In 1996, Elbadry and Ibrahim (23) determined the time-dependent temperature variations within the cross-section and along the length of curved concrete single-cell box girder bridges using a three-dimensional finite-element model used in heat transfer.

2.2.6 Thin-Walled Curved Beam Theory

The curved beam theory was first established by Saint-Venant for the case of solid curved beams loaded in a direction normal to their plane of curvature. The theory is based on the usual beam assumption, i. e. cross-sectional dimensions are small compared to the length; cross-sections do not distort and plane sections remain plane. Curved beam theory can only provide the designer with an accurate distribution of the resultant bending moments, torque, and shear at any section of a curved beam if the axial, torsional and bending rigidities of the section are accurately known. In general, curved beam theory cannot be applied to curved box girders bridges since it cannot account for warping, distortion, and bending deformations of the individual wall elements of the box. Therefore, the thin-walled beam theory was developed by Vlasov (73) for axisymmetric sections, and then extended by Dabrowski (18) for asymmetric section, to account for warping deformations caused by the gradient of normal stresses in individual box elements. The theory assumes non-distortional cross-section and, hence, does not account for all warping or bending stresses. The theory cannot predict shear lag or the response of deck slabs due to

local wheel loads. Using this theory, few authors (58, 37, 38, 55) analysed the curved multi-spine box girder bridges under dead and live loads.

In 1985, Hasebe et al. (34) presented a detailed analytical study, based on the refined thin-walled beam theory by Kano et al. (44), taking into account shear deformation and shear lag, to examine the influence of various parameters on the effective width of curved box beams. In 1989, Maisel (47) extended Vlasov's thin-walled beam theory to treat torsional, distortional, and shear lag effects of straight, thin-walled cellular box beams. In 1989, Mavaddat and Mirza (49) used Maisel's formulations to develop computer programs to analyse straight concrete box beams with one, two, or three cells and side cantilevers over a simple span or two spans with symmetric mid-span loadings. The structure is idealized as a beam and the normal and shear stresses are calculated using the simple bending theory and St-Venant's theory of torsion. Then, the secondary stresses arising from torsional and distortional warping and shear lag are calculated.

Several investigators (7, 51, 72, 78, 71, 74, 75, 30, 68) have combined thin-walled beam theory by Vlasov and the finite-element technique to develop a thin-walled box beam element for elastic analysis of cellular box girder bridges, in which transverse distortion and longitudinal torsional warping, and in some cases the shear lag effect, were accounted for. In 1992 and 1994, Li (45) and Razaqpur and Li (64) developed two thin walled box beam finite elements, straight and curved, which can model extension, flexure (including shear deformation), torsion, torsional warping, distortion, distortional warping, and shear lag

effects. The two elements, that were developed using an extended version of Vlasov's thin-walled beam theory, were used for the analysis of multi-cell box girder bridges with general geometry. Razaqpur and Li (63, 62) extended the application of these two elements to the analysis of straight and curved multi-branch multi-cell box girder assemblages, respectively. The results using the proposed element compared well with the shell element analysis. However, the element does not account for local stress distribution at the intersection of box girder assemblages.

2.3. Load Distribution and Codes of Practice for Box girder bridges

Composite girder bridges may take the form of I-girder, multi-cells, or multiple-spines. Bridges of concrete deck over steel boxes are more efficient and economical than those of composite steel-concrete I-girders since they exhibit better transverse load distribution due to their superior torsional stiffness. Further economies can be achieved by using a multiple box bridge section other than a cellular bridge section. The former weighs less than the latter, generally. The following paragraphs provide a summary of the research work done on load distribution in such bridge types.

In 1985, Yoo and Littrell (77) studied the effect of cross-bracing on the warping and bending stresses of curved I-girders using a full three-dimensional finite-element modelling. In 1986, Brockenbrough (10) used the finite-element modelling to derive load distribution factors, including the warping effects, of curved composite I-girder bridges as a function of the span length, radius of curvature, girder spacing, and cross-bracing spacing. In 1967, and

1968, Johanston and Mattock (42), and Fountain and Mattock (29) used a computer program for the analysis of folded plate structures to study the lateral distribution of load in simple span composite multiple-spine box girder bridges without transverse diaphragms. To verify their analysis and computer program, a one-quarter scale model of a two-lane, 80 ft span bridge supported by three box girders, and one-fifth scale model of a two-lane, 100 ft span bridge supported by two box girders were built and tested under concentric and eccentric AASHTO truck loadings. The results were used to develop an expression for the live load bending moment distribution factor for each box girder as a function of the roadway width, and number of boxes. Their findings formed the basis for the lateral distribution of loads for bending moment currently used by AASHTO (4) and by the Ontario Highway Bridge Design Code in 1983 (60) for the multi-spine box girder bridges. The drawback of this expression is that the beneficial effect of the cross-bracing inside and between the boxes was not taken into account. Moreover, it limits its application to bridges with a number of spines equal to the number of lanes. The AASHTO Load Resistance Factor Design (2) provides another expression for load distribution for the ultimate limit state to obtain the live load bending moment and shear force in each box of the multiple-spine box girder bridge cross-section.

In 1985, and 1992, Bakht and Jaeger (5, 6) presented a particular case of multiple-spine bridges having at least three spines, zero transverse bending stiffness, with the load transfer between the various spines through transverse shear. Based on these simplifications, they proposed load distribution factors for bending moment and shear.

These formed the basis for live load distribution used by the third edition of the OHBDC (61) for multiple-spine bridges. In 1994, Normandin and Massicotte (56) presented the results of a refined finite-element analysis to determine the distribution patterns in multiple-spine box girder bridges with different characteristics and geometry. Several parameters were considered in the analysis: the presence of the internal diaphragms, the use of external bracing, and the type of live load. The study proved that internal diaphragms, inside boxes, are essential components in a box girder bridge since they contribute largely to the reduction of the cross-sectional distortion. Moreover, external bracings between boxes do not significantly influence the distribution characteristics of bending moments and shear, since a fully loaded bridge usually governs the design. Results also indicate that, in some cases, both the AASHTO (4) and OHBDC (61) distribution factors underestimate the live load effects by a significant margin.

In 1978, Heins (35) extended the applicability of the straight multiple-spine box girder moment distribution equation provided by Fountain and Mattock (29) to horizontally curved composite multiple-spine box girder bridges. A modification factor to the straight girder moment distribution was proposed as a function of the radius of curvature provided that cross-bracings are used inside the boxes. In 1980, Mukherjee and Trikha (54), using the finite-strip method, developed a set of design coefficients for twin cell curved box girder reinforced concrete bridges as an aid to practical design of such bridges. These coefficients were for moment, shear, transverse moment, and vertical deflection under the webs. These coefficients were limited only to concrete bridges of two-lane, span length between 20 and

40 m, and radius of curvature between 45 and 150 m.

The AASHTO Guide Specification for Horizontally Curved Highway Bridges (3) pertained to both curved composite concrete deck-steel I-girder bridges and multiple-spine box girder bridges. The specifications for load distribution for both curved I-girders and multiple-spine box girders were based on a design-oriented research work done by Heins and Jin in 1984 (36) on live load distribution of single and continuous curved composite I-girder bridges. They utilized a space frame modelling to incorporate the interaction of diaphragms (cross-bracing in the radial direction) and bottom lateral bracing in some bays or in all bays. Appropriate design equations were presented for use in conjunction with a plane grid solution. For both curved I-girders and curved multiple-spine box girders, the AASHTO Guide Specification for Horizontally Curved Highway Bridges of 1993 (3) specifies that the moments and shears required to proportion the individual members shall be based on a rational analysis, other than a plane grid, of the entire structure which takes into account the complete distribution of loads to the various members. Otherwise, the code modifies the resulting maximum live load stresses, using the Heins-Jin design equation, considering additional warping stresses besides the normal bending stresses obtained from plane grid analysis.

In 1981, Davis and Bon (20) presented a correction factor for curvature for load distribution in concrete and prestressed concrete multi-cell box girder bridges. For all girders except the exterior girder farthest from the centre of curvature, this factor is a ratio

of the distance from the centre of curvature to the assigned girder to the centre-line radius of curvature of the bridge. For the outermost girder (farthest from the centre of curvature), they proposed straight bridge load distribution without any modifications. The drawback of this method is that the beneficial effect of the transverse diaphragms was not taken into consideration. In 1988, Nutt et al. (57) proposed a set of equations for moment distribution in straight, reinforced and prestressed concrete, multi-cell box girder bridges as a function of the number of lanes, cell width, span length, and number of cells. In 1989, Ho et al. (40) used the finite-strip method to analyse straight simply-supported, two-cell box girder and rectangular voided slab bridges without intermediate diaphragms. Empirical expressions were deduced for the ratio of the maximum longitudinal bending moment to the equivalent beam moment. This study was limited to a straight two-cell bridge section made of either steel or concrete. Moreover, the span lengths of the bridges in this study were up to 40 m in case of two-lane, 50 m in case of three-lane, and 67 m in case of four-lane. In 1995, using the finite-strip method, Cheung and Foo (17) proposed expressions for the ratio moment distribution factor of the curved multiple-spine box girder bridge to that of the straight one as a function of span length, number of lanes, box spacing, and radius of curvature. The disadvantage of this study is that it did not take into account the beneficial effect of diaphragms inside the boxes or cross-bracings between boxes. Further, the effect of the number of boxes and dead load distribution were not included.

The AASHTO code of 1996 (4) specified load distribution factors for bending moment in straight reinforced concrete box girder bridges, namely: $S/8$ for one-lane traffic

and $S/7$ for two or more traffic lanes, where S is the cell width in feet. The specified load distribution factors were based on suggestions made by California design engineers in 1959 (19). However, these distribution factors do not give the designer any indication on the behaviour of the bridge and the parameters influencing the response of the structure other than the cell width. In 1991, Zokaie et al. (69, 79) proposed other moment and shear distribution factors for reinforced and prestressed concrete multi-cell bridges. Their findings form the load distribution factors for moment and shear currently used by the AASHTO LRFD code (2) for straight concrete multi-cell bridges. In 1996, Brighton et al. (9) described a study to determine a live load distribution factor for a new type of precast concrete double cell box girders that was proposed for a prefabricated bridge system for rapid construction of short-span bridges. In 1994 and 1996, Dean (21) and Fu et al. (31) studied torsion on multi cellular members. In 1998, using the finite-element method, Sennah (66) proposed moment, shear, and deflection distribution factors, as well as maximum force in bracing, for curved composite concrete deck-steel cellular bridges.

Some of the aforementioned investigations on box girder bridges were confined to reinforced and prestressed concrete construction, and did not include composite concrete deck-steel construction. Others dealt with steel box girders but were limited to particular cases, or in their range of applicability of the research findings. Therefore, research work on moment and shear distribution of straight and curved composite concrete deck-steel multiple-spine bridges is required. The Canadian codes of practice for highway bridge design [OHBDC, 1992 (61); CAN/CSA-S6-88 (11); CHBDC, 1998 (59)] have no

specifications for the design of horizontally curved bridges including those of multi-box cross-sections, while the American code of practice for horizontally curved highway bridges [AASHTO Guide Specification, 1993 (3)] provides load distribution factors for curved composite bridges other than those of multi-box cross-section. Because of its superior torsional-to-bending stiffness ratio when compared to other types of bridge cross-sections, the multiple-spine bridge cross-section is required, specially, in sharply curved alignments to allow better load distribution characteristics. The American Association of State Highway and Transportation Officials code of 1996 (4) states the curved bridge may be designed as a straight bridge if the central angle $\leq 12^\circ$. On the other hand, the Canadian Highway Bridge Design Code of 1997 (59) states that for horizontally curved bridges, the effect of curvature may be neglected in structural design calculations as long as two conditions are met: L^2/bR ratio is less than 1.0, where L is the curved span length, b is half the bridge width, and R is the radius of curvature; or, when $R > 90$ m. These limitations are questionable in the case of moment and shear in curved composite multiple-spine bridges.

CHAPTER III

FINITE-ELEMENT ANALYSIS

3.1 General

Of all the available methods of analysis, the finite-element method is the most powerful, versatile, and flexible. Recent developments in the finite-element method of analysis make it possible to model a bridge in a more realistic manner and to provide a full description of its structural response within the elastic and post-elastic stages of loading. The most important advantage of this method is its capability to deal with problems that have arbitrary arrangements of structural elements, material properties, and boundary conditions. Therefore, the finite-element method is specially suitable for the analysis of curved composite multiple-spine bridges. Thus, the finite-element program named ABAQUS (39) was used throughout this study to determine the linear static response of curved composite multiple-spine bridges. The finite-element modelling of the different components of the composite multiple-spine bridges (i.e. the reinforced concrete deck slab, the steel top flanges, the steel webs, the steel bottom flange, the solid end-diaphragms, the cross-bracings, and the top chords) is described in subsequent sections in this chapter. A general description of the ABAQUS program is presented in this chapter. The finite-element method of structural analysis described herein was also used to perform the parametric studies on static responses of both straight and curved composite concrete deck-steel multiple-spine bridges. These parametric studies are described in detail in chapter IV.

3.2 Finite-Element Approach

The finite-element method is a discretization technique in which the entire structure is discretized into a finite number of regions (elements) that are interconnected at certain points (nodes). With a displacement formulation, the stiffness matrix of each element is derived and the global stiffness matrix of the entire structure can be formulated by the direct stiffness method. This global matrix, along with the given displacement boundary conditions and applied loads, is solved and thus the displacements and stresses can be determined. The global stiffness matrix represents the nodal force-displacement relationships and can be expressed in the following matrix equation form:

$$[P] = [K][U] \quad (3.1)$$

in which $[P]$ is the nodal load vector, $[K]$ is the global stiffness matrix, and $[U]$ is the nodal displacement vector. The steps for deriving the above equation can be summarized in the following basic relationships:

$$(a) \quad v(x, y) = [\Phi(x, y)][\alpha] \quad (3.2)$$

where $v(x, y)$ is the internal displacement vector of the element, $\Phi(x, y)$ is the displacement function, and α is a generalized coordinate.

$$(b) \quad [U] = [A][\alpha] \quad \text{then, } [\alpha] = [A]^{-1} [U] \quad (3.3)$$

where $[A]$ is the transformation matrix from local to global coordinates.

$$(c) \quad [\varepsilon(x, y)] = [B(x, y)][\alpha] = [B(x, y)][A]^{-1}[U] \quad (3.4)$$

in which $[B(x, y)]$ is the strain-displacement matrix, and $[\varepsilon(x, y)]$ is the strain matrix.

The stress matrix $[\sigma(x, y)]$ is given by:

$$(d) \quad [\sigma(x, y)] = [D][\varepsilon(x, y)] = [D][B(x, y)][A]^{-1}[U] \quad (3.5)$$

where $[D]$ is the constitutive matrix or the elasticity matrix. By using the principle of minimization of the local potential energy for the total external work equal to $1/2 [U]^T[P]$, it can be shown that:

$$(e) \quad (i) \quad W_E = [u']^T [P]$$

$$(ii) \quad W_I = \int_{vol.} [\varepsilon']^T [\sigma] dv = [u']^T [A']^T [k'] [A]^{-1} [U] \quad (3.6)$$

$$where \quad [k'] = \int_{vol.} [B(x, y)]^T [D] [B(x, y)] dv$$

and W_E is the external virtual work, W_I is the internal virtual work, $[u']$ is the vector of virtual displacement, $[\varepsilon']$ is the vector of virtual strain, and $[k']$ is the element stiffness matrix.

(f) From the principle of virtual work, $W_E = W_I$. By taking one element of virtual nodal displacement vector $[u']$ equal to unity successfully, the following is obtained.

$$[P] = [K][U] \quad where \quad [K] = \sum [k'] \quad (3.7)$$

Thus, the global structural stiffness matrix is an assemblage of the element stiffness matrix $[k']$.

(g) The solution of the resulting system of equations yields the values of nodal displacement [U] and the internal forces for each element can be obtained from equation (3.4) and (3.5). In a linear (elastic) problem, loads are applied to a model and the response is obtained directly.

3.3. Description of the Finite-Element Program 'ABAQUS'

ABAQUS (39) is designed as a flexible tool for numerical modelling of structural response in linear analysis. This computer program runs as a batch application to assemble a data deck that describes a problem so that it can provide an analysis. A data deck for this computer program contains model data and history data. Model data defines a finite-element model: the elements, nodes, element properties, material definitions, nodal constraints, and any data that specify the model itself. History data define what happens to the model, the sequence of events or loadings for which the model's response is sought. The computer program provides a TRANSFORM option to specify a local coordinate system at nodes by setting up a rotated direction for displacements and rotations at individual nodes and node sets. This option was used to rotate the two horizontal displacements (U_x and U_y) to radial and tangential displacement to apply the boundary conditions at the radial supports of curved bridges.

3.4 Finite-Element Modelling of Curved Composite Multi-Spine Bridges

A three-dimensional finite-element analysis is used to model curved composite concrete deck-steel box bridges. The structure is first divided into several components; namely: concrete deck slab, steel webs, steel bottom flange, steel solid-end-diaphragms, steel top flanges, and cross-bracing and top-chord members. The concrete slab is rigidly connected to the steel top flanges by means of shear stud connectors. In this section, element types used for different components as well as material modelling in the elastic loading stages are presented.

3.4.1 Geometric Modelling

(a) Modelling of Deck Slab, Webs, Bottom Flange, and End-Diaphragms

A mesh of three-dimensional shell elements was used to model the reinforced concrete deck slab, steel webs, steel bottom flange, and steel solid-end-diaphragms. A four-node doubly-curved general purpose shell element named S4R in the ABAQUS library was used. The element has either straight or curved boundaries depending on nodes definitions. The element had six degrees of freedom at each node, namely three displacements (U_1 , U_2 , U_3) and three rotations (Φ_1 , Φ_2 , Φ_3). A detailed description of the shell element S4R is shown in Fig. 3.1. The general-purpose shell element chosen herein uses thick shell theory as the shell thickness increases and becomes discrete Kirchhoff thin shell elements as the thickness decreases; the transverse shear deformation becomes very small as the shell thickness decreases. The criterion for neglecting shear deformation occurs when the

thickness of the shell is less than about 1/15 of a characteristic length on the surface of the shell, such as the distance between supports. However, the thickness of the shell may be larger than 1/15 of the element length. Element S4R accounts for finite membrane strains and allows for change in thickness caused by deformation. It is, therefore, suitable for large membrane strain analysis, besides large-rotation analysis, involving materials with Poisson's ratios.

(b) Modelling of Steel Top Flanges, Top-chords, and Cross-bracings

A three-dimensional two-node linear-interpolation element, named B31H in ABAQUS library, was adopted to model the steel top flanges, top-chords, and cross-bracings. The element had two nodes with six degrees of freedom at each node, three displacements (U_1 , U_2 , U_3) and three rotations (Φ_1 , Φ_2 , Φ_3). A detailed description of the beam element B31H is shown in Fig. 3.2. This hybrid element is designed to handle very slender situations, where the axial stiffness of the member is very large compared to its bending stiffness. Therefore, because of their insignificant flexural and torsional stiffness, cross-bracings and top-chord members are considered as axial members loaded in tension and compression.

3.4.2 Boundary Conditions

Two different nodal constraints were used in the analysis, namely: boundary constraints and multi-point constraints. Two different boundary constraints were used in

modelling the simply-supported bridges: the roller support at one end of the bridge constrained both vertical and radial displacements at the lower end nodes of each web; the hinge support at the other end of the bridge was modelled by restricting all possible translations at the lower end nodes of each web.

The multi-point constraint option in the ABAQUS software, type BEAM, which allows constraint between different degrees of freedom, was used between the shell nodes of the concrete deck and the beam element nodes of the steel top flanges. The finite-element formulation of the multi-point constraint BEAM type is described in ABAQUS (39.) This multi-point constraint option ensured full interaction between the concrete deck slab and the steel boxes, thus modelling the presence of the shear connectors. In this type of constraint, a linear set of constraint equations was utilized to couple the nodal degrees of freedom of the nodes of relevant elements as shown in Fig. 3.3. Proper spacing of the multi-point constraints was adopted in the transverse direction at the support lines to ensure full interaction of the concrete deck with the supporting steel boxes.

3.4.3 Material modelling

ABAQUS (39) requires that the material is sufficiently defined to provide suitable properties for those elements with which the material is associated, and for the analytical procedures through which the model will be run. Thus a material associated with the structural elements must include a mechanical category option to define its mechanical (stress-strain) properties such as elastic modulus and yield stress. Hence, values of $E_c =$

27,000 Mpa and $\nu_c = 0.3$ were assumed for the concrete, whereas values of $E_s = 200,000$ Mpa and $\nu_s = 0.3$ were taken for the steel.

3.5 Finite-Element Analysis of the Prototype Bridges

A convergence study was conducted to choose the finite-element mesh. The finite-element mesh is usually chosen based on pilot runs and is a compromise between economy and accuracy. Utilizing four elements in each box and between boxes in the transverse direction, 72 elements in the direction of traffic for a single span, with six elements in the webs proved to be enough for elastic analysis. Figure 3.3 shows a typical finite-element discretization of the cross-section of two-box bridge prototypes. The aspect ratio of the shell elements used in modelling the webs was 2.1 for bridges of span-to-depth ratio of 25. While the aspect ratio of the shell elements used in modelling the concrete deck slab and the steel bottom flange ranged from 1 to 4.8. This maximum limit of around 5 would be enough when stress evaluation is of prime concern. However, shell elements of aspect ratio between 1 to 2, 2 to 3, 3 to 4, and 4 to 5 were 52%, 30%, 14%, and 4%, respectively, of those used in modelling bridges of spans 20 to 100 m, used in the parametric study.

Pilot runs on the effect of vertical web stiffeners on the structural behaviour proved that these thin stiffeners have an insignificant effect on the response. Therefore, they were not included in the finite-element model. It was also proven that the steel reinforcement in the concrete deck slab has an insignificant effect in the bridge elastic response. In practice,

the cross-bracing system should be as deep as possible to accomplish its effect. The top surface of the top-chord members should be very close to the steel top flanges with a vertical distance equal to half the concrete deck slab thickness to allow for concrete form work and to prevent lateral instability of the steel top flanges during construction. Therefore, the connections of the top-chord and cross-bracing members to the steel boxes used in the finite-element modelling were shifted to the points of intersection of the steel webs and the steel top flanges.

The finite-element modelling was employed to perform several parametric studies on the structural response of curved composite multiple-spine prototype bridges as shown in chapter IV. In this respect, a wide range of prototype bridges was examined as described in chapter IV. Appendix A.2 shows a list of the finite-element computer program input data used in the analysis of a four-lane and three-box curved bridge having a span of 100 meters and a radius of 100 meters.

CHAPTER IV

PARAMETRIC STUDIES

4.1 General

The parametric studies were aimed to generate information not yet available on the structural behaviour of straight and curved composite concrete deck-steel multiple spine bridges. Although it was common practice for engineers to increase the design moment of an equivalent straight box girder by 5% to 20% for curved box girders, more refined specifications should be made available for the design of such bridges. The current parametric studies were intended to develop a simplified design method for these bridges. The time constraint in the completion of this research imposed the choice of one of the two design trucks used in North America, i.e. those defined by CHBDC and AASHTO. The latter was used in the parametric studies in order to provide the engineer with the flexibility and tools to design such bridges when using the AASHTO truck. Thus, the main objectives of the parametric studies were: (i) to investigate the influence of all major parameters affecting the straining actions of composite multiple spine bridges; (ii) to generate a database for these straining actions to develop empirical formulas for the design of different idealized girders for bending, shear, and deflection.

4.2 Description of the Bridge Prototypes Used in the Parametric Studies

In order to accurately determine the parameters affecting the structural response of straight and curved composite multiple spine bridges, it was necessary to define the

geometric parameters that may affect their behaviour. These parameters include: span length, number of boxes, number of traffic lanes, span-to-depth ratio, span-to-radius of curvature ratio, aspect ratio, cross-bracing and top-chord systems, and end-diaphragm thickness. For this study, the straight composite multiple spine bridges, presented in Table 4.1, which were designed according to AASHTO bridge specifications (4, 66), were modified into multiple spine bridges, and thus formed the basis of the prototype bridges used in the parametric studies. The symbols used in the first column in Table 4.1 represent designations of the bridge types considered: 1 stands for lane; b stands for box; ss stands for simply-supported and straight and sc stands for simply-supported and curved; and the number at the end of the designation represents the span length in meters. For example, 21-2b-sc-20 denotes a bridge of 2 lanes, 2 boxes, simply-supported, curved, and of 20 m span. Figure 4.1 shows the basic cross-sectional configurations and symbols as presented in Table 4.1.

In the parametric studies, the span length of the bridges ranged from 20 m to 100 m, representing medium span bridges. The number of traffic lanes was taken as 2, 3, and 4. One-lane bridges were not included in this study. Responses and distribution factor for such bridges can be found elsewhere (66). The bridge width was 9.30 m in the case of two-lane, 13.05 m in the case of three-lane, and 16.80 m in the case of four-lane bridges. The number of boxes ranged from 2 to 4 in the case of two-lane, 3 to 5 in the case of three-lane, and 3 to 6 in the case of four-lane bridges. To change the number of steel boxes for the same lane width, the thicknesses of the steel top flanges, webs, and bottom flanges were changed to maintain the same shear stiffness of the webs and overall flexural stiffness of the cross-section. Figure 4.2 shows the number of boxes along with the number of lanes considered in the parametric studies.

For each bridge included in the parametric study, the transverse geometry (including number and stiffness of cross-bracing and top-chord systems, and span-to-depth ratio) as well as radius of curvature were changed to study their effect on the structural response. The number of cross-bracings as well as the top-chords was varied from 1 to 17. For road-ways or ramps where structural depth is not severely limited, box girder, T-, or I-beam bridges have cost about the same for spans close to 24 m. For shorter spans, T- or I-beam bridges are usually cheaper, and for longer spans, box girder bridges tend to be more economical. However, in some cases, box girder bridges have been found to be economical for spans as short as 20 m when structural depth was restricted. The practical range of span-to-depth ratio for box girder bridges ranges from 20 to 30 (35). However, in this study, the range of span-to-depth ratio was taken from 10 to 40 in order to examine its effect.

The curved bridges considered in this study are assumed to have constant radii of curvature and concrete decks with constant elevations. The degree of curvature can be defined by the span-to-radius ratio, L/R , where the span of the bridge, L , is the arc length along the centre line of its cross-section and the radius of curvature, R , is the distance from the origin of the circular arc to the centre line of the cross-section. The L/R ratios used in this study ranged from 0.0 to 2.0. The higher values of L/R along with the lower value of the span length, 20 m, are theoretically possible to analyze but practically uncommon for curved highway bridges since the Geometric Design Standards for Ontario Highways, 1985, (52) only allow using curved bridges when a radius of curvature ≥ 45 m. However, the inclusion in this study of a smaller radius of curvature serves to show the trend of the structural response of curved bridges within certain limits of L/R .

The full ranges of all the parameters used in this study are listed in Table 4.2. These ranges were based on an extensive survey of actual designed multi-cell bridges [Johanston et al., 1967, (42); Chapman et al., 1971, (13); Heins, 1978, (35)] and modified into multiple-spine bridges for the purpose of this study. For the parametric studies, the material properties (modulus of elasticity, Poisson's ratio, and mass density) for the concrete deck, steel boxes, diaphragms, and bracing systems were taken to be the same for all the cases studied and are listed in Table 4.3. Complete listing of the geometries of the bridge prototypes used in the parametric studies is shown in Appendix A.1.

The key parameters investigated in this study are: span length, number of traffic lanes, number of cross-bracings and top-chord systems, number of boxes, and degree of curvature. Solid end-diaphragms considered in this study were provided at both ends of the bridge in the radial direction. The end-diaphragms material and thickness were taken to be the same as those of the webs. Changing the flexural stiffness of a bridge was performed by: changing the plate thickness or the span-to-depth ratio of the steel section. The sensitivity study proved that the latter option has a more significant effect on the structural response than the former option. When investigating the effect of the number of cross-bracing systems, X-type bracings as well as top chords were first provided inside the boxes only, in the radial direction, at different locations along the span. Later, additional X-type bracings were added between the boxes at the same location and orientation as the bracings inside the boxes. In practice, these bracings are made from single or back-to-back angles. Sensitivity study proved that replacing the area of angle cross-section by rectangular cross-section has no effect on the structural response. However, changing the stiffness of these rectangular bracing systems was found to have an effect on the shear only. Thus the cross-sectional area of the X-type bracings was varied from 144 mm^2 to 22500 mm^2 when

studying the shear response of the bridges, and in all other cases it was decided to conduct the parametric studies with X-type bracings and top chords of 100×100 mm rectangular cross section. The effects of the bridge span length and width were studied, maintaining the same flexural rigidity per unit width of the bridge.

4.3 Loading Conditions of Composite Multiple-Spine Bridges at Service

Considerations were given to the effects of highway truck loading and bridge dead loads on the load distribution characteristics of straight and curved composite cellular bridges. The North American Codes of Practice (2, 4, 11, 59) provide load distribution factors for truck loading on straight bridges only and not for dead load since the dead load is considered distributed equally between girders. However, in curved bridges, the curvature affects the uniform distribution of the dead load. Highway truck loading considered in this study is AASHTO truck loading (4). The highway truck loading includes a highway truck and lane loading. The lane loading, which governs the design live load longitudinal moments for spans greater than about 45 m, is provided merely as a convenience to avoid the placing of more than one truck in one lane in bridges with large spans.

4.3.1 Dead Load

To simulate the dead load due to self-weight, the GRAV option in ABAQUS was used to account the dead load of the structure through the gravity action. A concrete density of 24 kN/m³ and steel density of 78 kN/m³ were assumed.

4.3.2 Live Load

Highway live loads included AASHTO truck load HS20-44 and equivalent lane

load (4), consisting of superimposed load of 9.34 kN/m uniformly and centrally distributed within a strip of 3 m width plus a single concentrated load (80 kN for bending stresses and 116 kN for shear) distributed over 3 m width on a line normal to the centre line of the lane. Modification factors of 1, 0.9, and 0.75 for two-, three- and four-lane loadings, respectively, were applied. Figure 4.3 summarizes the configurations of the AASHTO truck loading.

The two types of live load (the truck loading and the equivalent lane loading) was first applied on a straight girder to determine which case produces the maximum effect in bridges of 20, 40, 60, 80, and 100 m span. When studying stress distribution, deflection distribution, and the distribution of axial forces in bracings, the loadings on the bridge prototypes were applied at mid-span in such a way to produce maximum mid-span longitudinal stresses. In case of studying shear distribution at the supports, the live loads were located very close to the support lines in the longitudinal direction in such a way to produce maximum support reactions and in such a way that no wheel load was applied directly over the support since the load would be transmitted directly to the support producing little effect on the value of web shear. The last wheel load in the truck was placed 1 m from the support line to allow transverse distribution of shear forces between webs. Subsequently, four loading cases were considered for each bridge prototype: three different truck loading (or equivalent lane-loadings) are shown in Fig. 4.4. The fourth case of loading was the bridge dead load. In the two partial loading cases, Fig. 4.4.b and 4.4.c, the wheel loads close to the curbs were applied at a distance of 0.6 m from the inside edge of the curbs.

4.4 Parametric Studies

4.4.1 Stress Distribution in Simply-Supported Straight and Curved Composite Multiple-Spine Bridges

A parametric study was conducted on simply-supported curved composite concrete deck-steel multiple-spine bridge prototypes to (i) investigate the influence of all major parameters affecting the stress distribution throughout the bridge cross-section; (ii) generate a database for stress distribution factors; (iii) develop empirical expressions for stress distribution factors for truck loading as well as for dead load. The parameters chosen for this study were: span length, number of traffic lanes, number of boxes, number and stiffness of bracing systems, span-to-depth ratio, span-to-radius of curvature ratio and loading conditions. The parametric study was based on the following assumptions: (i) the reinforced concrete slab deck had complete composite action with the top steel flange of the boxes; (ii) the bridges were simply-supported; (iii) all materials were elastic and homogenous; (iv) the effect of road superelevation, outer web slope, and curbs were insignificant and therefore, ignored; (v) solid end-diaphragms were used in the radial direction and their material and thickness were taken to be the same as those of the webs; and, (vi) bridges had constant radii of curvature between support lines. Regarding superelevation in curved bridges, it was observed (6) that live load applied to composite I-girder bridges produced essentially the same moments, twisting moments, and deflections for any angle of bridge superelevation between 0 and 10 percent. The details of the parametric study are described in the following sections.

The multiple-spine cross-section was divided into girders as shown in Fig. 4.5. Each idealized girder consisted of the web, steel top flange, concrete deck slab, and bottom

flange. For each girder, the width of the concrete deck equaled the web spacing whereas the bottom flange width was taken as half the web spacing. In order to determine the stress distribution factor, D_σ , carried by each curved girder, the maximum stress, σ , was calculated for a simply-supported straight girder subjected to: a line of wheel loads of an AASHTO truck, or a line of half the lane loading with a single concentrated load and then to dead load, as a line load per meter long of the bridge. Based on the finite-element modelling, the average maximum normal flexural stress of each girder, σ_{\max} , was obtained at mid-span for the two types of loading, namely AASHTO truck loading and dead load. The multi-lane loading modification factor was taken into account. The design stress distribution factors, D_σ for the two types of loading was then calculated from the following relationship:

$$D_\sigma = \frac{\sigma_{\max}}{\sigma} \quad (4.1)$$

A sensitivity study was first undertaken to determine the different factors that may influence the lateral load distribution. The sensitivity study revealed that the extreme bottom fiber stresses are always greater than the extreme top fiber stresses in the bridge cross-section at mid-span. For design purpose, the bottom fiber stresses in the steel bottom flange were found to be of more importance to design engineers, and hence, were used in the calculations of σ , and σ_{\max} . The sensitivity study also revealed that the span-to-depth ratio has an insignificant effect on the stress distribution. In practice, X-type bracings as well as top-chords (lateral ties to the steel top flanges) are made from single or back-to-back angles. The sensitivity study showed that replacing the angle cross-section by a rectangular one, or changing the bracing cross-section from 12×12 mm to 150×150 mm, has no effect on the stress distribution. Moreover, the sensitivity study showed that using additional X-type

bracings between boxes has no effect on the stress distribution in the bottom flange. Therefore, it was decided to conduct the parametric study with span-to-depth ratio of 25 and with X-bracings and top-chords having a 100×100 mm rectangular cross-section inside the box along the span.

4.4.2 Deflection in Simply-Supported Straight and Curved Composite Multiple-Spine Bridges

The North American codes of Practice (4, 59) limit deflection of a straight bridge in the form of a limiting ratio of the span length or in the form of a limiting span-to-depth ratio. In curved bridges, the curvature increases the deflection when compared to that in straight bridges. The effects of several parameters, adopted for bending stress distribution, on the deflection at the mid-span of the simply-supported bridge prototypes were also studied. Based on those parameters, empirical design equations for the mid-span deflection of straight bridges, Δ_s and of curved bridges, Δ_c were developed.

4.4.3 Axial Forces in Bracing System in Simply-Supported Straight and Curved Composite Multiple-Spine Bridges

Bracing systems are used to provide torsional resistance against both the bridge curvature and eccentric loading on the bridge. The output from all the computer runs used to investigate the stress distribution on curved bridges provided also the axial force in the bracing and top-chord members. The key parameters adopted for stress distributions were also adopted herein to study their effect on the maximum tensile and compressive forces in the bracing system.

4.4.4 Shear Distribution in Simply-Supported Straight and Curved Composite Multiple-Spine Bridges

A parametric study was conducted on simply-supported curved composite concrete deck-steel multiple-spine bridge prototypes to (i) investigate the influence of all major parameters affecting the shear distribution between the webs; (ii) generate a database for shear distribution factors; (iii) develop empirical expressions for shear distribution factors for AASHTO truck loading as well as for dead load. The parameters chosen for this study were the same as those for the stress distribution. However, in this case, the sensitivity study showed that the stiffness of the X-type bracings has also an effect on the shear forces carried by the webs. However, additional bracings between the boxes had no effect on the shear. Hence, the cross-sectional area of the bracings, A_b , was taken into consideration. In order to determine the shear distribution factor, D_{sc} , the maximum reaction, V , was calculated in a simply-supported straight girder when subjected to: a line of wheel loads of an AASHTO truck, or a line of half the lane loading with a single concentrated load; then, dead load as a line load per meter long of the bridge. The spans of the simply-supported girders were the same as those for the prototype bridges considered. Based on the finite-element modelling, the maximum reaction under each web, V_{max} , was obtained for each bridge prototype taking into account the modification factor for multi-lane loading. The shear distribution factors, D_{ss} or D_{sc} , for straight bridges and curved bridges respectively and for the two types of loading were then calculated from the following relationship:

$$D_{ss \text{ or } sc} = \frac{V_{max}}{V} \quad (4.2)$$

RESULTS FROM THE PARAMETRIC STUDY

5.1 General

This chapter presents the results from an extensive parametric study, using the finite-element modelling, in which 50 simply-supported composite multi-spine bridge prototypes are analyzed, to evaluate their structural response when used in curved alignments. The parametric study conducted herein includes the following: (i) stress distribution in simply-supported straight and curved composite multi-spine bridges; (ii) deflection distribution in simply-supported curved composite multi-spine bridges; (iii) axial forces in the bracing members; (iv) shear distribution in simply-supported straight and curved composite multi-cell bridges. Based on the data generated from the parametric study, a simplified design method is proposed for straight and curved simply-supported composite multi-spine bridges.

5.2 Stress Distribution in Simply-Supported Straight and Curved Composite Multiple-Spine Bridges

Unlike the conventional method in the current codes and previous literature which propose moment distribution factors, it was found more practical in this study to propose stress distribution factors to estimate the flexural response of bridge girders. The bottom flexural stress distribution factor can be calculated using:

$$D_{\sigma} = \frac{(\sigma_h)_{\max}}{\sigma_h} \quad (5.1)$$

where $(\sigma_b)_{\max}$ is the maximum flexural stress in the outside fibers of the bottom flange obtained from the finite element analysis (FEA) program. And σ_b , is the bottom flexural stress of an equivalent straight and simply supported girder. It is obtained from the simple beam analysis (SBA) using:

$$\sigma_b = M \frac{y_b}{I} \quad (5.2a)$$

where M is the bending moment due to AASHTO truck loading or dead load on a simply supported straight idealized girder; y_b is the distance of the idealized girder's neutral axis from the bottom surface, and I is the moment of inertia of the idealized girder.

Similarly, top flexural stress distribution factors could be obtained by using the stresses in the top fibers of the concrete deck. Table 5.1 shows the results of a sensitivity study carried on a two-lane, two-box bridge of 60 meter span, with different degree of curvature, and subjected to full AASHTO truck loading. It can be observed, as expected, that the maximum tensile stresses in the bottom flange are always higher, in absolute value, than the maximum compressive stresses in the concrete deck. Therefore, only the tensile stresses in the bottom flange were considered in determining the stress distribution factors for multi-spine bridges. However, if needed, the compressive stresses can be obtained, conservatively, using:

$$(\sigma_t)_{\max} = D_\sigma \left(\frac{y_t}{ny_b} \right) \sigma_b \quad (5.2b)$$

where y_t is the distance of the neutral axis from the top surface, n is the modular ratio, D_σ is the factor obtained from Eq.(5.1), and σ_b is calculated from Eq.(5.2a).

Further sensitivity study was then undertaken to determine the different factors that may influence the lateral bending stress distribution. The sensitivity study revealed that changing either the concrete slab thickness or the bottom flange thickness has an

insignificant effect on the moment distribution. This was also confirmed by Nutt et al. (57) in the case of straight reinforced and prestressed concrete multi-cell bridges, and later, by Sennah (66) for composite steel multi-cell bridges. The sensitivity study also revealed that changing the span-to-depth ratio within the practical range of 20 to 30 found by Heins (35) has also an insignificant effect on the stress distribution. Therefore, it was decided to conduct the parametric study using a span-to-depth of 25. The sensitivity study showed that cross-bracings, degree of curvature, span length, number of boxes, and number of lanes are the key parameters affecting the structural response of composite multiple-spine bridges.

5.2.1 Effect of Cross-Bracing System

The effect of cross-bracing system on the longitudinal bending stresses encountered in the composite bridge cross-section under service loading was examined.

The torsional stiffness of a box girder results from three components: the St-Venant rigidity, the warping rigidity, and the distortional rigidity. Increasing the flexibility of any of these components reduces the rigidity of the box girder. Adding bracings between support lines is generally required for stability purposes at the construction phase. Table 5.2 shows the effect of bracings on the stress distribution factors for each of the idealized girders of two-lane, two-box, 60 meter bridge of different curvatures and different live load conditions. For straight bridges, it can be observed that in the case of fully loaded bridges adding one cross-bracing system at mid-span increases the bending stress by a maximum of 6% in the outer girder and decreases it by approximately the same amount in the central girder. While in the case of partially loaded bridges, the maximum bending stress carried by the loaded outer girder is considerably reduced by more than 40%. It can be also observed that adding more cross-bracings improves the ability of the cross-section to transfer loads from one girder to the adjacent ones. The same trends were observed for curved bridges also.

The critical loading case for the maximum design stress distribution factor is affected by the loading conditions. For two-, three-, and four-lane bridges, the fully loaded bridge is the governing case for design. This is clearly evident from the results in Table 5.2 for a two-lane bridge.

The warping stresses due to torsion and distortion effects are significantly reduced to the extent that adding at least three cross-bracings with a spacing less than the maximum spacing of 7.5 m specified by the AASHTO code (4) has an insignificant effect on the longitudinal stress distribution. For this reason, it was decided to conduct the parametric study with the number of bracing and top-chord systems of 3, 5, 7, 11, and 17 for bridge spans of 20, 40, 60, 80, and 100 m, respectively.

In practice, X-type bracings as well as top-chords are made of single back-to-back angles. The sensitivity study showed that replacing the angle cross-section by rectangular one has no effect on the response. Table 5.5 shows the effect of cross-sectional area of bracing members on the structural response of curved two-lane, two-box, bridges. It can be observed that an increase in the cross-sectional area of bracings has no effect on the stress distribution and deflection. However, the maximum force in bracing members increases with increase in the cross-sectional area of bracing members. Thus, it was decided to conduct the parametric study with cross-bracings and top-chords having an 100×100 mm rectangular cross-section.

The sensitivity study also showed that adding X-type bracing systems between boxes has no effect on the stress distribution. Figure 5.1 and 5.2 show the effect of number of internal and external cross-bracings on the stress distribution factor for the inner girder and outer girder, respectively, of a two-lane, two-box and 60 meter span bridge under dead load and different curvatures. It can be observed, from both figures, that adding external

bracings has no effect on the stress distribution factor. The same trend was noticed for other type of bridges and under different truck loading. Thus, it was decided to conduct the parametric study with only internal cross-bracings and top-chords.

5.2.2 Effect of Curvature

The effect of curvature on bending stresses carried by the outer, central, and inner girders was investigated. Figure 5.3 and 5.4 show the stress distribution factors for each girder of four-box, two-lane, bridge of 100 m span with different curvatures when subjected to dead load as well as AASHTO truck loading in all lanes. It can be observed that the inner girder, closest to the centre of curvature, carries the smallest moment. The farther the girder is from the center of curvature the higher is the stress carried by that girder. Moreover, these stresses appear to increase with increase in curvature. Similar behaviour was observed in case of three-, and four-lane bridges with different number of boxes. For simplicity, expressions for the moment distribution factors will be derived for the outer girder, inner girder, and the internal girder representing either the central girder or the intermediate girder, shown in Fig. 4.5.

Figure 5.5 and 5.6 present the effect of span-to-radius of curvature ratio, L/R , on the stress carried by the inner and outer girders, respectively, of 41-100 bridges due to dead load. While figure 5.7 shows the effect of span-to-radius of curvature ratio on the stress carried by the outer girders of 41-100 bridges due to full AASHTO truck loading. It is observed that the stress distribution factor increases with increase in the L/R ratio. However, for the case of dead loading and curved bridges, increasing the number of boxes decreases slightly the stress carried by the inner girders, and increases the stress distribution factor of

the central and outer girders for the same bridge width. This can be explained by the effect that, for curved bridges, there is more dead load for outer girders and less dead load for inner girders when compared to straight equivalent girder. For Fully loaded lanes, the stress distribution factors increases with an increase of curvature and decreases with an increase of the number of boxes. Similar behaviour was observed for the inner and central girders in the case of two-, and three-lane bridge of different span under full AASHTO loading.

5.2.3 Effect of Bridge Aspect Ratio

In examining this effect on the bridge response, the bridge width was kept constant while changing the span length. Figure 5.8 shows the effect of span length on the stress distribution factor of the central girder of four-lane, five-box bridges under full AASHTO truck loading. It can be observed that, for straight bridges, the increase in the span length has no effect on the stress distribution. That trend can be explained by the fact that, in the analysis of determining the stresses, the thicknesses of the steel box were changed with the increase in span length in order to maintain the overall flexural stiffness of the cross-section of a given width. However, the stress distribution factor increases with an increase in span length for curved bridges. This increase is more and more pronounced as the curvature increase, as expected.

The above observations were made for all idealized girders of different combinations of bridge widths and span lengths, for different curvatures, and for all different loading conditions.

5.2.4 Effect of Number of boxes and Number of Lanes

The variation in the number of steel boxes for the same bridge span length was studied for different number of lanes. Fig. 5.9 shows the effect of both the number of boxes

and the number of lanes on the bending stress carried by the outer girders of straight bridges of 60 m span due to full AASHTO loading. While Fig. 5.10 shows these effects on the bending stress carried by the central girders of bridges of 100 m span and span-to-radius of curvature ratio of 1, under the condition of fully loaded lanes. It is observed that the bending stresses carried by a girder decrease significantly with increase in the number of boxes. It is also revealed that for the same number of steel boxes, the stress distribution factors increase with an increase in the number of traffic lanes.

5.2.5 Empirical Formulas for the bending stress Distribution Factor, D_σ

From the results of the parametric study, it became evident that the bending stress distribution factor, D_σ , for simply-supported curved composite multi-spine bridges is governed by the following parameters: (i) bridge span length, L ; (ii) span-to-radius of curvature ratio, L/R ; (iii) number of steel boxes, N_B ; and (iv) number of traffic lanes, N_L . Using the least square method available in the solver of the 2000 Microsoft Excel software, empirical expressions were generated for the bending stress distribution factors at the extreme fibers of the bottom flange. All dimensions used in these expressions are in meters and the expressions are calibrated to obtain a dimensionless distribution factor. For proper use of these expressions in design, at least three cross-bracing systems, with spacing not exceeding 7.5 m as specified by the AASHTO code, are required. Good comparison is shown in Figs. 5.11 and 5.12 between the results from the finite-element analysis and the proposed empirical expressions listed below. It should be mentioned that these proposed expressions follow a similar trend to that introduced by the AASHTO code (4) in presenting load distribution factors. The modification factor for multi-presence of vehicles in multi-lane bridges has been included.

a) For Two-lane bridges due to dead load:

$$D_{\sigma} \text{ (inner)} = 1 + 0.09 \frac{L^{0.14}}{N_B^{0.02}} \left(\frac{L}{R} \right)^{2.92} \quad (5.3a)$$

$$D_{\sigma} \text{ (internal)} = 1 + 0.09 L^{0.19} N_B^{0.26} \left(\frac{L}{R} \right)^{2.14} \quad (5.3b)$$

$$D_{\sigma} \text{ (outer)} = 1 + 0.15 L^{0.11} N_B^{0.61} \left(\frac{L}{R} \right)^{1.61} \quad (5.3c)$$

b) For Three-lane bridges due to dead load:

$$D_{\sigma} \text{ (inner)} = 1 + \frac{0.1}{L^{0.01} N_B^{0.03}} \left(\frac{L}{R} \right)^{3.67} \quad (5.4a)$$

$$D_{\sigma} \text{ (internal)} = 1 + 0.11 L^{0.15} N_B^{0.22} \left(\frac{L}{R} \right)^{2.05} \quad (5.4b)$$

$$D_{\sigma} \text{ (outer)} = 1 + 0.2 \frac{N_B^{0.69}}{L^{0.03}} \left(\frac{L}{R} \right)^{1.44} \quad (5.4c)$$

c) For four-lane bridges due to dead load:

$$D_{\sigma} \text{ (inner)} = 1 + 0.09 \left(\frac{N_B}{L} \right)^{0.06} \left(\frac{L}{R} \right)^{4.28} \quad (5.5a)$$

$$D_{\sigma} \text{ (internal)} = 1 + 0.27 \frac{N_B^{0.13}}{L^{0.02}} \left(\frac{L}{R} \right)^{2.1} \quad (5.5b)$$

$$D_{\sigma} \text{ (outer)} = 1 + 0.4 \frac{N_B^{0.64}}{L^{0.17}} \left(\frac{L}{R} \right)^{1.35} \quad (5.5c)$$

d) For two-lane bridges due to full AASHTO truck loading:

$$D_{\sigma} \text{ (inner)} = \frac{2.09}{N_B^{1.01}} \left[1 + 0.03 \frac{L^{0.34}}{N_B^{0.08}} \left(\frac{L}{R} \right)^{3.33} \right] \quad (5.6a)$$

$$D_{\sigma} \text{ (internal)} = 1.59 \frac{L^{0.04}}{N_B^{0.88}} + 0.11 \frac{L^{0.29}}{N_B^{0.76}} \left(\frac{L}{R} \right)^{2.2} \quad (5.6b)$$

$$D_{\sigma} \text{ (outer)} = \frac{2.09}{N_B^{1.01}} \left[1 + 0.1 L^{0.22} N_B^{0.65} \left(\frac{L}{R} \right)^{1.7} \right] \quad (5.6c)$$

e) For three-lane bridges due to full AASHTO truck loading:

$$D_{\sigma} \text{ (inner)} = \frac{2.64}{N_B^{1.01}} \left[1 + 0.05 \frac{L^{0.2}}{N_B^{0.11}} \left(\frac{L}{R} \right)^{3.55} \right] \quad (5.7a)$$

$$D_{\sigma} \text{ (internal)} = 2.51 \frac{L^{0.01}}{N_B^{0.93}} + 0.13 \frac{L^{0.32}}{N_B^{0.82}} \left(\frac{L}{R} \right)^{2.12} \quad (5.7b)$$

$$D_{\sigma} \text{ (outer)} = \frac{2.64}{N_B^{1.01}} \left[1 + 0.12 L^{0.15} N_B^{0.63} \left(\frac{L}{R} \right)^{1.33} \right] \quad (5.7c)$$

f) For four-lane bridges due to full AASHTO truck loading:

$$D_{\sigma} \text{ (inner)} = \frac{3.11}{N_B^{1.01}} \left[1 + \frac{2.5}{100} \frac{L^{0.2}}{N_B^{0.12}} \left(\frac{L}{R} \right)^{4.56} \right] \quad (5.8a)$$

$$D_{\sigma} \text{ (internal)} = 2.25 \frac{L^{0.03}}{N_B^{0.35}} + 0.17 \frac{L^{0.3}}{N_B^{0.93}} \left(\frac{L}{R} \right)^{2.14} \quad (5.8b)$$

$$D_{\sigma} \text{ (outer)} = \frac{3.11}{N_B^{1.01}} \left[1 + 0.08 L^{0.17} N_B^{0.64} \left(\frac{L}{R} \right)^{1.48} \right] \quad (5.8c)$$

It should be noted that by putting $L/R = 0$ in the above mentioned expressions, bending stress distribution factors for straight composite multi-spine bridges can be obtained. Different methods found in the literature for load distribution of multi-spine bridges were limited to reinforced and prestressed concrete sections. Good comparison is shown between the results from the finite-element analysis and the proposed expressions.

5.3 Deflection in Simply-Supported Curved Composite Multiple-spine Bridges

5.3.1 Cross-Bracings Versus Degree of Curvature

The effect of the cross-bracing system on the deflection distribution at the mid-span section was studied under various truck loading conditions as well as dead load. Figure 5.13 shows the outer girder deflection distribution for 21-2b-60 bridges due to full AASHTO truck loading conditions. It can be observed that the presence of cross-bracings has no effect on straight bridges but reduces the deflection for increasing curvature. It was also found that the required minimum spacing, as specified by AASHTO, is enough to provide a better deflection distribution. Moreover, it can be observed that additional cross-bracing systems

between the steel boxes along the span has no effect on the deflection at mid-span. The same trends were noticed for the case of dead load. Table 5.3 shows the deflection distribution of 21-2b-60 bridge of different curvature due to different loading conditions. Results revealed that the case of fully-loaded lanes provided the maximum design deflection required for the serviceability limit state. Figure 5.14 presents the mid-span deflection of a straight 21-2b-60 bridge due to either fully loaded or partially loaded lanes. It can be confirmed that for straight multi-spine bridges, cross-bracings has an insignificant effect on the deflection distribution at the mid-span in case of fully loaded lanes. While it significantly enhances the deflection at the mid-span section in case of partially loaded lanes. Table 5.5 shows the deflection for a 21-2b-60 bridge with different cross-sectional area of bracing members. It can be observed that the change in the cross-sectional area of cross-bracings members has no effect on the deflection as long as the bracing system is provided between the supporting line with the maximum spacing recommended by the code (4) and that bracing system is provided at the supporting line between the boxes.

5.3.2 Number of Boxes and Number of Lanes Versus Curvature

The effect of number of boxes as well as bridge curvature on deflection was also examined. Figure 5.15 shows the effect of number of boxes and span-to-radius ratio on the average mid-span deflection of four-lane bridges of 100 m span under dead load. It can be observed that, for straight bridges, increasing the number of boxes has no effect on the deflection. However, for curved bridges, the increase in the number of boxes increases the deflection with increasing curvature. The same trend was observed for the case of dead load on the same bridge. Figure 5.16 shows the effects of the number of traffic lanes and curvatures on the deflection in case of four-box bridges of 40 m span under full AASHTO truck loading. It can be confirmed that for the same number of traffic lanes, the deflection

increases with an increase of curvature. It can be observed, also, that an increase in traffic lanes decreases the deflection for a given bridge. This can be explained by the fact that the multi-lane loading reduction factor is in effect.

5.3.3 Aspect Ratio Versus Curvature

In examining this effect on the mid-span average deflection, the bridge width was kept constant while changing the span length. Figure 5.17 shows the effect of span length on the deflection of 41-5b bridges under full AASHTO loading conditions. It can be observed that the mid-span average deflection increases with increase in the aspect ratio as well as curvature. Similar trend was observed for all other cases where all other parameters are fixed and the span length is varied, and for all type of loading conditions.

5.3.4 Empirical Expressions for Straight and Curved Bridge Deflection

Based on the data generated from the parametric study, the following empirical expressions for the mid-span average deflection, Δ_s , for straight bridges, and the mid-span average deflection, Δ_c , for the curved bridges were generated for dead load condition as well as for full AASHTO truck loading condition. The dimensions in the expressions listed below are in meters. Thus, using these expressions to calculate the dead load deflection, one can determine the camber at mid-span section required during the fabrication of the steel boxes. The live load deflection can be used to examine the serviceability conditions of this type of bridges.

(a) For straight bridges under dead load condition:

$$\Delta_s = \frac{4.5}{10^5} \frac{L^{1.90}}{N_L^{0.05}} \quad (5.9)$$

(b) For curved bridges under dead load condition:

(i) For $\frac{L^2}{R} \leq 40$

$$\Delta_c = \Delta_s \left[1 + 7.45 \times 10^{-4} \frac{L^{1.04} N_B^{1.1}}{N_L^{2.98}} \left(\frac{L}{R} \right) + 0.04 L^{0.01} N_B^{0.14} N_L^{0.22} \left(\frac{L}{R} \right)^2 \right]^{8.65} \quad (5.10a)$$

(ii) For $\frac{L^2}{R} > 40$

$$\Delta_c = \Delta_s \left[1 + 216 \frac{N_L^{1.61}}{L^{2.67} N_B^{0.76}} \left(\frac{L}{R} \right) + 2.28 \times 10^{-2} \frac{L^{0.4} N_B^{0.53}}{N_L^{0.46}} \left(\frac{L}{R} \right)^2 \right]^{4.88} \quad (5.10b)$$

(c) For straight bridges under full AASHTO truck loading condition:

$$\Delta_s = 4 \times 10^{-4} \frac{L^{1.16}}{N_L^{0.38}} \quad (5.11)$$

(d) For curved bridges under full AASHTO truck loading condition:

(i) For $\frac{L^2}{R} \leq 40$

$$\Delta_c = \Delta_s \left[1 - 3.13 \times 10^{-6} L^{0.58} N_L^{5.69} \left(\frac{L}{R} \right) + 0.11 \frac{N_B^{0.14} N_L^{0.17}}{L^{0.23}} \left(\frac{L}{R} \right)^2 \right]^{6.8} \quad (5.12a)$$

(ii) For $\frac{L^2}{R} > 40$

$$\Delta_c = \Delta_s \left[1 - 2 \times 10^{-5} L^{0.88} N_B^{0.48} N_L^{2.23} \left(\frac{L}{R} \right) + 1.5 \times 10^{-2} \frac{L^{0.45} N_B^{0.51}}{N_L^{0.26}} \left(\frac{L}{R} \right)^2 \right]^{5.11} \quad (5.12b)$$

5.4 Axial Forces in Bracing Members

A sensitivity study revealed that the critical loading cases for moment at mid-span also produced maximum axial forces in the bracing members. Figure 5.18 shows the effect of the number of cross-bracings on the maximum axial force in bracings on 21-2b-60

bridges of different curvatures under full AASHTO truck loading. It is observed that the maximum compressive force is higher than the maximum tensile force, the maximum force increasing with increase in curvature and decreasing with increase in the number of cross-bracings. Similar trends were observed for other bridges considered in the study. Table 5.4 shows again the effect of the number of cross-bracings on the maximum axial force in the bracings of 21-2b-60 bridges of various curvatures under different AASHTO loading conditions. It can be observed that the case of fully loaded lanes provides the maximum design axial force in bracing members. The sensitivity study also revealed that the presence of additional bracing systems between the boxes decreases the maximum axial force in the bracings as expected.

Figure 5.19 shows the effect of the span length as well as the degree of curvature on the maximum compressive force in bracing members of 21-2b under full AASHTO truck loading. The results indicate that the compressive force increases with increase in the bridge span length as well as with the bridge curvature, as expected. The same trend was observed for the case of bridges under dead load. Figure 5.20 shows the effect of the number of boxes on the maximum compressive force in 41-100 bridges under dead. It can be observed that the increase in the number of boxes has an increasing effect on the maximum compressive force in bracings with increasing curvature of the bridge. Figure 5.21 presents the effect of the number of traffic lanes on the compressive force in bracings of four-box bridges of 40 m span under dead load. The increase in the number of traffic lanes increases the maximum compressive force in bracings. Such increase increases with increasing curvature.

Based on the data generated from the parametric study, the following expressions for the maximum axial force in a bracing member were deduced:

(a) Maximum compressive force, in kN, in the bracing system members due to dead load:

(i) For straight bridges

$$(F_C)_s = \frac{8.43}{N_L^{0.01} N_B^{0.08}} (3L^{0.58} - 9) \quad (5.13a)$$

(ii) For curved bridges

$$\frac{(F_C)_c}{(F_C)_s} = 1 + \frac{0.18}{N_L^{0.01} N_B^{0.09}} (0.03L^{1.83} + 43) \left[0.15 \left(\frac{L}{R} \right)^3 - 0.12 \left(\frac{L}{R} \right)^2 + 0.39 \left(\frac{L}{R} \right) \right] \quad (5.13b)$$

(b) Maximum compressive force, in kN, in a diagonal bracing member due to live load:

(i) For straight bridges

$$(F_C)_s = \frac{11.5}{N_L^{0.08} N_B^{0.28}} (0.25L^{0.6} + 4.4) \quad (5.14a)$$

(ii) For curved bridges

$$\frac{(F_C)_c}{(F_C)_s} = 1 + \frac{0.05}{N_L^{0.01} N_B^{0.09}} (0.1L^{1.80} + 96) \left[0.16 \left(\frac{L}{R} \right)^3 - 0.17 \left(\frac{L}{R} \right)^2 + 0.42 \left(\frac{L}{R} \right) \right] \quad (5.14b)$$

It should be noted that the above mentioned expressions for the design forces in bracing members represent the upper-bound of maximum forces in bracing members in all the bridge geometries considered in the parametric study since the weight of bracing members compared to the weight of the bridge is negligible.

5.5 Shear Distribution in Simply-Supported Straight and Curved Composite Multiple-Spine Bridges

A sensitivity study was first undertaken to determine the different factors that may

influence the shear distribution at the supports. Table 5.6 shows a sensitivity study on the effect of the span-to-depth ratio on the shear distribution of three-lane, three-box bridges of 60 m span. This sensitivity study revealed that the increase of the span-to-depth ratio redistributes slightly the shear forces within webs of the intermediate boxes for partially loaded bridges. It has no significant effect on the shear forces carried by the inner and outer webs that carry higher shear forces. For fully loaded bridges, it has no significant effect either. Hence, the span-to-depth ratios within the practical range of 20 to 30, found by Heins (36), has an insignificant effect on the shear distribution. Therefore, it was decided to conduct the parametric study using a span-to-depth ratio of 25. The sensitivity study also showed that number and stiffness of cross-bracings, degree of curvature, aspect ratio, number of boxes, and number of lanes are the key parameters affecting the shear distribution of composite multi-spine bridges.

5.5.1 Effect of Cross-Bracing

X-type bracings as well as top-chords (lateral ties for the top steel flanges) are usually used in the radial direction between boxes at the support lines, and inside boxes, at equal intervals from the support lines, to minimize distortional, longitudinal warping, and transverse bending stresses encountered in an open-cell cross-section during the construction phase. Table 5.7 shows the effect of cross-bracings on the distribution of shear forces between webs at the support line of straight composite 21-2b-60 bridges under an AASHTO truck loading. It is observed that adding cross-bracings enhances slightly the shear distribution between webs for the fully loaded bridges. However, internal cross-bracing systems enhance considerably the shear distribution between webs for partially loaded bridges. As an example, for the partially loaded case shown Table 5.7, when using eight cross-bracing systems, the maximum shear force in the loaded outer web is reduced by

5%, and is increased by 13% in the central web. The up-lift force in the outer web away from load is reduced by 19%. Moreover, additional bracing systems between boxes, at the same location as the internal bracings systems, enhances further the shear distribution between webs for fully loaded bridges, but has no significant effects for partially loaded bridges. Thus the presence of cross-bracings enhances the torsional characteristics and the load transfer of straight multi-spine bridges subjected to AASHTO truck loadings.

Figure 5.22 shows the effect of the number of bracings on the shear force carried by the outer web due to dead load in 21-2b-60 bridges. It can be observed that, for straight bridges, the cross-bracings have no effects on the shear distribution factor. But, It is observed that, for curved bridges, the shear distribution factor decreases with the presence of at least one cross-bracing system. This decrease increases with increase in the degree of curvature. It can be also observed that additional bracings between boxes have no effect on the shear distribution. It can be concluded that three cross-bracings as well as top-chords, spaced at equal intervals between radial support lines, and having a maximum spacing of 7.5 m specified by the AASHTO code (4), are enough to produce fairly uniform shear distribution factors and hence uniform reactions on the substructure. Table 5.8 shows the effect of the cross-sectional area of cross-bracings on the shear distribution factor of 21-2b-60 straight bridges under AASHTO truck loading. It can be observed that the increase in the bracing stiffness decreases the shear force carried by the exterior webs and increases the shear force carried by the central webs for the fully loaded case. This effect is due to the presence of cross-bracings between the boxes at the support lines. For partially loaded bridges, the use of stiffer cross-bracings reduces the uplift force in the girder away from the loaded area and decreases the shear forces carried by the loaded webs, while it increases the shear force in the central webs. Figure 5.23 shows the effect of cross-sectional area of the

bracing system on the shear carried by the webs of two-lane, two-box curved bridge of 60 m, with $L/R=2$, under full AASHTO truck loading. It is interesting to note that, for such a curved bridge, the increase of the bracing stiffness reduces the uplift forces, decreases the shear force in the outer webs, and transfer the forces from one box to the adjacent through the stiffer cross-bracing members at the support line. Similar characteristics were observed in the case of dead load. Therefore, it was decided to conduct the parametric study taking into account the effect of cross-sectional area of the bracing systems. Moreover, 3, 5, 8, 11, and 17 top-chords and X-type bracing systems for bridge spans of 20, 40, 60, 80, and 100 m, respectively were used only inside the boxes between support lines. Top-chord and X-type cross-bracing systems were used between the boxes at the support lines for all cases.

5.5.2 Effect of Curvature

In case of straight bridges, shear forces in the webs at support lines are distributed in a manner quite different from that for bending moment, since the governing loading case occurs when the truck loading is located close to the web and to the support line. Results shown in Table 5.7 revealed that, for the partial loading case, the reaction at some outer bearings may be downward as a result of twisting. However, this effect is more than neutralized by the dead load effect in the case of straight bridges.

The effect of curvature on the reaction forces carried by the outer, central, and inner webs was investigated. Figures 5.24 and 5.25 present the effect of span-to-radius of curvature ratio, L/R , on the shear force carried by the outer web and the inner web of 21-2b bridges due to dead load, respectively. It is observed that the shear distribution factor for the outer web increases with increase in the span-to-radius ratio due to the presence of increasing torsional effects as a result of increase in the degree of curvature. It is also

observed that the shear distribution factors for the inner webs under dead load decrease with increase in curvature, changing from upward forces to downward forces causing support uplift. Similar behaviour was observed in the case of three-, and four-lane bridges with different number of boxes.

5.5.3 Effect of Aspect Ratio

The aspect ratio is presented herein as the ratio of the span length to the bridge width. Figure 5.27 shows that for $L/R = 1$, the shear distribution factor carried by the outer web due to dead load in 2I-2b bridges is 0.69, 0.90, 1.14, 1.40, and 1.69 for span lengths of 20, 40, 60, 80, and 100 m, respectively. These span lengths correspond to aspect ratios of 2.15, 4.30, 6.45, 8.60, and 10.75 respectively. Therefore, an increase in the shear force carried by the outer web can be expected with increase in the aspect ratio. It was also observed that uplift reaction forces carried by the inner web due to dead load increase with increase in the aspect ratio as shown in Fig. 5.25. Similar behaviour was observed in the case of three-, and four-lane bridges.

Figure 5.26 shows that the loading case of partially loaded lane(s) close to the outer side of curvature always produces higher shear distribution factors in the outer and inner webs than those in the case of partially loaded lane(s) close to the inner side of curvature. Therefore, only the case of partially loaded lane(s) close to the outer side of curvature has been considered in the parametric study. Moreover, Figure 5.27 shows that, for straight bridges, the partially loaded lane(s) produces higher shear distribution factors in the exterior webs than the fully loaded lanes. However, for curved bridges, it can be observed that the fully loaded lane(s) produces higher shear forces in the outer webs than the case of partially loaded lane(s) close to the outer side of curvature.

5.5.4 Effect of Number of Boxes and Number of Traffic Lanes

The variation in the number of boxes for the same bridge span length was studied for different number of lanes. Figures 5.28 shows the effect of number of boxes on the shear force carried by the outer webs of curved bridges, with $L/R = 2$, under dead load. It can be observed that an increase in number of boxes decreases the shear distribution factor as expected. It can be noted that the increase in traffic lanes decreases the shear distribution factor as well. Similar behavior was observed for straight bridges as well as bridges of different span lengths and different curvatures.

Figures 5.29 shows the effect of number of boxes on the shear force carried by the inner webs of curved bridges, with $L/R = 1$, under full AASHTO truck loading. It can be observed that the inner webs for curved bridges experience uplift forces as noted earlier. Such uplift forces decrease with increase in the number of boxes for a fixed number of traffic lanes. They increase with increase in the number of traffic lanes for a fixed number of boxes. This trend was observed for other bridges of different span length and different curvatures. Similar observations were made for the case of partially loaded lanes with truck(s) in the outer lanes.

5.5.5 Empirical formulas for the shear distribution factor, D_s

From the results of the parametric study, it became evident that the shear distribution factor, D_s , is governed by the following parameters: (i) bridge span length, L ; (ii) span-to-radius of curvature ratio, L/R ; (iii) number of boxes, N_B ; (iv) number of lanes, N_L . Using a statistical package for best fit, empirical expressions were generated for the shear distribution factors for straight multiple-spine bridges, D_{SS} , as well as for curved multiple-spine bridges, D_{SC} , due to dead load as well as AASHTO truck loading. The dimensions used in these expressions are in meters. For proper use of these expressions in

design, at least three cross-bracing systems with spacing not exceeding 7.5 m as specified by the AASHTO code (4) are required. It should be noted that the modification factor for multi-presence of vehicles in multi-lane bridges has been included:

(1) Dead Load Case:-

(i) For straight bridges

(a) For exterior webs

$$D_{ss} = 0.57 \frac{L^{0.01} A_h^{0.02}}{N_B^{0.91} N_L^{0.05}} \quad (5.15)$$

(b) For central webs

$$D_{ss} = 0.54 \frac{L^{0.02} A_h^{0.03}}{N_B^{0.93} N_L^{0.07}} \quad (5.16)$$

(ii) For curved bridges

(a) For the inner webs

$$D_{sc} = -0.03 \frac{L^{0.68} N_L^{0.14}}{N_B^{0.34} A_h^{0.06}} \left(\frac{L}{R} \right)^{2.41} \quad \text{for } L < 60 \text{ meters} \quad (5.17a)$$

$$D_{sc} = -2.65 \frac{L^{0.89}}{100 N_B^{0.76} N_L^{0.30} A_h^{0.12}} \left(\frac{L}{R} \right)^{1.78} \quad \text{for } L \geq 60 \text{ meters} \quad (5.17b)$$

(b) For the outer webs

$$D_{sc} = 0.14 \frac{L^{0.62} N_L^{0.07}}{N_B^{0.91} A_h^{0.07}} \left(\frac{L}{R} \right)^{0.91} \quad \text{for } L < 60 \text{ meters} \quad (5.18a)$$

$$D_{sc} = 4.55 \frac{L^{0.88}}{100 N_B^{0.92} N_L^{0.36} A_h^{0.14}} \left(\frac{L}{R} \right)^{1.36} \quad \text{for } L \geq 60 \text{ meters} \quad (5.18b)$$

(c) For the central webs

$$D_{sc} = 0.53 \frac{L^{0.08} A_h^{0.02}}{N_B^{0.96} N_L^{0.19}} \left(\frac{L}{R} \right)^{0.55} \quad \text{for } L < 60 \text{ meters} \quad (5.19a)$$

$$D_{sc} = 0.55 \frac{L^{0.10} A_h^{0.09}}{N_B^{0.61} N_L^{0.23}} \left(\frac{L}{R} \right)^{0.55} \quad \text{for } L \geq 60 \text{ meters} \quad (5.19b)$$

(2) Full AASHTO truck loading:-

(i) For straight bridges

(a) For exterior webs

$$D_{sx} = 0.29 \frac{L^{0.2} N_L^{2.19}}{N_B^{2.21} A_h^{0.01}} \quad \text{for } L < 60 \text{ meters} \quad (5.20a)$$

$$D_{sx} = 0.06 \frac{L^{0.6} N_L^{0.94}}{N_B^{1.68} A_h^{0.07}} \quad \text{for } L \geq 60 \text{ meters} \quad (5.20b)$$

(b) For central webs

$$D_{sx} = 2.2 \frac{N_L^{0.87} A_h^{0.01}}{L^{0.12} N_B^{0.97}} \quad (5.21)$$

(ii) For curved bridges

(a) For the inner webs

$$D_{sc} = -0.57 \frac{N_L^{0.65}}{L^{0.29} N_B^{0.11} A_h^{0.07}} \left(\frac{L}{R} \right)^{2.31} \quad \text{for } L < 60 \text{ meters} \quad (5.22a)$$

$$D_{sc} = -1.68 \frac{L^{1.07} N_L^{0.71}}{100 N_B^{0.74} A_h^{0.13}} \left(\frac{L}{R} \right)^{1.72} \quad \text{for } L \geq 60 \text{ meters} \quad (5.22b)$$

(b) For the outer webs

$$D_{sc} = 0.74 \frac{L^{0.10} N_L^{1.02}}{N_B^{1.13} A_h^{0.10}} \left(\frac{L}{R} \right)^{0.78} \quad \text{for } L < 60 \text{ meters} \quad (5.23a)$$

$$D_{sc} = 1.65 \frac{L^{1.17} N_L^{0.65}}{100 N_B A_h^{0.16}} \left(\frac{L}{R} \right)^{1.36} \quad \text{for } L \geq 60 \text{ meters} \quad (5.23b)$$

(c) For the central webs

$$D_{vc} = 2.55 \frac{N_L^{0.22} A_h^{0.02}}{L^{0.01} N_B^{0.79}} \left(\frac{L}{R} \right)^{0.1} \quad \text{for } L < 60 \text{ meters} \quad (5.24a)$$

$$D_{vc} = 1.65 \frac{N_L^{0.70} A_h^{0.08}}{L^{0.01} N_B^{0.59}} \left(\frac{L}{R} \right)^{0.42} \quad \text{for } L \geq 60 \text{ meters} \quad (5.24b)$$

(3) Partially Loaded Lanes with AASHTO truck(s) in the outer lane(s):-

(i) For straight bridges

(a) For exterior webs under the loaded side

$$D_{sx} = 0.85 \frac{L^{0.05} N_L^{0.64}}{N_B^{0.58} A_h^{0.03}} \quad \text{for } L < 60 \text{ meters} \quad (5.25a)$$

$$D_{sx} = 0.28 \frac{L^{0.22} N_L^{0.73}}{N_B^{0.81} A_h^{0.12}} \quad \text{for } L \geq 60 \text{ meters} \quad (5.25b)$$

(b) For exterior webs away from the loaded side

$$D_{ss} = -0.17 \frac{N_L^{0.19}}{L^{0.09} N_B^{0.64} A_h^{0.12}} \quad \text{for } L < 60 \text{ meters} \quad (5.26a)$$

$$D_{sv} = -0.01 \frac{L^{0.39} N_L^{0.79}}{N_B^{0.35} A_h^{0.25}} \quad \text{for } L \geq 60 \text{ meters} \quad (5.26b)$$

(c) For central webs

$$D_{sv} = 0.8 \frac{N_L^{0.67} A_h^{0.08}}{L^{0.01} N_B^{0.13}} \quad (5.27)$$

(ii) For curved bridges

(a) For the inner webs

$$D_{sc} = -0.8 \frac{N_L^{0.75}}{L^{0.28} N_B^{0.28} A_h^{0.06}} \left(\frac{L}{R} \right)^{1.97} \quad \text{for } L < 60 \text{ meters} \quad (5.28a)$$

$$D_{sc} = -3.64 \frac{L^{0.85} N_L^{0.70}}{100 N_B^{0.62} A_h^{0.12}} \left(\frac{L}{R} \right)^{1.59} \quad \text{for } L \geq 60 \text{ meters} \quad (5.28b)$$

(b) For the outer webs

$$D_{sc} = 1.38 \frac{N_L^{0.67}}{L^{0.01} N_B^{0.61} A_h^{0.07}} \left(\frac{L}{R} \right)^{0.45} \quad \text{for } L < 60 \text{ meters} \quad (5.29a)$$

$$D_{sc} = 4.58 \frac{L^{0.88} N_L^{0.66}}{100 N_B^{0.83} A_h^{0.16}} \left(\frac{L}{R} \right)^{1.18} \quad \text{for } L \geq 60 \text{ meters} \quad (5.29b)$$

(c) For the central webs

$$D_{sc} = 1.35 \frac{N_L^{0.96} A_h^{0.01}}{L^{0.21} N_B^{1.4}} \left(\frac{L}{R} \right)^{0.32} \quad \text{for } L < 60 \text{ meters} \quad (5.30a)$$

$$D_{vc} = 0.45 \frac{L^{0.22} N_L^{0.57} A_b^{0.11}}{N_B^{0.59}} \left(\frac{L}{R} \right)^{0.63} \quad \text{for } L \geq 60 \text{ meters} \quad (5.30b)$$

5.5.6 AASHTO and Proposed Equations: Brief Comparison for Shear

Figure 5.30 shows the effect of the number of steel boxes on the shear force carried by the central webs of straight 60 meter bridges having 100 mm X 100 mm cross-bracing and top-chord systems and subjected to full AASHTO truck loading. It can be observed that for two-lane bridges, the AASHTO design formula for shear distribution and the proposed equation herein are in good agreements. For four-lane bridges, the proposed equation is slightly more conservative. Figure 5.31 shows the same as in Figure 5.30 but for a span of 20 meters. It can be observed that for shorter spans, the AASHTO design formula underestimates in general the transverse shear distribution of the bridge. Such underestimation can go up to 25% in the case of four-lane bridges having three-box cross-section. It is important to note that half of the value given by the AASHTO formula is used in the comparison since it provides the fraction of wheel loads taken by the entire steel box and not the individual webs. It implies also that the response of the bridge depends on the number of steel boxes and the number of traffic lanes only. Moreover, the AASHTO equation is used for both shear and moment distribution factors.

5.6 Illustrative Design Examples

5.6.1 Design Example No. 1

Consider a two-lane three-box simply-supported bridge with a concrete deck slab composite with a steel section to be designed according to AASHTO specifications for truck loadings (4) to accommodate a ramp of 50 m radius. The bridge details are as follows: span length = 54 m; deck width = 9.3 m; deck slab thickness = 225 mm; all steel plate

thicknesses = 11 mm; top steel flange width = 500 mm; steel section depth = 2.2 m; modulus of elasticity of steel = 200 GPa; and modular ratio = 7.41. The superimposed dead load due to asphaltite material = 10 N/m^2 . Calculate the design moments, averaged deflection, and maximum force in cross-bracing members, assuming a dynamic load allowance, DLA, of 25%, and seven cross-bracings between the radial support lines inside the boxes.

Taking the concrete and steel densities as 2400 and 7800 N/m^3 , respectively, the total dead load per meter length for the bridge is 66.80 kN/m . Hence, the total dead load per meter length for each of the six idealized girder is 11.13 kN/m . Based on this value, the maximum dead load moment at mid-span of an idealized straight girder, M_{DL} , is $11.13 \times (54)^2 / 8 = 4056.9 \text{ kN.m}$. The moment of inertia, I , of an idealized girder is $6.19 \times 10^{-2} \text{ m}^4$, and the distance of the neutral axis to the bottom extreme fiber is 1.73 m . Therefore, the maximum flexural stress due to dead load, σ_{DL} , in the straight idealized girder is 85.2 Mpa . Now, applying a line of AASHTO wheel loads and half the lane loadings on a simply-supported straight girder of span 54 m , the maximum moment at mid-span, M_{LL} , is 2270 kN.m . Similarly, the maximum flexural stress due to wheel loads, σ_{LL} , in the straight idealized girder is 63.44 Mpa . Using Eqs. (5.3c) and (5.6c), the bottom flexural stress distribution factors for the outer girder of the bridge can be calculated, respectively, as: 1.51 due to dead load, and 1.08 due to truck loading. Using Eqs. (5.3b) and (5.6b), the bottom flexural stress distribution factors for the internal girders can be calculated, respectively, as: 1.30 due to dead load, and 0.89 due to truck loading. Using Eqs. (5.3a) and (5.6a), the bottom flexural stress distribution factors for the inner girder of the bridge can be calculated, respectively, as: 1.19 due to dead load, and 0.79 due to truck loading. By multiplying each stress distribution factor by σ_{DL} for dead load and by $\sigma_{LL}(1+DLA)$ for live

load, the total maximum bending stresses carried by each girder due to dead load and AASHTO truck loading are found. Thus, these resulting design bending stresses are as follows: $[85.2 \times 1.51 + 63.44 \times 1.08 \times (1+0.25)] = 214.29$ Mpa, $[85.2 \times 1.30 + 63.44 \times 0.89 \times (1+0.25)] = 181.34$ Mpa, and $[85.2 \times 1.19 + 63.44 \times 0.79 \times (1+0.25)] = 164.04$ Mpa for the outer, internal, and inner girders, respectively. It is interesting to note that these final design bending stresses for the curved bridge are 23%, 9%, and 0% greater than those for the outer, internal, and inner girders of a straight bridge, $L/R = 0$, of similar characteristics, respectively. The deflection at mid-span of an equivalent straight bridge can be calculated from Eqs. (5.9) and (5.11) as: 85 mm and 31 mm for dead and live load respectively. Use Eqs. (5.10b) and (5.12b) to calculate the mid-span deflection for the curved bridges as: 189 mm and 63 mm for the dead and live load respectively. The maximum compressive force in the diagonal bracing members for an equivalent straight bridge can be obtained from Eqs. (5.13a) and (5.14a) as: 163.5 kN due to dead load, and 57 kN due to live load. Use Eqs. (5.13b) and (5.14b) to calculate the maximum compressive force in the diagonal bracing members for the curved bridge as: 1238 kN due to dead load, and 324 kN due to live load. Therefore, the design compressive force in the bracing members is $[1238 + 324(1+0.25)] = 1643$ kN.

5.6.2 Design Example No. 2

Consider a two-lane two-box simply-supported curved bridge with a concrete deck slab composite with a steel section to be designed according to the AASHTO code (4) to accommodate a ramp of 50 m radius. The bridge details are as follows: curved span = 50 m; deck width = 9.3 m; deck slab thickness = 225 mm; all plate thicknesses = 25 mm; top steel flanges width = 400 mm; steel section depth = 1.6 m; 7 cross-bracing systems of 0.01 m^2 cross-sectional area along the span and one cross-bracing of the same cross-sectional area

between the boxes at the supports; modulus of elasticity of steel = 200 GPa, and modular ratio = 7.41. The superimposed dead load due to pavement material = 15 N/m². The dynamic load allowance is 25 %. Calculate the design shear forces carried by the webs.

Considering the concrete and steel densities as 2400 and 7800 N/m³, respectively, the maximum reaction due to dead load, V_{DL} , carried by each support line is 1830.5 kN. Applying a line of wheel loads of an AASHTO truck on a simply-supported straight girder of span = 50 m, the maximum reaction is 151 kN. Applying half the lane loading with a single concentrated load on a simply-supported straight girder of span 50 m, the maximum reaction is 174.7 kN. Thus, the maximum reaction due to live load, V_{LL} , is 174.7 kN. Using Eqs. (5.18a), (5.23a) and (5.29a), the shear distribution factors for the outer web can be calculated as: 1.22 due to dead load, 1.61 due to fully loaded lanes, and 1.91 due to truck loading in the outer lane. Using Eqs. (5.19a), (5.24a) and (5.30a), the shear distribution factors for the central web are: 0.30 due to dead load, 1.51 due to fully loaded lanes, and 0.42 due to truck loading in the outer lane. Using Eqs. (5.17a), (5.22a), and (5.28a), the shear distribution factors for the inner web are calculated as: -0.49 due to dead load, -0.37 due to fully loaded lanes, and -0.49 due to truck loading on the outer lane. By multiplying each shear distribution factor by V_{DL} for dead load and $V_{LL}(1 + DLA)$ for live load, the shear forces due to the different loading cases are obtained. Thus, the resulting shear forces are as follows: 2233 kN, 549 kN, and -897 kN for the outer, central, and inner webs, respectively, due to dead load; 352 kN, 330 kN, and -81 kN for the outer, central, and inner web, respectively, due to fully loaded lanes; and 417 kN, 92 kN, and -107 kN for the outer, central, and inner webs, respectively, due to truck on the outer lane. These results are used to design the webs, the shear connectors, the bridge bearings, and the supporting frame of the abutment.

CHAPTER VI

SUMMARY AND CONCLUSIONS

6.1 Summary

Extensive theoretical studies were carried out to investigate the static responses of straight and curved composite concrete deck-steel multiple-spine bridges. A literature review was conducted in order to establish the foundation for this study. It was observed that there is lack of information regarding the load distribution characteristics of this type of bridges. While the current design practices in North America recommend few analytical methods for the design of straight composite multiple-spine box girder bridges, practical requirements in the design process call for a simplified design method in the form of expressions for bending stress and shear distribution factors for both straight and curved multiple-spine bridges. Therefore, the current research described in this thesis was carried out with the goal to fill most of the gaps found in previous studies as well as bridge codes.

Fifty simply-supported composite concrete deck-steel multiple-spine box prototype bridges were considered in this study. The finite-element method was used throughout this study to describe linear responses of such bridges. It should be noted that the effects of temperature, vehicle-bridge interaction, and deck surface roughness were not considered herein because they are outside the scope of this study. In the parametric study, the prototype bridges were subjected to dead load and AASHTO truck loadings. Based on the data generated from the parametric studies, a simplified design method was proposed for both straight and curved multiple-spine bridges of composite construction. This simplified design method involved maximum values for the load distribution factors for girder bending stress and shear, as well as empirical expressions for mid-span deflection and maximum design values for the axial force in bracing members. It should also be noted that the

proposed expressions for shear forces would lead to the design of shear connectors, bridge bearing, and supporting frames or abutments. It should be emphasized the derived expressions apply only to the AASHTO truck loading.

6.2 Conclusions

The most important conclusions drawn from the theoretical results in this study are summarized below:

- 1- The presence of solid end-diaphragms at the support lines along with a minimum of three bracing systems between the radial support lines, with a maximum spacing of 7.5 m, significantly enhances the transverse load distribution for bending stress and shear in the girders, as well as the transverse distribution of deflection.
- 2- Stiffer cross-bracings enhance significantly the transverse distribution of shear but have no significant effects on the bending stress and deflection. It was found a cross-sectional area of 0.01 m^2 for the cross-bracing systems provides an optimum transverse distribution for shear.
- 3- Provided that the above mentioned requirements for cross-bracings are met, the case of fully loaded lanes is the governing case for design for girder bending stresses, deflection, design axial force in bracing members of both straight and curved composite multiple-spine bridges. While in case of shear distribution between webs, the case of fully loaded lanes produce the maximum shear effect in the outer, internal, and inner webs at the support lines, whereas the case of partially loaded lanes with truck(s) in the outer lane(s) produce uplift forces in the inner support points.
- 4- Curvature is the most critical parameter that influences the design of girders and bracing members in curved multiple-spine bridges. Increase in the degree of curvature increases the flexural stress distribution factors, the deflection at mid-span,

the maximum axial force in a bracing member, as well as the upward shear forces in webs close to the outer side of curvature and the downward shear forces in webs close to the inner side of curvature.

- 5- For the same number of lanes, the flexural stress and shear distribution factors as well as the maximum axial force in a bracing member decrease with increase in the number of boxes.
- 6- Increasing the bridge span increases the bending stress distribution factors for the outer and inner girders and decreases it for the internal girders. It also increases the deflection at mid-span and maximum axial force in bracing members.

6.3 Recommendation for Future Research

It is recommended that further research efforts be directed towards the following:

1. The study of load distribution in this type of bridges when subjected to CHBDC truck loadings.
2. Further comparisons between the current AASHTO formula as well as proposed ones by previous researchers for transverse load distribution and the proposed equations in this study for bending stress and shear.

REFERENCES

- 1- Al-Rifaie, W. N., and Evans, H. R. 1979. **An approximate method for the analysis of box girder bridges that are curved in plan.** Proceedings of International Association of Bridges and Structural Engineering, IABSE, 1-21.
- 2- American Association of State Highway and Transportation Officials, AASHTO. 1994. **AASHTO LRFD Bridge Design Specifications.** Washington, D.C.
- 3- American Association of State Highway and Transportation Officials, AASHTO. 1993. **Guide specifications for horizontally curved highway bridges.** Washington, D.C.
- 4- American Association of State Highway and Transportation Officials, AASHTO. 1996. **Standard specifications for highway bridges.** Washington, D.C.
- 5- Bakht, B., and Jaeger, L. G. 1992. **Simplified methods of bridge analysis for the third edition of OHBDC.** Canadian Journal of Civil Engineering, 19(4): 551-559.
- 6- Bakht, B. and Jaeger, L. G. 1985. **Bridge deck simplified.** McGraw-Hill, New York, N.Y.
- 7- Bazant, Z. P., and El Nimeiri, M. 1974. **Stiffness method for curved box girders.** ASCE Journal of the Structural Division, 100(ST10): 2071-2090.
- 8- Bradford, M. A., and Wong, T. C. 1992. **Local buckling of composite box girders under negative bending.** The Structural Engineer, 70(21): 377-380.
- 9- Brighton, J., Newell, J. and Scanlon, A. 1996. **Live load distribution factors for double cell box girders.** Proceeding of the 1st Structural Specialty Conference, Alberta, Canada, 419-430.
- 10- Brockenbrough, R. L. 1986. **Distribution factors for curved I-girder bridges.** ASCE Journal of Structural Engineering, 112(10): 2200-2215.

- 11- Canadian Standard Association. 1988. **Design of highway bridges (CAN/CSA-S6-88)**. Rexdale, Ontario, Canada.
- 12- Chan, M. Y. T., Cheung, M. S., Beauchamp, J. C., and Hachem, H. M. 1990. **Thermal stresses in composite box-girder bridges**. Proceeding of the 3th International Conference on Short and Medium Span Bridges, Toronto, Ontario, Canada, 2: 355-366.
- 13- Chapman, J. C., Dowling, P. J., Lim, P. T. K., and Billington, C. J. 1971. **The structural behaviour of steel and concrete box girder bridges**. The Structural Engineer, 49(3): 111-120.
- 14- Cheung, M. S. 1984. **Analysis of continuous curved box-girder bridges by the finite strip method**, In Japanese. Japanese Society of Civil Engineers, 1-10.
- 15- Cheung, M. S., and Chan, M. Y. T. 1978. **Finite strip evaluation of effective flange width of bridge girders**. Canadian Journal of Civil Engineering, 5(2): 174-185.
- 16- Cheung, M. S., and Cheung, Y. K. 1971. **Analysis of curved box girder bridges by the finite-strip method**. International Association of Bridges and Structural Engineering, IABSE, 31(I): 1-8.
- 17- Cheung, M. S., and Foo, S. H. C. 1995. **Design of horizontally curved composite box girder bridges: a simplified approach**. Canadian Journal of Civil Engineering, 22(1): 93-105.
- 18- Dabrowski, R. 1968. **Curved thin-walled girders, Theory and analysis**. Springer, New York.
- 19- Davis, R. E., Bon V. D., and Semans, F. M. 1982. **Live load distribution in concrete box girder bridges**. Transportation Research Record, Transportation Research Board, 871:47-52.
- 20- Davis, R. E., Bon V. D. 1981. **Transverse distribution of loads in box girder bridges (Volume 7): Correction for curvature**. California Department of Transportation,

Socramento, CA, Report No. FHWA-CA-SD-81/16 Final Report.

- 21- Dean, D. L. 1994. **Torsion of regular multicellular members**. ASCE Journal of Structural Engineering, 120(12): 3675-3678.
- 22- Dilger, W. H., Ghoneim, G. A., and Tadros, G. S. 1988. **Diaphragms in skew box girder bridges**. Canadian Journal of Civil Engineering, 15(5): 869-878.
- 23- Elbadry, M. M., and Ibrahim, A. M. 1996. **Temperature distributions in curved concrete box-girder bridges**. 1st Structural Specialty Conference, Canadian Society of Civil Engineering, Edmonton, Alberta, Canada, 1-12.
- 24- Evans, H. R. 1982. **Simplified methods for the analysis and design of bridges of cellular cross-section**. Proceedings of the NATO Advanced Study Institute on Analysis and Design of Bridges, Cesme, Izmir, Turkey, 95-115.
- 25- Evans, H. R., and Shanmugam, N. E. 1984. **Simplified analysis for cellular structures**. ASCE Journal of the Structural Division. 110(ST3): 531-543.
- 26- Fam, A. R. M. 1973. **Static and free-vibration analysis of curved box bridges**. Structural Dynamic Series No. 73-2, Department of Civil Engineering and Applied Mechanics, McGill University, Montreal, Quebec, Canada.
- 27- Fam, A. R., and Turkstra, C. J. 1975. **A finite element scheme for box bridge analysis**. Computers and Structures Journal, Pergamon Press, 5: 179-186.
- 28- Fam, A. R., and Turkstra, C. J. 1976. **Model study of horizontally curved box girder**. ASCE Journal of the Structural Division, 102(ST5): 1097-1108.
- 29- Fountain, R. S., and Mattock, R. S. 1968. **Composite steel-concrete multi-box girder bridges**. Proceedings of the Canadian Structural Engineering Conference, Toronto, 19-30.
- 30- Fu, C. C., and Hsu, Y. T. 1995. **The development of an improved curvilinear thin-walled Vlasov element**. Computers and Structures Journal, Pergamon Press, 54(1): 147-159.

- 31- Fu, C. C., and Yang, D. 1996. **Designs of concrete bridges with multiple box cells due to torsion using softened truss model.** ACI Structural Journal, 93(6): 696-702.
- 32- Galuta, E. M., and Cheung, M. S. 1995. **Combined boundary element and finite element analysis of composite box girder bridges.** Computers and Structures Journal, Pergamon Press, 57(3): 427-437.
- 33- Hambly, E. C., and Pennells, E. 1975. **Grillage analysis applied to cellular bridge decks.** The Structural Engineer, 53(7): 267-275.
- 34- Hasebe, K., Usuki, S., and Horie, Y. 1985. **Shear lag analysis and effective width of curved girder bridges.** ASCE Journal of Engineering Mechanics, 111(1): 87-92.
- 35- Heins, C. P. 1978. **Box girder bridge design-State-of-the-Art.** AISC Engineering Journal, 2: 126-142.
- 36- Heins, C. P., and Jin, J. O. 1984. **Live load distribution on braced curved I-girders.** ASCE Journal of Structural Engineering, 110(3): 523-530.
- 37- Heins, C. P., and Oleinik, J. C. 1976. **Curved box beam bridge analysis.** Computers and Structures Journal, Pergamon Press, London, 6(2): 65-73.
- 38- Heins, C. P., and Sheu, F. H. 1982. **Design/analysis of curved box girder bridges.** Computers and Structures Journal, 15(3): 241-258.
- 39- Hibbitt, H. D., Karlson, B. I., and Sorenson, E. P. 1996. **ABAQUS version 5.6, finite element program.** Hibbitt, Karlson & Sorenson, Inc, Providence, R. I.
- 40- Ho, S., Cheung, M. S., Ng, S. F., and Yu, T. 1989. **Longitudinal girder moments in simply supported bridges by the finite strip method.** Canadian Journal of Civil Engineering, 16(5): 698-703.
- 41- Ishac, I. I., and Smith, T. R. G. 1985. **Approximations for moments in box girders.** ASCE Journal of Structural Engineering, 111(11): 2333-2342.
- 42- Johanston, S. B., and Mattock, A. H. 1967. **Lateral distribution of loads in composite**

- box girder bridges.** Highway Research Record, Highway Research Board, 167: 25-33.
- 43- Kabir, A. F. and Scordelis, A. C. 1974. **Computer programs for curved bridges on flexible bents.** Structural Engineering and Structural Mechanics Report No. UC/SESM 74-10, University of California, Berkeley, CA.
- 44- Kano, T., Usuke, S., and Hasebe, K. 1982. **Theory of thin-walled curved members with shear deformation.** Ingenieur-Archiv, 51.
- 45- Li, H. G. 1992. **Thin-walled box beam finite elements for static analysis of curved haunched and skew multi-cell box girder bridges.** Ph.D. Thesis, Department of Civil Engineering, Carleton University, Ottawa, Ontario, Canada.
- 46- Li. W. Y., Tham, L. G., and Cheung, Y. K. 1988. **Curved box-girder bridges.** Journal of Structural Engineering, American Society of Civil Engineers, 114(6): 1324-1338.
- 47- Maisel, B. I. 1985. **Analysis of concrete box beams using small computer capacity.** Canadian Journal of Civil Engineering, 12(2): 265-278.
- 48- Malcolm, D. J., and Redwood, R. G. 1970. **Shear lag in stiffened box girders.** ASCE Journal of the Structural Division, 96(ST7): 1403-1419.
- 49- Mavaddat, S., and Mirza, M. S. 1989. **Computer analysis of thin walled concrete box beams.** Canadian Journal of Civil Engineering, 16(6): 902-909.
- 50- Meyer, C. and Scordelis, A. C. 1971. **Analysis of curved folded plate structures.** ASCE Journal of the Structural Division, 97(ST10): 2459-2480.
- 51- Mikkola, M., and Paavola, J. 1980. **Finite element analysis of box girders.** ASCE Journal of the structural Division, 106(ST6): 1343-1357.
- 52- Ministry of Transportation and Communications. 1985. **Geometric design standards for Ontario highways.** Downsview, Ontario, Canada.
- 53- Moffatt, K. R., and Dowling, P. J. 1975. **Shear lag in steel box girder bridges.** The Structural Engineer, 53(10): 439-448.

- 54- Mukherjee, D. and Trikha, D. N. 1980. **Design coefficient for curved box girder concrete bridges**. Indian Concrete Journal, 54(11): 301-306.
- 55- Nakai, H., and Heins, C. P. 1977. **Analysis criteria for curved bridges**. ASCE Journal of Structural Division, 103(ST7):1419-1427.
- 56- Normandin, P., and Massicotte, B. 1994. **Load distribution in composite steel box girder bridges. Proceedings of the 4th International Conference on Short and Medium Span Bridges**. Halifax, N.S., Canada, 165-176.
- 57- Nutt., R. V., Schamber, R. A., and Zokaie, T. 1988. **Distribution of wheel loads on highway bridges**. Transportation Research Board, National Cooperative Highway Research Council, Imbsen & Associates Inc., Sacramento, Calif.
- 58- Oleinik, J. C., and Heins, C. P. 1975. **Diaphragms for curved box beam bridges**. ASCE Journal of the Structural Division, 101(ST10): 2161:2179.
- 59- Ontario Ministry of Transportation and Communications. 1998. **Canadian highway bridge design code, CHBDC**. Downsview, Ontario
- 60- Ontario Ministry of Transportation and Communications. 1983. **Ontario highway bridge design code, OHBDC**. Second edition, Downsview, Ontario.
- 61- Ontario Ministry of Transportation and Communications. 1992. **Ontario highway bridge design code, OHBDC**. Third edition, Downsview, Ontario
- 62- Razaqpur, A. G., and Li, H. G. 1997. **Analysis of curved multi-cell box girder assemblages**. Structural Engineering and Mechanics, 5(1): 33-49.
- 63- Razaqpur, A. G., and Li, H. G. 1990. **Analysis of multi-branch multi-cell box girder bridges**. Proceeding of the 3th International Conference on Short and Medium Span Bridges, Toronto, Ontario, Canada, 2: 153-164.
- 64- Razaqpur, A. G., and Li, H. G. 1994. **Refined analysis of curved thin-walled multi-cell box girders**. Computers and Structures Journal , Pergamon Press, 53(1): 131-142.

- 65- Sargious, M. A., Dilger, W. H., and Hawk, H. 1979. **Box girder diaphragms with openings**. ASCE Journal of the Structural Division, 105(ST1): 53-65.
- 66 – Sennah, K. M. 1998. **Load Distribution and Dynamic Characteristics of Curved Composed Concrete Deck-Steel Cellular Bridges**. PhD dissertation, Civil and Environmental Engineering Program, University of Windsor, Windsor, Ontario, Canada.
- 67- Sisodiya, R. G., Cheung, Y. K., and Ghali, A. 1970. **Finite-element analysis of skew, curved box girder bridges**. International Association of Bridges and Structural Engineering, IABSE, 30(II): 191-199.
- 68- Tesar, A. 1996. **Shear lag in the behaviour of thin-walled box bridges**. Computers & Structures Journal, 59(4): 607-612.
- 69- Transportation Research Board, National Research Council. 1992. **Distribution of wheel loads on highway bridges**. National Cooperative Highway Research Program, Research results Digest, RRD 187.
- 70- Trukstra, C. J., and Fam, A. R. 1978. **Behaviour study of curved box bridges**. ASCE Journal of the Structural Division, 104(ST3): 453-462.
- 71- Usuki, T. 1987. **The theory of curved multi-cell box girder bridges under consideration of cross-sectional distortion**. Structural Engineering/Earthquake Engineering, 4(2): 277-287.
- 72- Van Zyl, S. 1978. **Analysis of curved segmentally erected prestressed concrete box girder bridges**. Structural Engineering and Structural Mechanics, Report No. UC/SESM 78-2, University of California, Berkeley, CA.
- 73- Vlasov, V. Z. 1965. **Thin-walled elastic beams**. OTS61-11400, National Science Foundation, Washington, D. C.
- 74- Waldron, P. 1988. **The significance of warping torsion in the design of straight concrete box-girder bridges**. Canadian Journal of Civil Engineering, 15(5): 879-889.

- 75- Williams, R. G. M., Cassell, A. C., and Boswell, L. F. 1992. **A computer design aid for prestressed box beams**. Proceedings of the Institute of Civil Engineering Structures & Bridges, 94: 61-72.
- 76- Willam, K. J., and Scordelis, A. C. 1972. **Cellular structures of arbitrary plan geometry**. ASCE Journal of the Structural Division, 98(ST7): 1377-1394.
- 77- Yoo, C. H., and Littrell, P. C. 1985. **Cross-bracing effects in curved stringer bridges**. ASCE Journal of Structural Engineering, 112(9): 2127-2140.
- 78- Zhang, S. H., and Lyons, L. P. R. 1984. **Thin-walled box beam finite element for curved bridge analysis**. Computers and Structures Journal, 18(6): 1035-1046.
- 79- Zokaie, T., Imbsen, R. A., and Osterkamp, T. A. 1991. **Distribution of wheel loads on highway bridges**. Transportation Research Record, Transportation Research Board, 1290: 119-126.
- 80- Zienkiewicz, O. C. 1977. **The finite-element method**. McGraw-Hill Book Company, Third Edition.

Table 4.1. Geometries of the prototype bridges in the parametric study

Bridge Type	Span L(m)	No. of lanes	No. of boxes	Cross-section dimensions (mm)								
				A	B	C	D	F	t ₁	t ₂	t ₃	t ₄
21-2b-sc-20	20	2	2	9300	2325	300	800	1025	16	10	15	225
31-3b-sc-20		3	3	13050	2175	300	800	1025	16	10	17	225
41-4b-sc-20		4	4	16800	2100	300	800	1025	16	10	18	225
21-2b-sc-40	40	2	2	9300	2325	375	1600	1825	28	14	18	225
31-3b-sc-40		3	3	13050	2175	375	1600	1825	28	14	20	225
41-4b-sc-40		4	4	16800	2100	375	1600	1825	28	14	21	225
21-2b-sc-60	60	2	2	9300	2325	450	2400	2625	40	18	23	225
31-3b-sc-60		3	3	13050	2175	450	2400	2625	40	18	25	225
41-4b-sc-60		4	4	16800	2100	450	2400	2625	40	18	26	225
21-2b-sc-80	80	2	2	9300	2325	530	3200	3425	52	22	26	225
31-3b-sc-80		3	3	13050	2175	530	3200	3425	52	22	28	225
41-4b-sc-80		4	4	16800	2100	530	3200	3425	52	22	30	225
21-2b-sc-100	100	2	2	9300	2325	600	4000	4225	64	26	30	225
31-3b-sc-100		3	3	13050	2175	600	4000	4225	64	26	33	225
41-4b-sc-100		4	4	16800	2100	600	4000	4225	64	26	35	225

Note: Symbols A, B, C, D, F, t₁, t₂, t₃, t₄ are explained in Fig. 4.1.

Table 4.2. Ranges of the parameters considered in the sensitivity and parametric studies

Parameters	No. of traffic lanes		
	2	3	4
Span length (m), L	20-100	20-100	20-100
Number of boxes, N_b	2-4	3-5	3-6
Box width (mm), B	1160-2325	1305-2175	1400-2800
Bridge width (mm), A	9300	13050	16800
Overhanging length (mm)	580-1163	653-1088	700-1400
Span-to-depth ratio, L/D	10-40	10-40	10-40
External web slope factor	0	0	0
Top slab thickness (mm), t_4	225	225	225
Bottom flange thickness (mm), t_3	14-30	16-34	17-35
Web thickness (mm), t_2	8-26	8-26	10-35
Top flange thickness (mm), t_1	10-64	10-64	11-85
Top flange width (mm), C	300-600	300-600	300-600
End-diaphragms thickness (mm)	0-26	0-26	0-35
Number of bracing systems	0-23	0-23	0-23
Bracing area (mm^2), A_b	144-22500	144-22500	144-22500

Table 4.3. Material properties for concrete and steel in the parametric study

Material Properties	Concrete	Steel
Modulus of Elasticity, E (Mpa)	27,000	200,000
Poisson's ratio, ν	0.20	0.30
Density, ρ (kg/m^3)	2400	7800

Table 5.1. Finite Element Analysis versus Straight Simple Beam Analysis

N _L	N _B	$\frac{L}{R}$	L	Tensile stress in bottom flange (Mpa)					Compressive stress in concrete (Mpa)				
				FEA ¹				SBA ²	FEA				SBA
				G1	G2	G3	G4		G1	G2	G3	G4	
2	2	0	20	33	32	32	33	33	2	2	2	2	15
			40	31	30	30	31	30	2	2	2	2	14
			60	28	29	29	28	29	2	2	2	2	15
			80	29	29	29	29	29	2	2	2	2	17
			100	28	28	28	28	28	2	2	2	2	17
		1.0	20	36	35	37	40	33	2	2	2	3	15
			40	33	34	35	39	30	2	2	2	3	14
			60	35	31	39	35	29	2	2	3	2	15
			80	34	34	37	38	29	2	3	3	3	17
			100	34	33	38	37	28	2	3	3	3	17
		2.0	20	58	55	46	56	33	4	4	2	4	15
			40	52	56	48	59	30	3	4	3	3	14
			60	61	51	63	51	29	4	3	3	3	15
			80	57	59	58	60	29	4	4	3	4	17
			100	60	58	60	59	28	4	4	3	4	17

¹ Results from finite element analysis

² Results from straight beam analysis

Table 5.2. Effect of number of inner cross-bracing system on stress distribution of straight and curved bridges

Bridge type	$\frac{L}{R}$	No. of Cross-bracings	Stress Distribution factor, D_{σ} , due to															
			Fully Loaded Lanes ¹				Truck Loading in the outer lane				Truck Loading in the inner lane							
			Inner Girder	Girder No. 1	Girder No. 2	Outer Girder	Inner Girder	Girder No. 1	Girder No. 2	Outer Girder	Inner Girder	Girder No. 1	Girder No. 2	Outer Girder				
21-2b-ss-60	0	0	0.98	1.03	1.03	0.98	0.34	0.40	0.67	0.74	0.67	0.40	0.74	0.74	0.67	0.40	0.34	
		1	1.04	0.96	0.96	1.04	0.56	0.40	0.61	0.43	0.61	0.40	0.40	0.43	0.61	0.40	0.56	
		3	1.01	0.99	0.99	1.01	0.49	0.43	0.58	0.50	0.58	0.43	0.58	0.50	0.58	0.43	0.49	
		5	1.01	0.99	0.99	1.01	0.48	0.44	0.56	0.52	0.56	0.44	0.56	0.52	0.56	0.44	0.48	
		7	1.00	0.99	0.99	1.00	0.47	0.44	0.56	0.53	0.56	0.44	0.56	0.53	0.56	0.44	0.47	
		11	1.00	1.00	1.00	1.00	0.47	0.45	0.55	0.53	0.55	0.45	0.55	0.53	0.55	0.45	0.47	
		17	1.01	1.00	1.00	1.01	0.47	0.45	0.55	0.54	0.55	0.45	0.55	0.54	0.55	0.45	0.47	
		0	1.39	1.20	0.94	0.77	0.51	0.48	0.59	0.56	0.56	0.48	0.59	0.56	0.60	0.67	0.36	0.67
		1	0.82	1.10	0.89	1.32	0.47	0.48	0.58	0.60	0.58	0.48	0.59	0.58	0.58	0.60	0.41	0.53
		3	0.94	1.05	0.98	1.15	0.48	0.48	0.59	0.58	0.59	0.48	0.59	0.58	0.58	0.60	0.44	0.50
5	0.97	1.01	1.03	1.10	0.49	0.47	0.59	0.58	0.59	0.47	0.59	0.58	0.58	0.56	0.44	0.50		
7	0.99	1.00	1.05	1.09	0.49	0.49	0.59	0.58	0.59	0.49	0.59	0.58	0.58	0.55	0.45	0.49		
11	0.99	1.00	1.06	1.08	0.49	0.49	0.59	0.58	0.59	0.49	0.59	0.58	0.58	0.54	0.46	0.48		
17	0.99	1.00	1.07	1.07	0.49	0.49	0.59	0.58	0.59	0.49	0.59	0.58	0.58	0.54	0.46	0.48		
21-2b-sc-60	0.4	0	1.96	1.31	1.14	0.78	0.88	0.63	0.65	0.63	0.63	0.65	0.52	1.06	0.63	0.51	0.32	
		1	0.51	1.46	0.85	1.94	0.36	0.71	0.57	0.94	0.71	0.57	0.94	0.11	0.80	0.33	0.94	
		3	0.97	1.28	1.04	1.47	0.54	0.64	0.63	0.77	0.64	0.63	0.77	0.44	0.68	0.41	0.66	
		5	1.07	1.18	1.17	1.34	0.58	0.60	0.68	0.72	0.60	0.68	0.72	0.51	0.62	0.48	0.59	
		7	1.11	1.14	1.23	1.30	0.59	0.59	0.70	0.70	0.59	0.70	0.70	0.54	0.59	0.51	0.56	
		11	1.13	1.12	1.26	1.27	0.60	0.58	0.71	0.69	0.60	0.58	0.71	0.69	0.55	0.57	0.53	0.54
		17	1.14	1.11	1.28	1.26	0.61	0.58	0.72	0.69	0.61	0.58	0.72	0.69	0.56	0.57	0.54	0.54
		0	1.96	1.31	1.14	0.78	0.88	0.63	0.65	0.63	0.63	0.63	0.65	0.52	1.06	0.63	0.51	0.32
		1	0.51	1.46	0.85	1.94	0.36	0.71	0.57	0.94	0.71	0.57	0.94	0.11	0.80	0.33	0.94	
		3	0.97	1.28	1.04	1.47	0.54	0.64	0.63	0.77	0.64	0.63	0.77	0.44	0.68	0.41	0.66	
5	1.07	1.18	1.17	1.34	0.58	0.60	0.68	0.72	0.60	0.68	0.72	0.51	0.62	0.48	0.59			
7	1.11	1.14	1.23	1.30	0.59	0.59	0.70	0.70	0.59	0.70	0.70	0.54	0.59	0.51	0.56			
11	1.13	1.12	1.26	1.27	0.60	0.58	0.71	0.69	0.60	0.58	0.71	0.69	0.55	0.57	0.53	0.54		
17	1.14	1.11	1.28	1.26	0.61	0.58	0.72	0.69	0.61	0.58	0.72	0.69	0.56	0.57	0.54	0.54		

¹ AASHTO lane loading

Table 5.3. Effect of number of inner cross-bracing system on deflection of curved bridges

Bridge type	$\frac{L}{R}$	No. of Cross-bracings	Deflection at mid-span, mm, due to																	
			Fully Loaded Lanes ¹						Truck Loading in the outer lane						Truck Loading in the inner lane					
			Inner Girder No. 1	Girder No. 2	Outer Girder	Inner Girder No. 1	Girder No. 2	Outer Girder	Inner Girder No. 1	Girder No. 2	Outer Girder	Inner Girder No. 1	Girder No. 2	Outer Girder						
21-2b-sc-60	0.4	0	55	48	42	34	17	18	20	21	39	30	21	14						
		1	33	35	35	37	15	17	19	21	18	18	16	16						
		3	31	33	35	36	15	17	19	21	16	16	15	16						
		5	31	33	35	36	15	17	19	21	16	16	15	15						
		7	31	33	35	36	15	17	19	21	16	16	15	15						
		11	31	33	35	36	15	17	19	21	16	16	15	15						
		17	31	33	35	36	15	17	19	21	16	16	15	15						
		0	156	139	124	108	66	61	58	54	92	78	65	54						
		1	55	61	63	69	28	32	36	40	27	29	27	30						
		3	45	51	56	62	25	29	33	38	21	23	23	25						
		5	44	50	55	61	24	28	33	37	20	22	23	25						
		7	43	49	55	61	24	28	33	37	20	21	22	24						
		11	43	49	55	61	24	28	32	37	19	21	22	24						
		17	43	49	54	60	24	28	32	37	19	21	22	24						

¹ AASHTO lane loading

Table 5.4. Effect of number of inner cross-bracing system on maximum bracing axial force

Bridge Type	L/R	No. of Cross-bracings	Bracing axial force, kN, due to							
			Fully loaded lanes ¹			Truck loading in the outer lane				
			Tension	Compression		Tension	Compression			
2.1-2b-sc-60	0.4	0 ²	111	242		89	138		34	99
		1	139	197		88	136		137	139
		3	77	174		85	133		73	85
		5	52	170		85	133		47	61
		7	52	170		85	133		40	49
		11	53	168		86	133		38	36
		17	54	167		87	133		36	28
		0	364	526		237	299		139	214
		1	365	452		222	271		245	251
		3	255	373		198	248		133	143
		5	249	366		196	245		88	117
		7	248	365		195	245		69	116
		11	250	364		197	246		69	115
		17	251	362		198	246		69	114

¹ AASHTO truck loading

² No bracing systems along span. Only bracing systems at support lines between boxes

Table 5.5. Effect of the area of cross-bracings on structural response of curved multiple-spine bridge

Bridge Type	Cross-bracing and top-chord area (mm ²)	Stress distribution factor, $D\sigma$				Maximum force in bracings (kN)		Deflection at mid-span section (m)			
		Inner girder	Girder No. 1	Girder No.2	Outer girder	Tension	Compression	Inner girder	Girder No. 1	Girder No.2	Outer girder
21-2b-sc-60 ¹	0	1.98	1.28	1.19	0.83	-	-	0.52	0.46	0.42	0.37
	144	1.33	1.12	1.20	1.05	252	255	0.23	0.23	0.24	0.25
	625	1.26	1.14	1.29	1.18	288	301	0.17	0.18	0.20	0.22
	2500	1.25	1.14	1.33	1.22	406	529	0.15	0.17	0.19	0.21
	5625	1.24	1.14	1.34	1.23	673	909	0.15	0.16	0.18	0.21
	10000	1.24	1.14	1.34	1.23	870	1222	0.14	0.16	0.18	0.20
	15625	1.24	1.14	1.34	1.23	1001	1465	0.14	0.16	0.18	0.20
22500	1.24	1.14	1.34	1.23	1083	1651	0.14	0.16	0.18	0.20	

¹ span-to-radius ratio, L/R=1.0; seven cross-bracing and top-chord system inside each box; dead load condition

Table 5.6. Effect of span-to-depth ratio on shear distribution factor of 3L-3B-60 straight bridge under AASHTO truck loading

Bracing ¹ Type	L/D	Shear Distribution factor, D _{SS}											
		Fully loaded Lanes						Partially Loaded Lanes					
		W ₁	W ₂	W ₃	W ₄	W ₅	W ₆	W ₁	W ₂	W ₃	W ₄	W ₅	W ₆
Internal Bracings Only	15	0.51	0.86	1.04	1.04	0.86	0.51	-0.30	0.12	0.39	0.78	1.11	1.31
	20	0.47	0.89	1.05	1.05	0.89	0.47	-0.28	0.14	0.36	0.80	1.06	1.33
	25	0.45	0.92	1.05	1.05	0.92	0.45	-0.27	0.18	0.32	0.84	0.98	1.36
	30	0.43	0.94	1.05	1.05	0.94	0.43	-0.27	0.23	0.26	0.89	0.90	1.39
	35	0.41	0.96	1.04	1.04	0.96	0.41	-0.27	0.28	0.21	0.94	0.82	1.43
Internal and External Bracings	15	0.62	0.87	0.93	0.93	0.87	0.62	-0.31	0.16	0.41	0.76	1.07	1.32
	20	0.62	0.87	0.92	0.92	0.87	0.62	-0.31	0.20	0.41	0.76	1.00	1.36
	25	0.64	0.85	0.92	0.92	0.85	0.64	-0.31	0.25	0.38	0.77	0.91	1.41
	30	0.65	0.84	0.92	0.92	0.84	0.65	-0.31	0.30	0.34	0.80	0.82	1.46
	35	0.66	0.83	0.92	0.92	0.83	0.66	-0.32	0.36	0.29	0.84	0.73	1.51

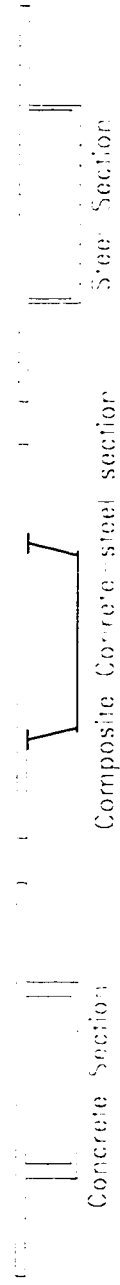
¹ Eight 100 mm x 100 mm cross-bracing systems along the span

Table 5.7. Effect of number of cross-bracing systems on shear distribution factor of two-lane, two-box bridges of 60 m span under AASHTO truck loading

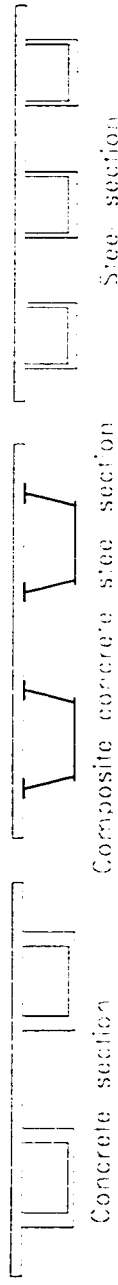
Bracing Type	Number Of cross-racing	Shear distribution factor, D_{SS}							
		Fully Loaded Lanes				Partially Loaded Lanes			
		W_1	W_2	W_3	W_4	W_1	W_2	W_3	W_4
Internal Bracings Only	0	0.69	1.26	1.26	0.69	-0.27	0.27	0.70	1.25
	1	0.67	1.28	1.28	0.67	-0.22	0.31	0.66	1.21
	2	0.67	1.28	1.28	0.67	-0.22	0.32	0.65	1.20
	3	0.68	1.27	1.27	0.68	-0.22	0.32	0.65	1.20
	5	0.70	1.25	1.25	0.70	-0.22	0.31	0.66	1.20
	7	0.71	1.24	1.24	0.71	-0.22	0.32	0.66	1.19
	8	0.72	1.23	1.23	0.72	-0.22	0.31	0.66	1.19
	11	0.73	1.22	1.22	0.73	-0.22	0.31	0.67	1.19
	17	0.74	1.21	1.21	0.74	-0.22	0.31	0.67	1.18
23	0.74	1.21	1.21	0.74	-0.22	0.31	0.67	1.19	
Internal And External Bracings	0	0.69	1.26	1.26	0.69	-0.27	0.27	0.70	1.25
	1	0.69	1.25	1.25	0.69	-0.22	0.31	0.66	1.20
	2	0.72	1.23	1.23	0.72	-0.22	0.33	0.65	1.19
	3	0.75	1.20	1.20	0.75	-0.22	0.34	0.64	1.19
	5	0.78	1.17	1.17	0.78	-0.23	0.35	0.64	1.19
	7	0.79	1.16	1.16	0.79	-0.23	0.35	0.65	1.18
	8	0.80	1.15	1.15	0.80	-0.23	0.35	0.65	1.18
	11	0.81	1.14	1.14	0.81	-0.23	0.35	0.66	1.18
	17	0.83	1.12	1.12	0.83	-0.23	0.34	0.67	1.17
23	0.83	1.12	1.12	0.83	-0.23	0.34	0.68	1.16	

Table 5.8. Effect of cross-bracing area on the shear distribution factor of two-lane, two-box straight bridges of 60 m span under AASHTO truck loading

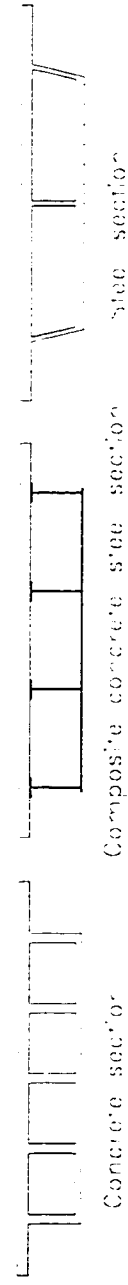
Bracing Type	Cross-bracing area (mm ²)	Shear distribution factor, D _{SS}							
		Fully Loaded Lanes				Partially Loaded Lanes			
		W ₁	W ₂	W ₃	W ₄	W ₁	W ₂	W ₃	W ₄
Internal Bracings Only	12x12	0.76	1.19	1.19	0.76	-0.30	0.57	0.33	1.35
	25x25	0.76	1.19	1.19	0.76	-0.29	0.58	0.32	1.33
	50x50	0.75	1.20	1.20	0.75	-0.26	0.50	0.43	1.29
	75x75	0.73	1.22	1.22	0.73	-0.24	0.39	0.55	1.24
	100x100	0.70	1.25	1.25	0.70	-0.22	0.31	0.66	1.20
	125x125	0.67	1.28	1.28	0.67	-0.21	0.26	0.73	1.16
	150x150	0.64	1.31	1.31	0.64	-0.20	0.23	0.79	1.13
Internal And External Bracings	12x12	0.75	1.19	1.19	0.75	-0.30	0.60	0.30	1.35
	25x25	0.78	1.17	1.17	0.78	-0.30	0.61	0.30	1.34
	50x50	0.80	1.15	1.15	0.80	-0.27	0.52	0.41	1.29
	75x75	0.80	1.15	1.15	0.80	-0.24	0.42	0.54	1.23
	100x100	0.78	1.17	1.17	0.78	-0.23	0.35	0.64	1.19
	125x125	0.75	1.20	1.20	0.75	-0.22	0.29	0.73	1.15
	150x150	0.72	1.23	1.23	0.72	-0.22	0.26	0.79	1.12



a) types of single box girders



b) types of multi-bay (multi-box) box girders



c) types of multi-bay (corrugated) box girders

Fig. 1.1. Box girder cross sections

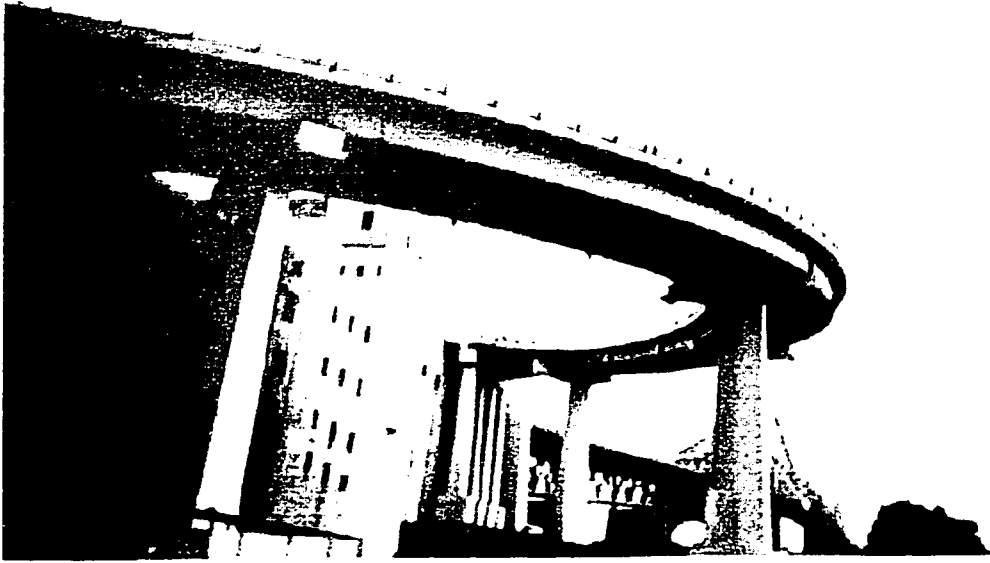


Fig.1.2. Jacques Cartier I-girder bridge in Montreal, Quebec

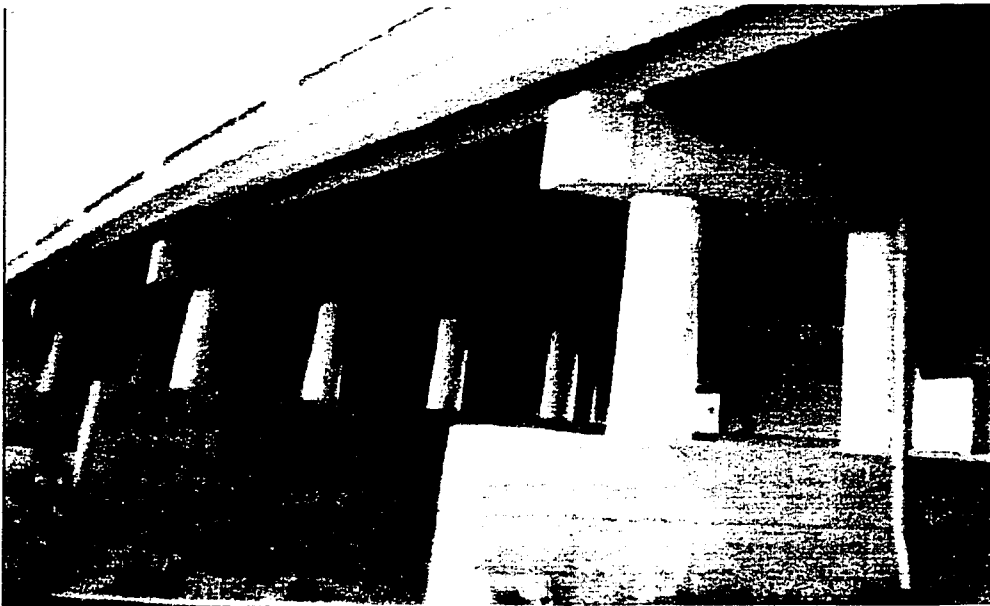
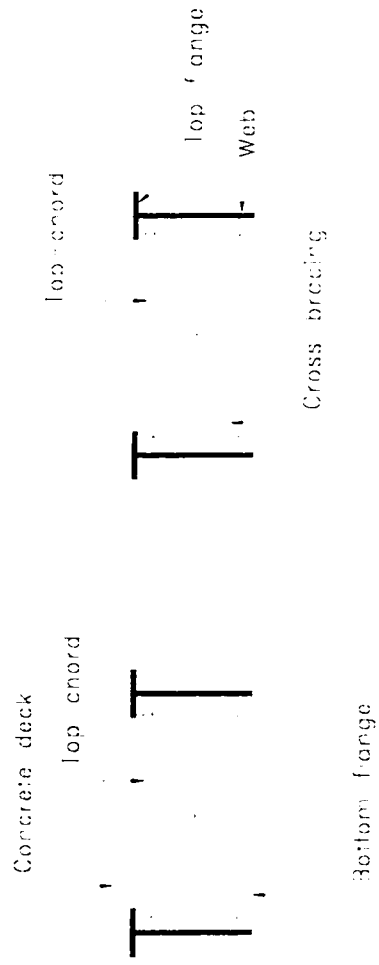
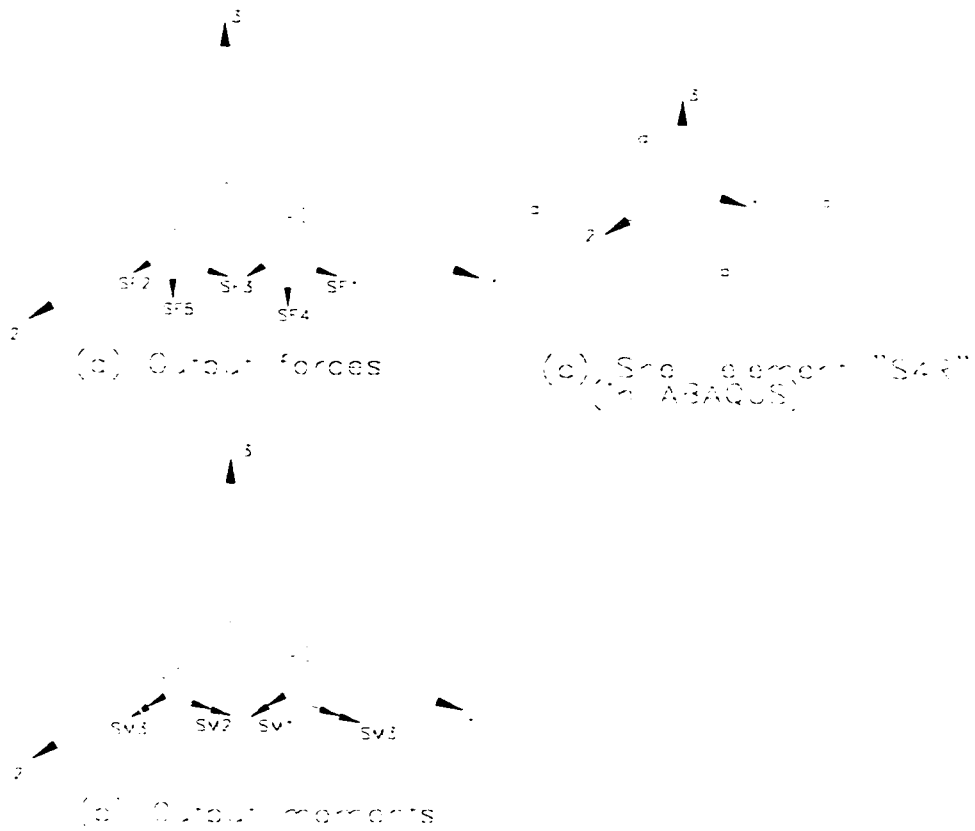


Fig.1.3. Box girder bridge in Downtown Toronto

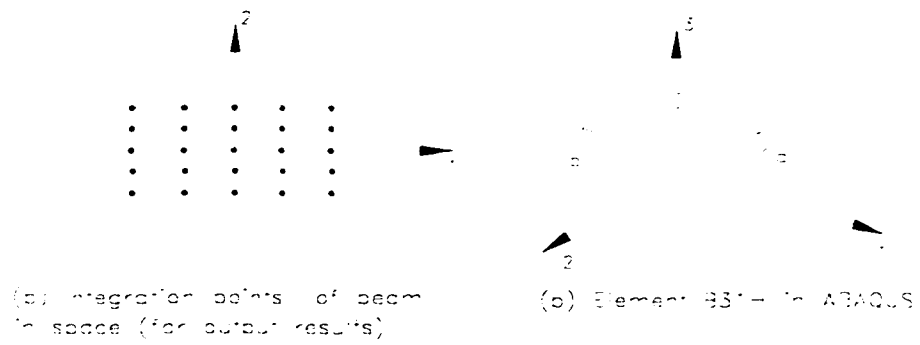
Bridge Weir





- Four-node element
- Degrees of freedom : $U1, U2, U3, \phi1, \phi2, \phi3$
- Output forces : SF1, SF2, SF3, SF4, SF5
- Output moments : MV1, MV2, MV3
- Stress components : S11, S22, S12

Fig. 3.1. Shear element "S4R" used for plate modeling



- Two node element
- Degrees of freedom : $U1, U2, U3, \phi1, \phi2, \phi3$
- Output forces : $SF1, SF2, SF3$
- Output moments : $SM1, SM2, SM3$
- Stress components : $S11, S12$

Fig. 3.2 beam element "B31" for beam in space

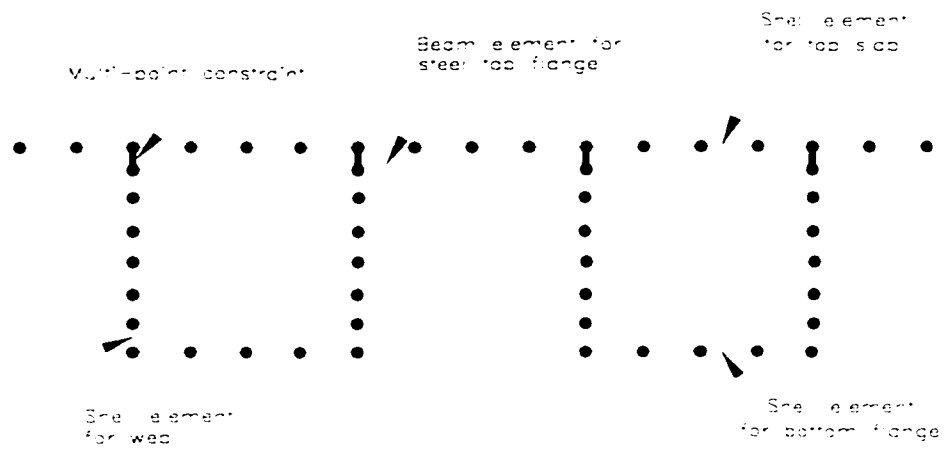
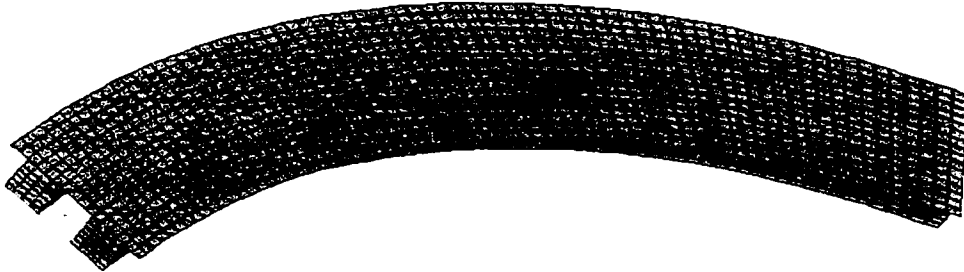


Fig. 3.3. Finite element discretization of cross section of the bridge



a) Top view of the curved bridge

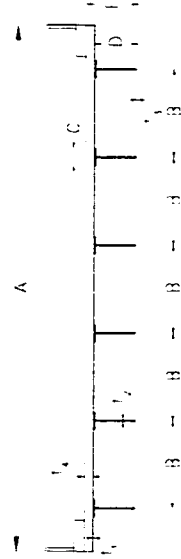


b) View of the bridge

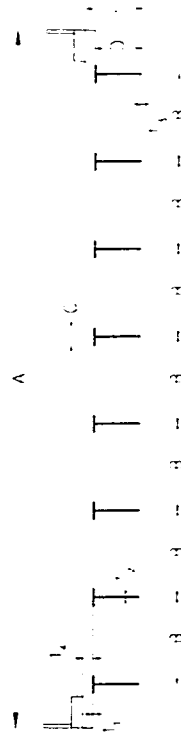
Fig.3.4. Typical finite-element mesh for a composite bridge prototype



(a) two lane two box cross section



(b) three lane three box cross section



(c) four lane four box cross section

Fig. 4.1.1. Box cross section configurations and symbols

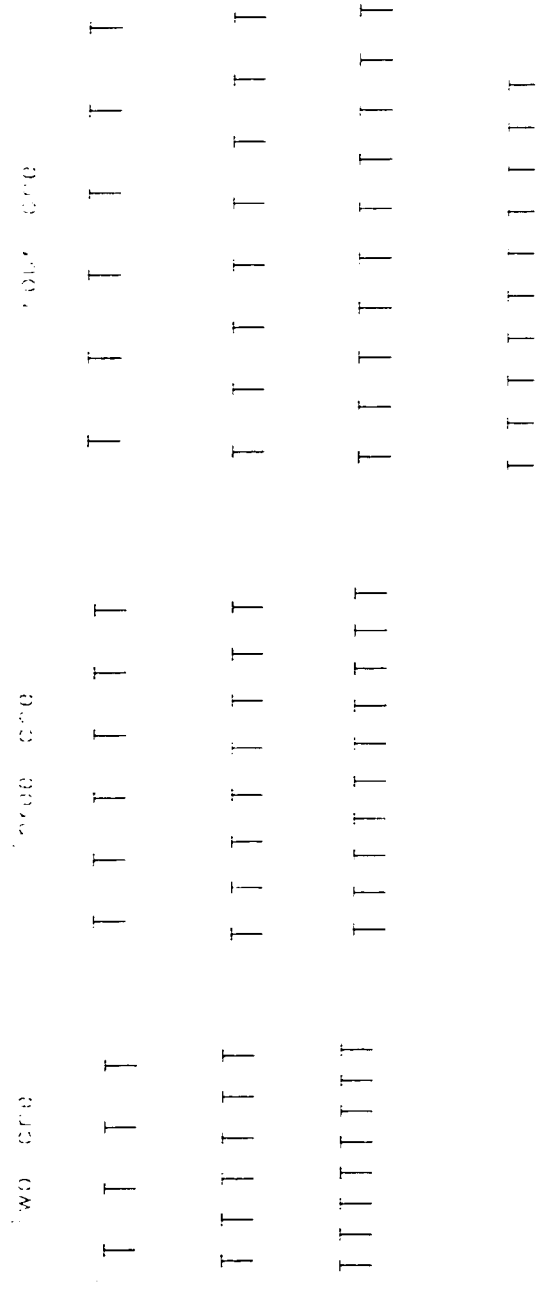
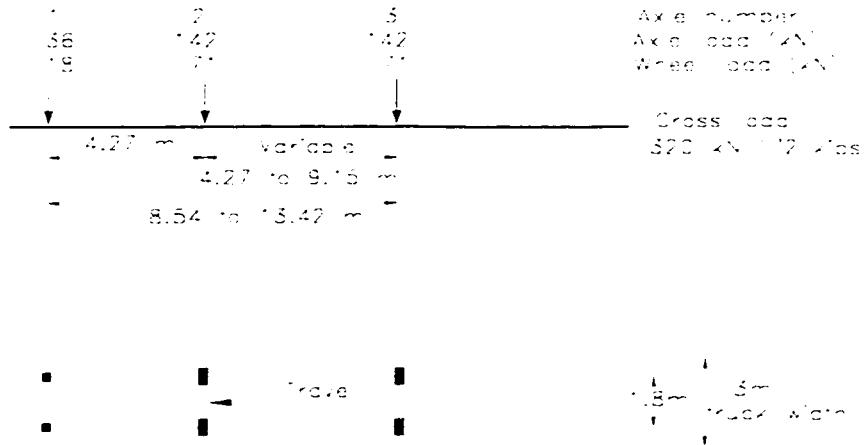
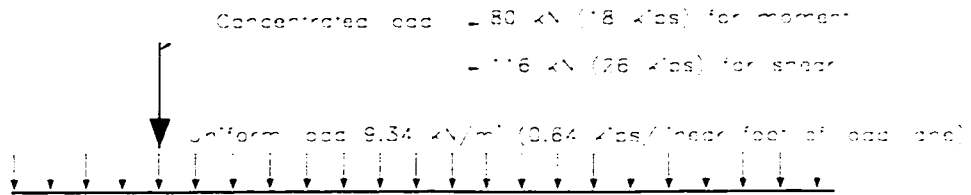


Fig. 4.2. Cross section configurations used in the present study



(a) HS20-44 AASHTO loading truck



(b) lane loading for HS20-44 AASHTO loading truck

Fig.4.3. Truck loading configuration according to "AASHTO" specifications

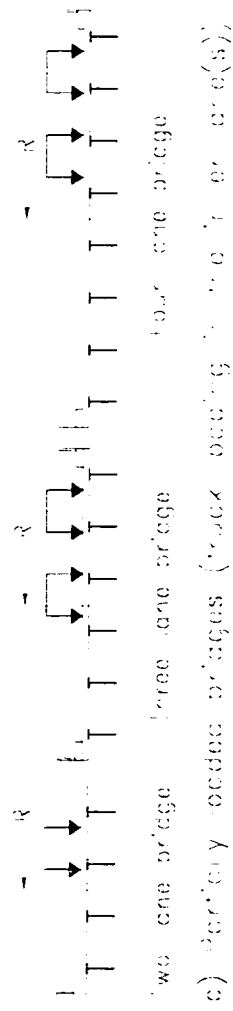
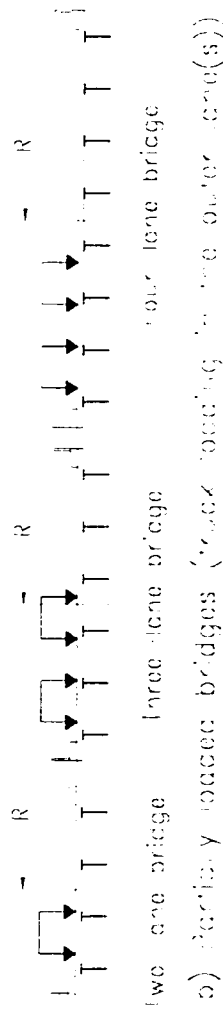
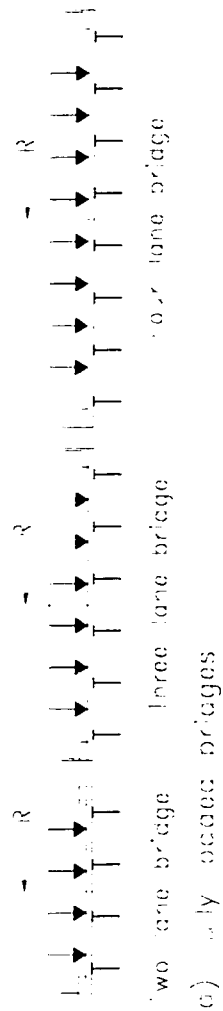
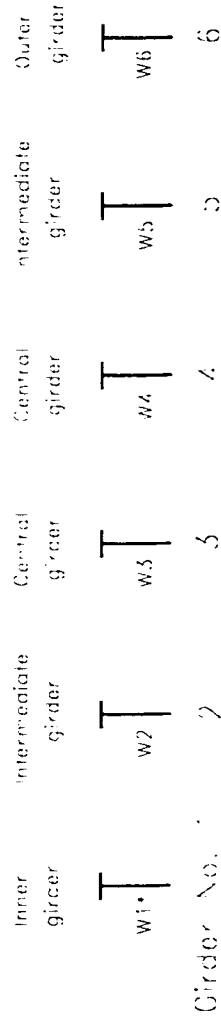


Fig. 6.6. Access cases considered in the present study



(a) Cross section of three box bridge

3-



(b) Identified girders for flexure stress distribution

W1* Web

Fig. 4.5. Identified girders for flexure stress distribution

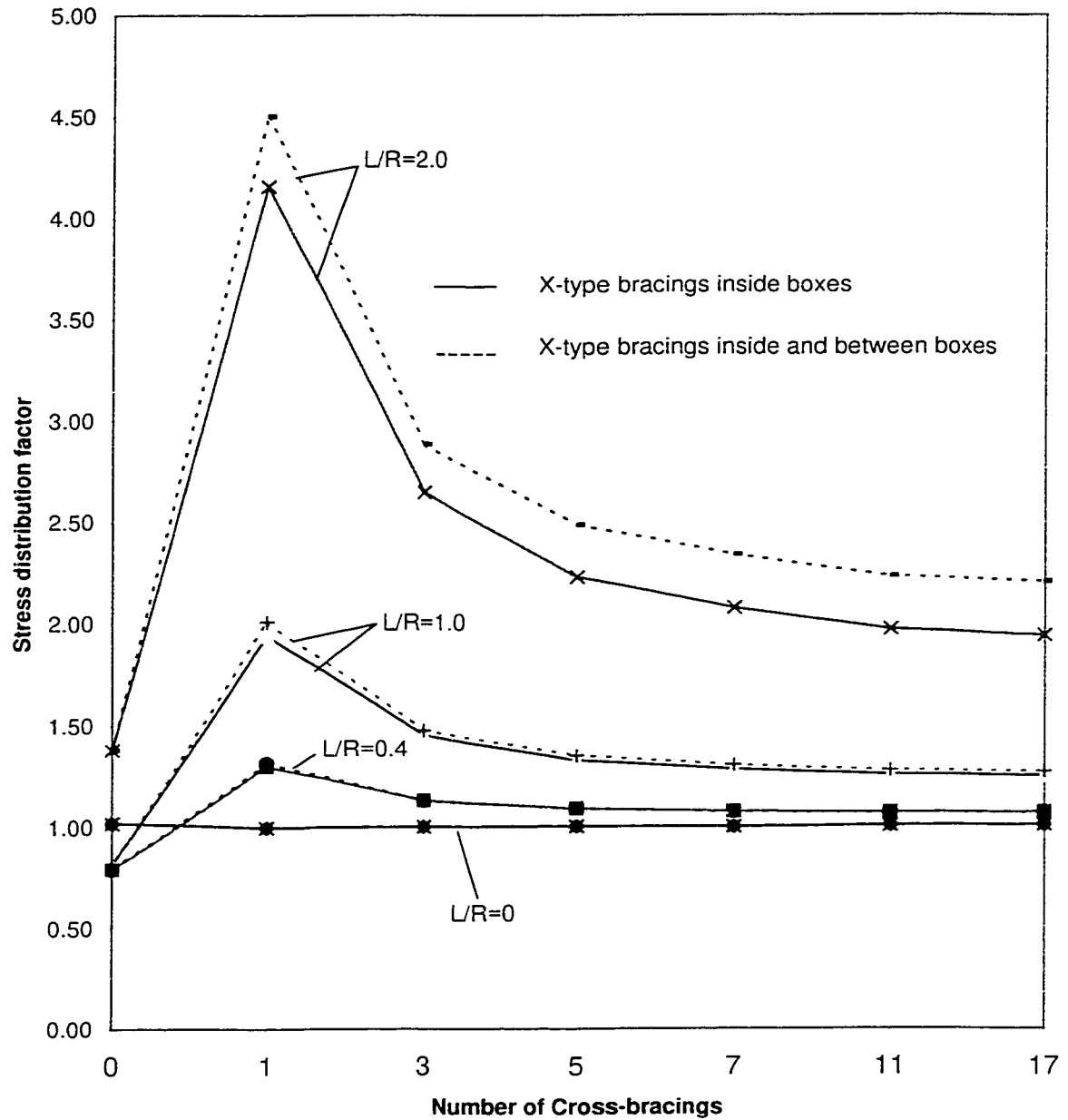


Fig.5.1. Effect of number of cross-bracing system on stress distribution factor of the outer girder for a two-lane, two-box bridge of 60 m under dead load

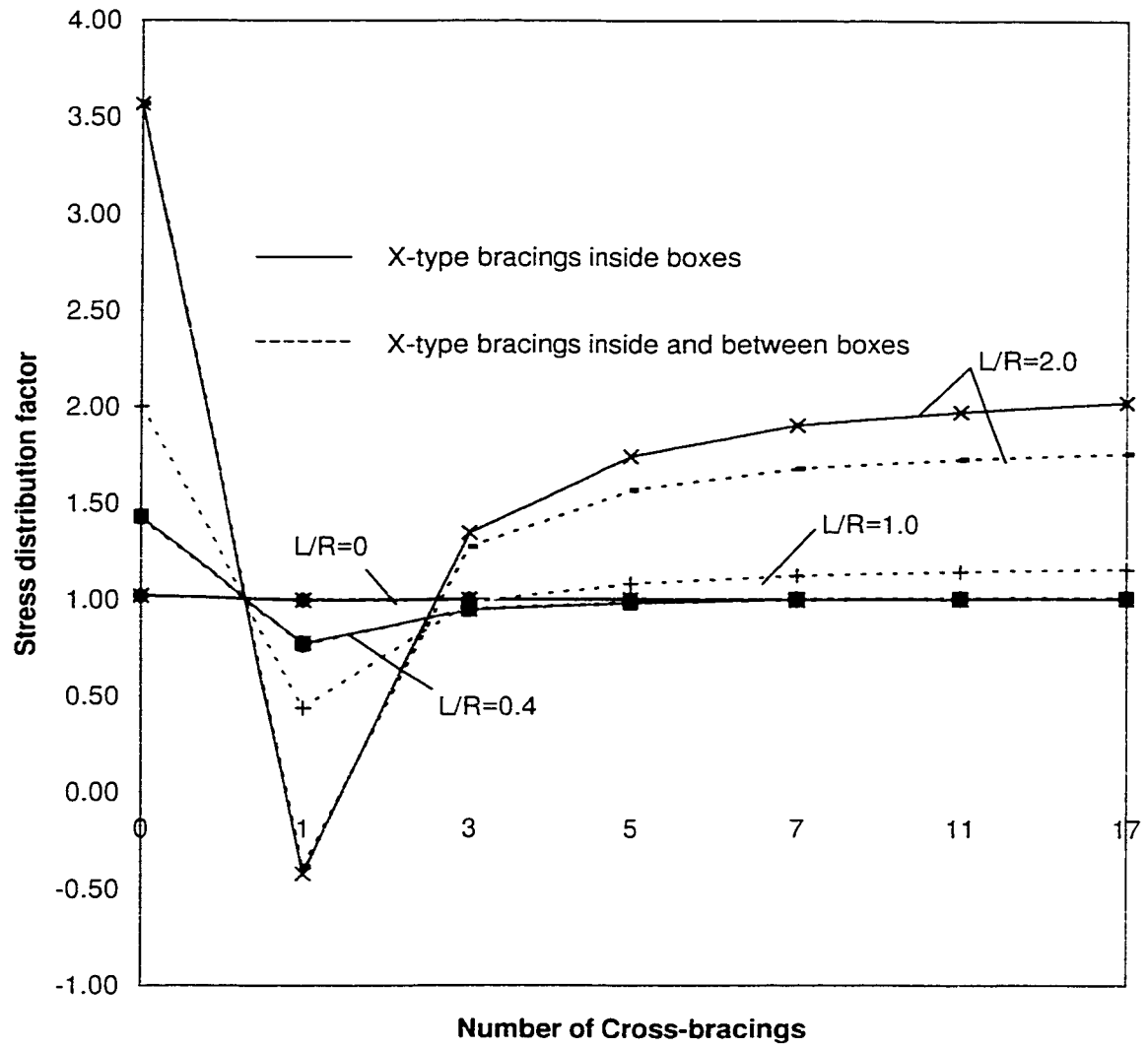


Fig.5.2 Effect of Number of Cross-bracing systems on stress distribution factor of inner girder of two-lane, two-box bridge of 60 m under dead load

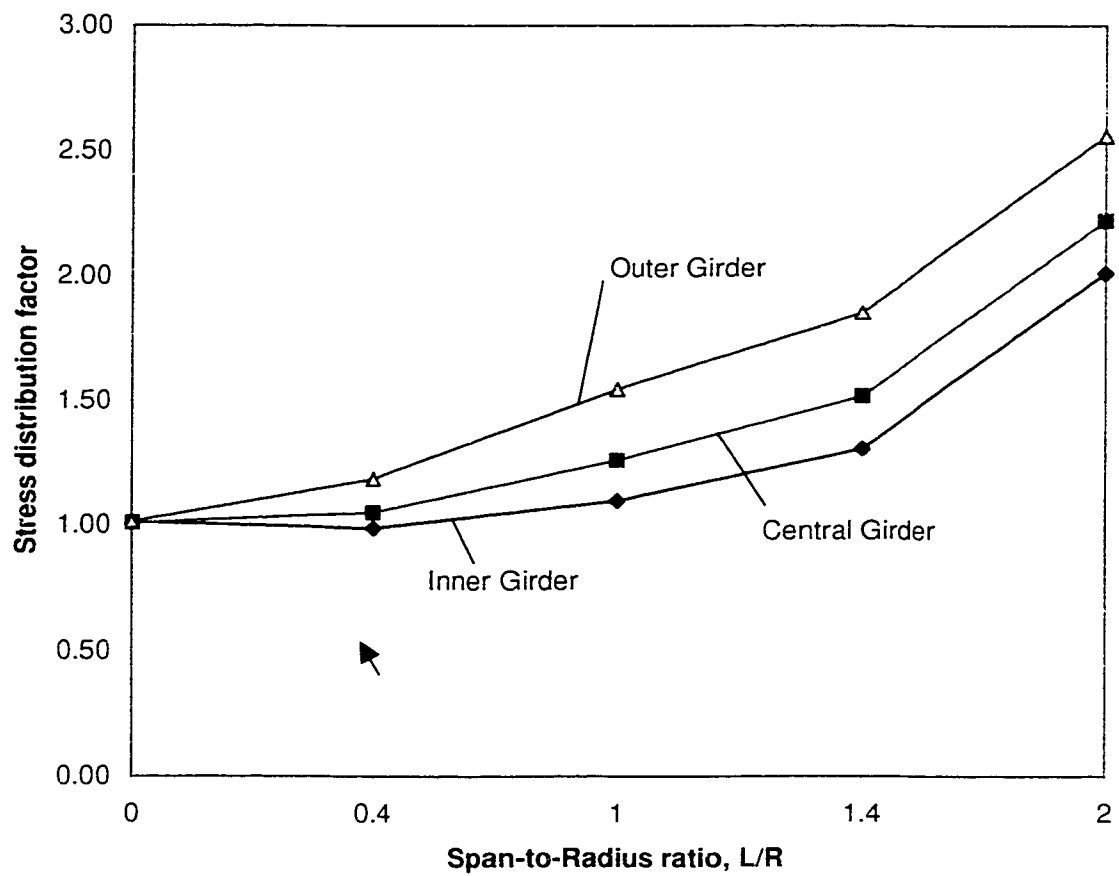


Fig.5.3. Effect of curvature on stress distribution factor of two-lane, four-box and 40 m bridge under dead load

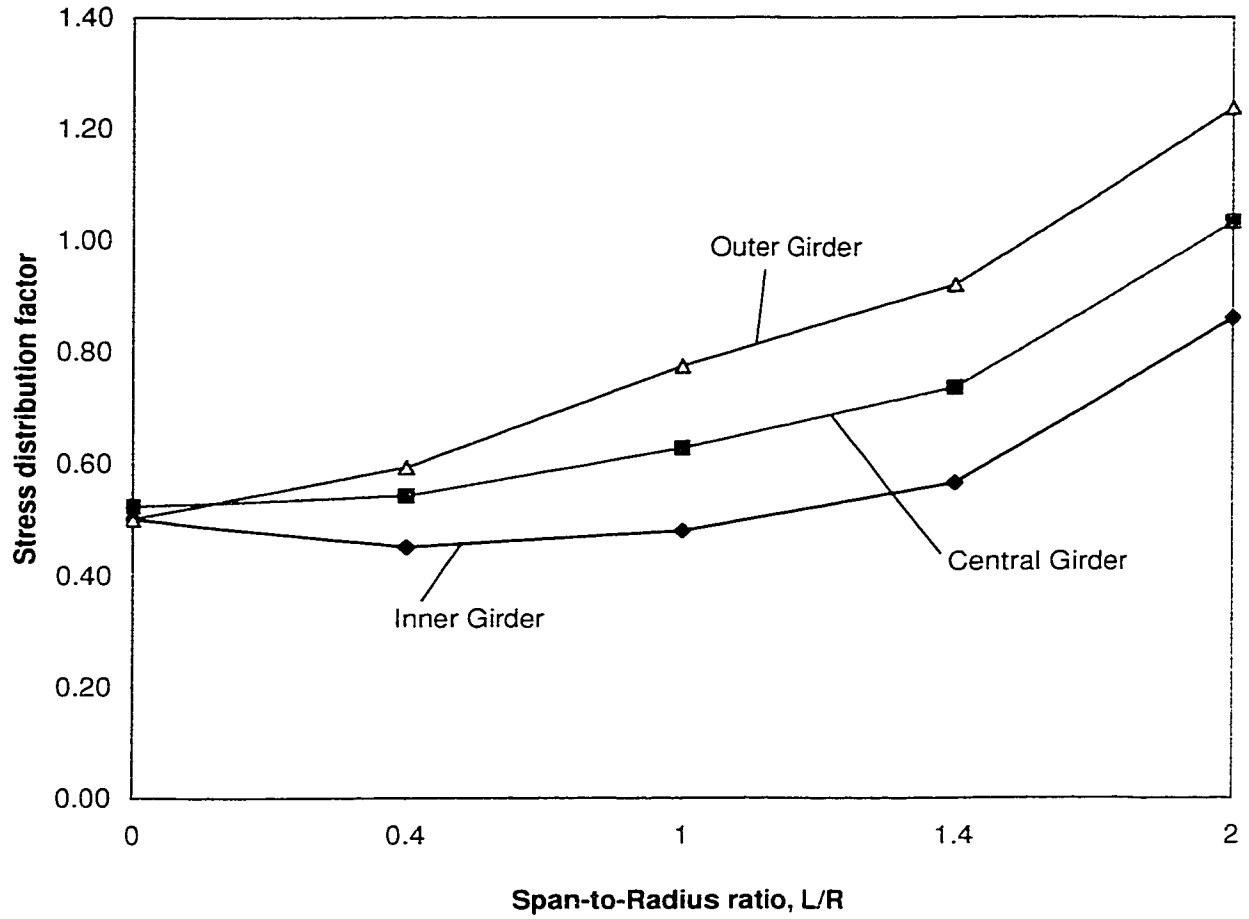


Fig.5.4. Effect of curvature on stress distribution of two-lane, four-box and 40 m bridge under Full AASHTO truck loading

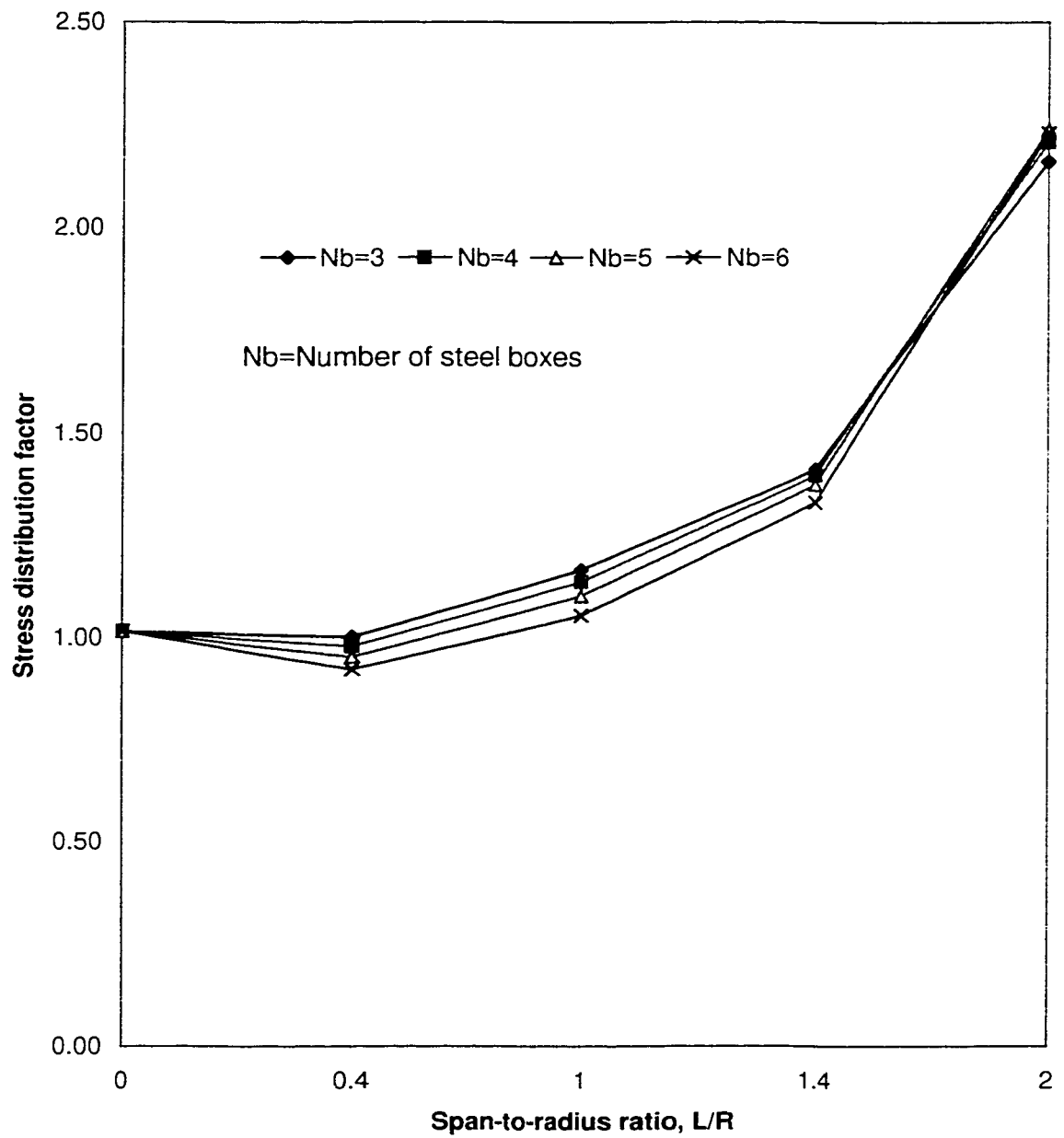


Fig.5.5 Effect of curvature on stress distribution factor for the inner girder of 4-lane bridges of 100 m span under dead load

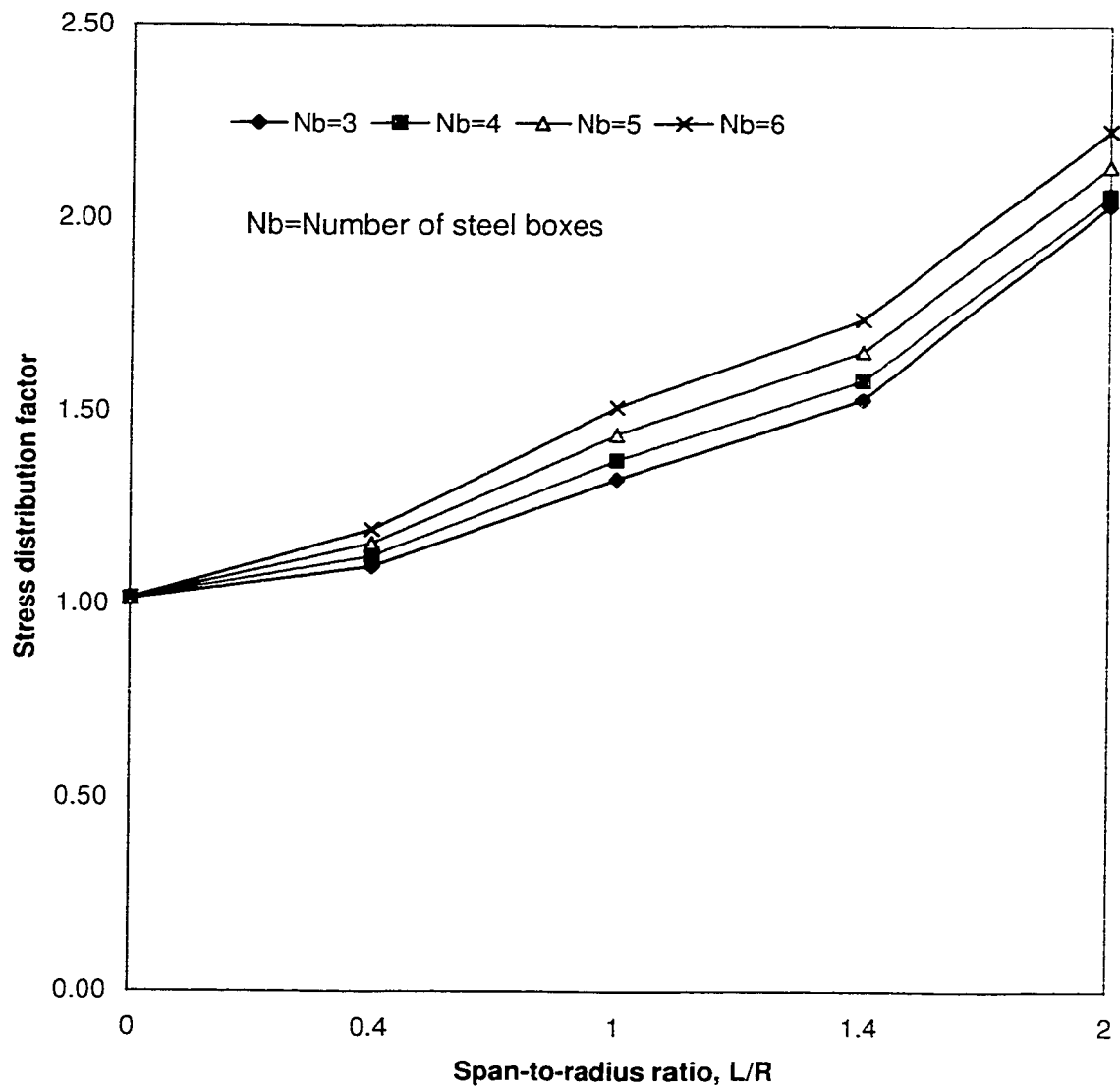


Fig.5.6 Effect of curvature on stress distribution for the outer girder of four-lane bridges of 100 m span under dead load

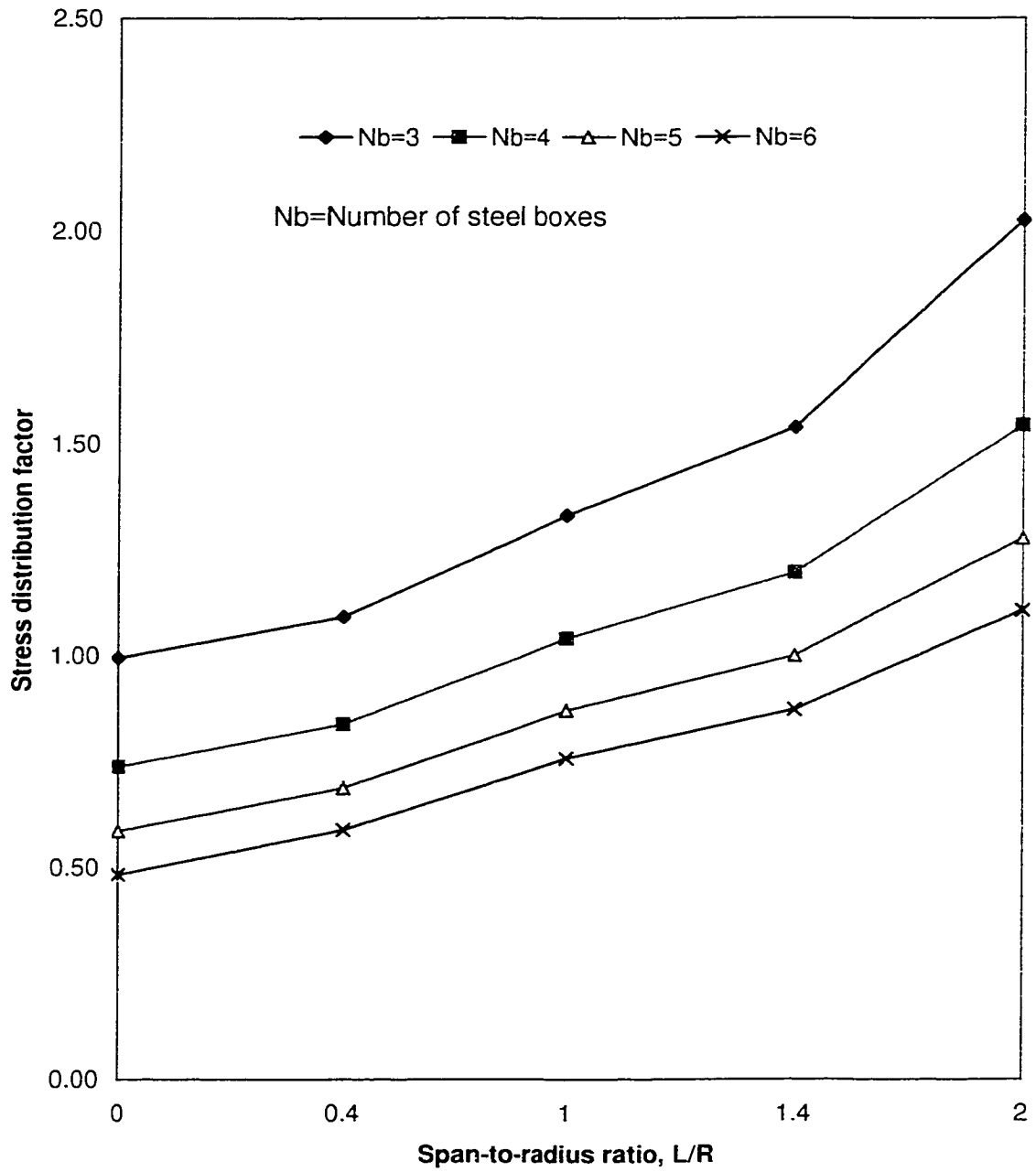


Fig.5.7. Effect of curvature on stress distribution for the outer girder of four-lane bridges of 100 m span under full AASHTO truck loading

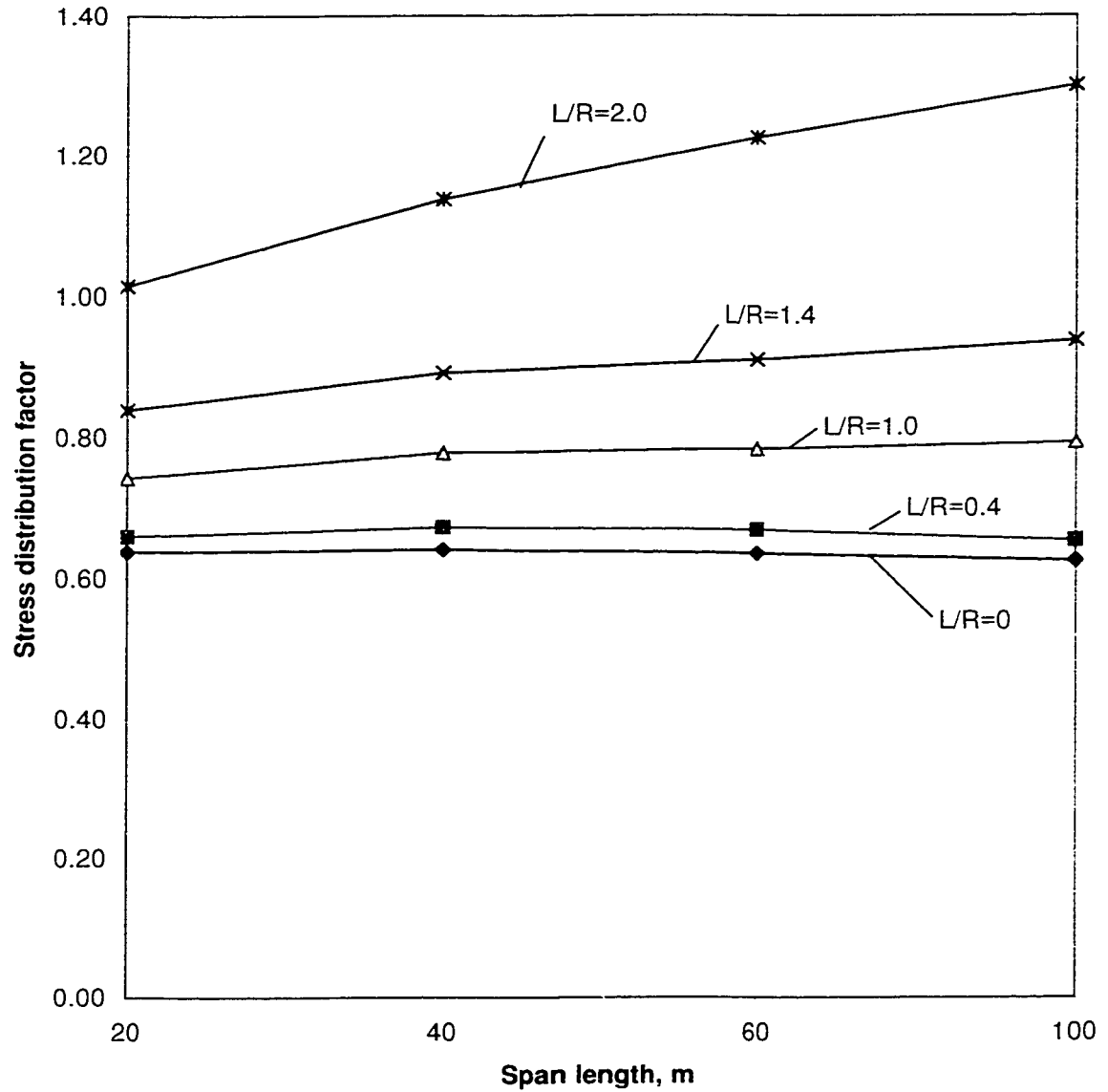


Fig.5.8. Effect of span length on the stress distribution factor for the central girders of four-lane, five-box bridges under full AASHTO truck loading

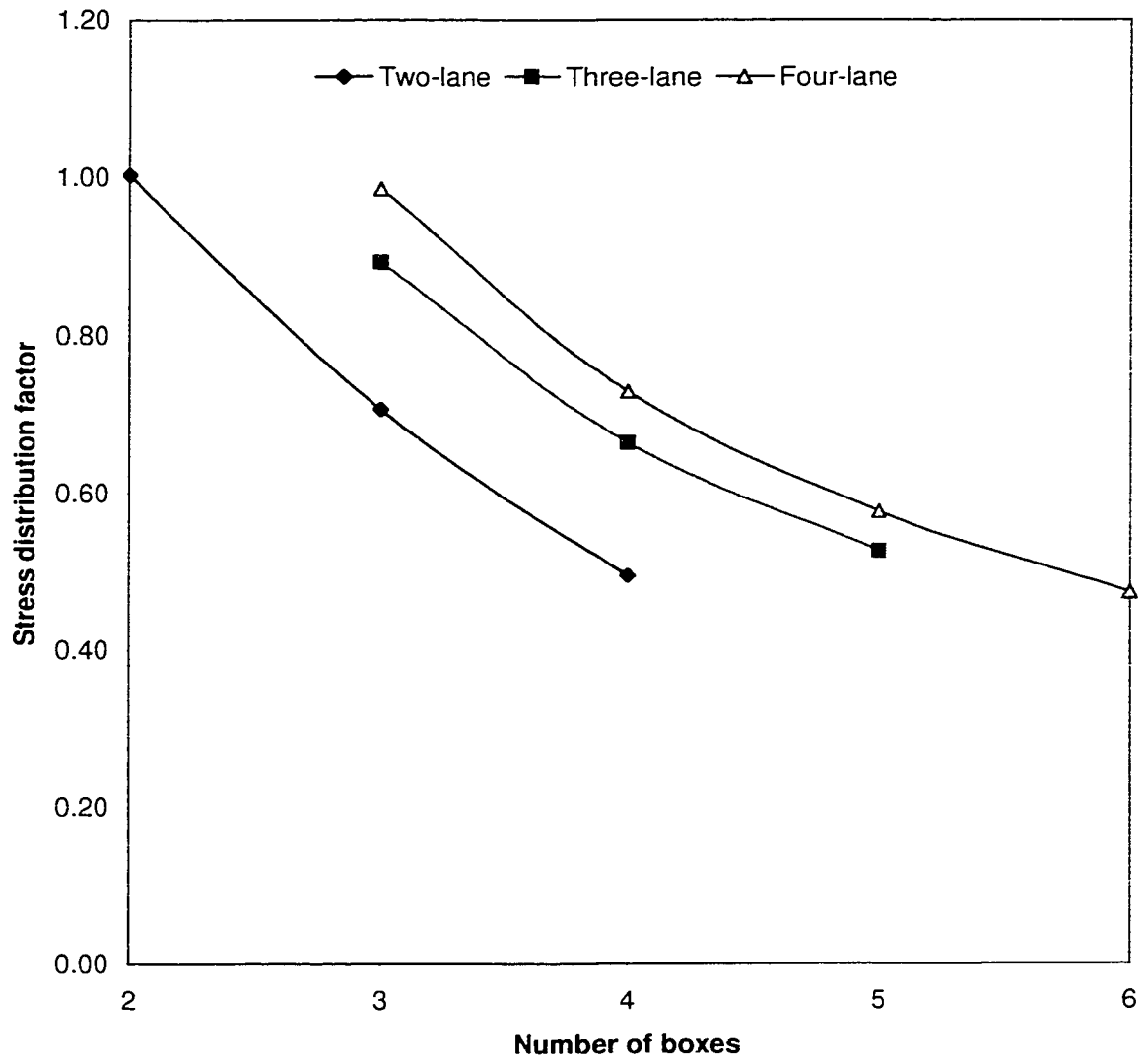


Fig.5.9. Effect of number of boxes on stress distribution factor for the outer girder of straight bridges of 60 m span due to full AASHTO truck loading

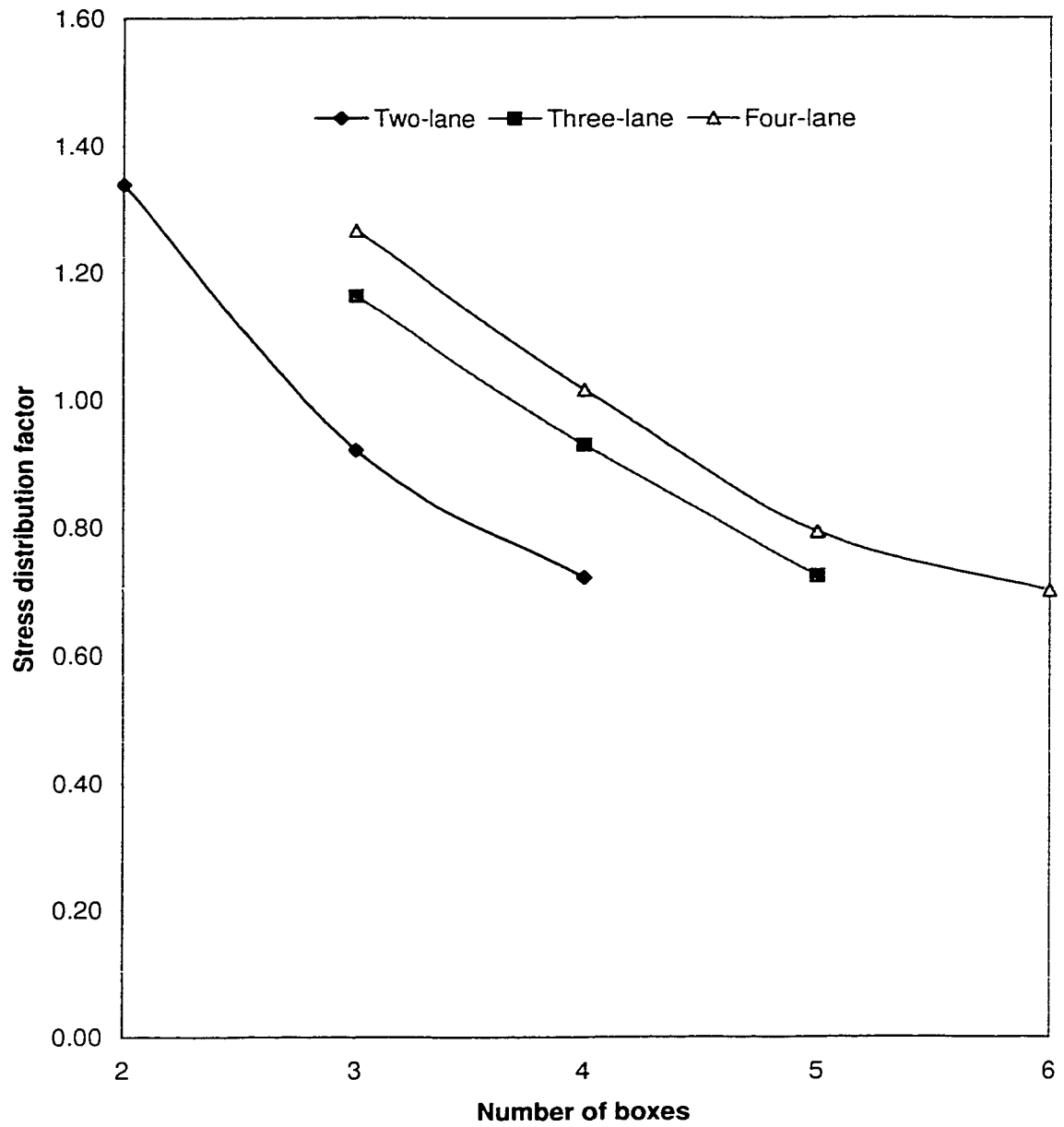


Fig.5.10. Effect of number of traffic lanes on stress distribution factor for the central girders of bridges of 100 m span and $L/R=1$, under full AASHTO truck loading

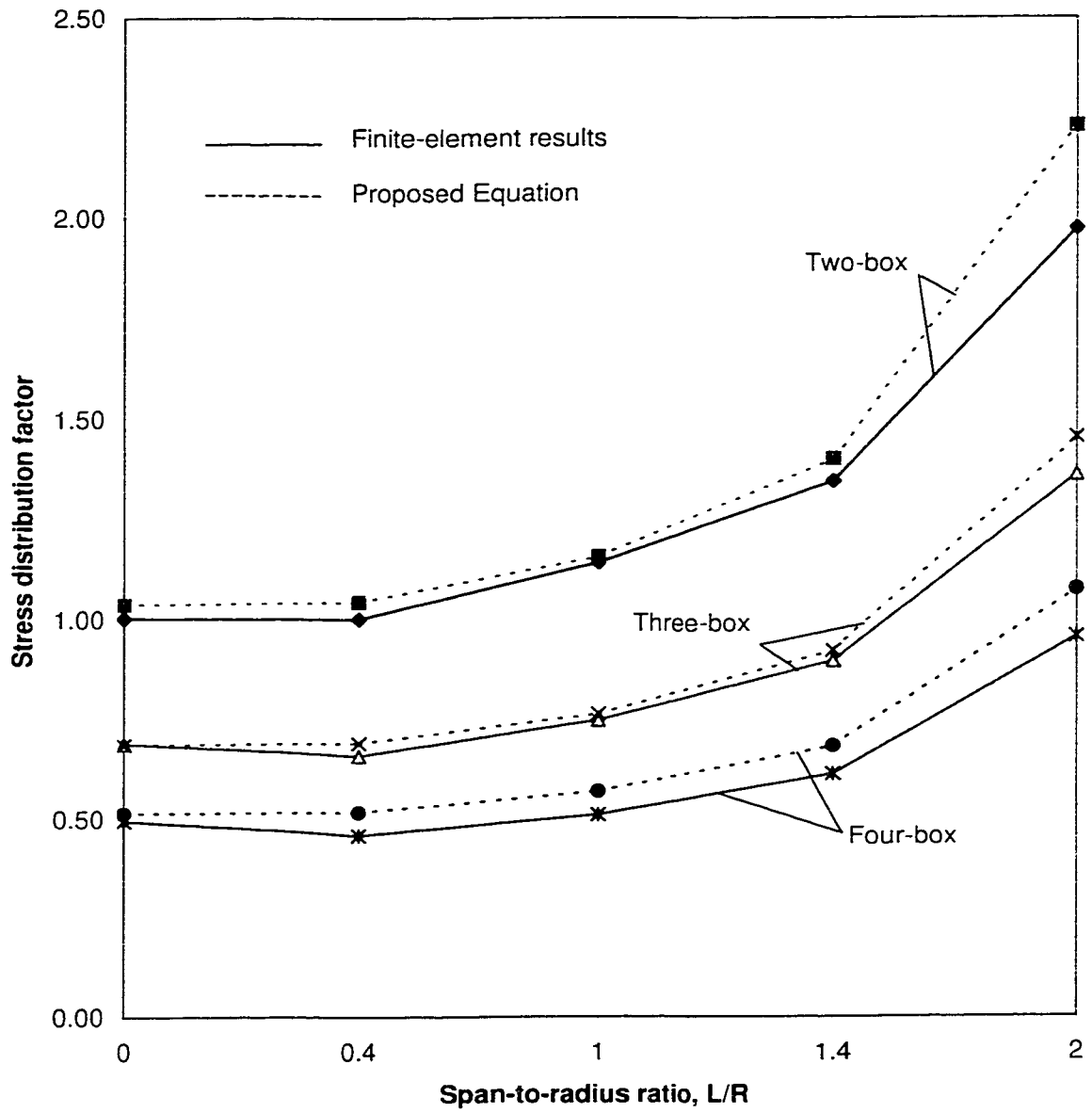


Fig.5.11. Effect of curvature on stress distribution factor for the inner girder of two-lane bridges of 60 m span under full AASHTO truck loading

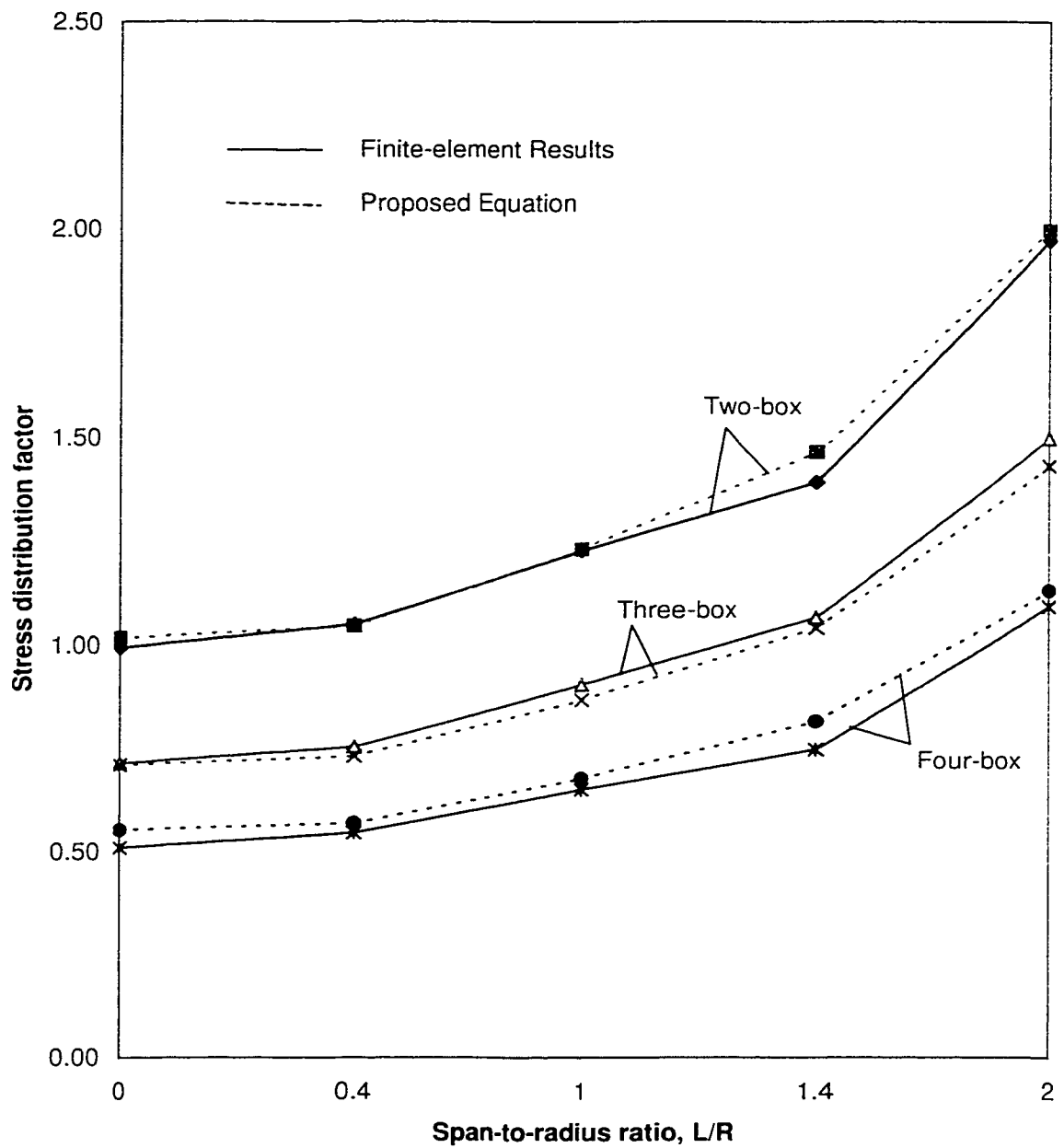


Fig.5.12. Effect of curvature on stress distribution factor for the internal girders of two-lane bridges of 60 m span under full AASHTO truck loading

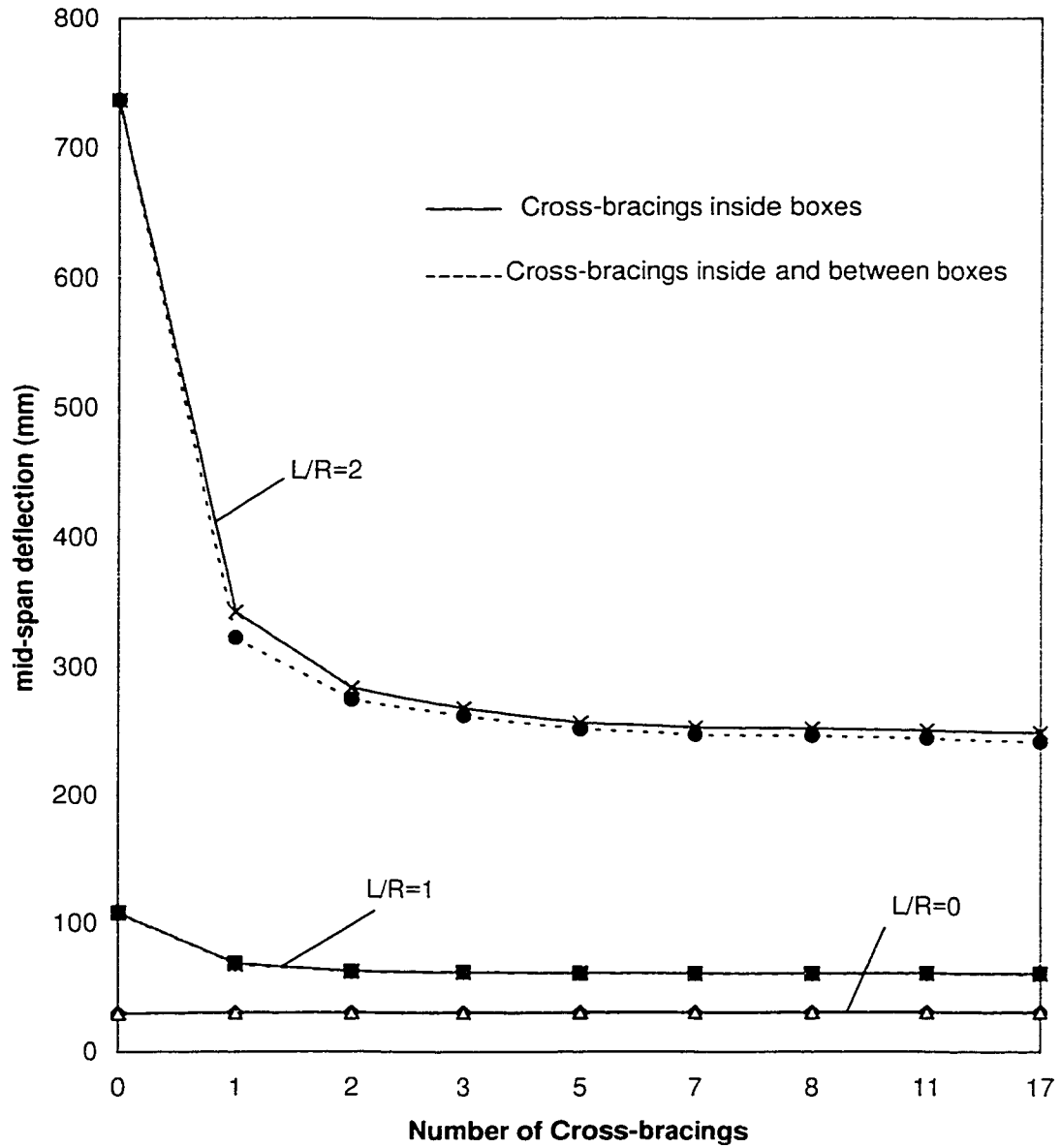


Fig.5.13. Effect of Number of cross-bracings on the mid-span deflection of the outer girder of two-lane, two-box bridges of 60 m span under full AASHTO truck load

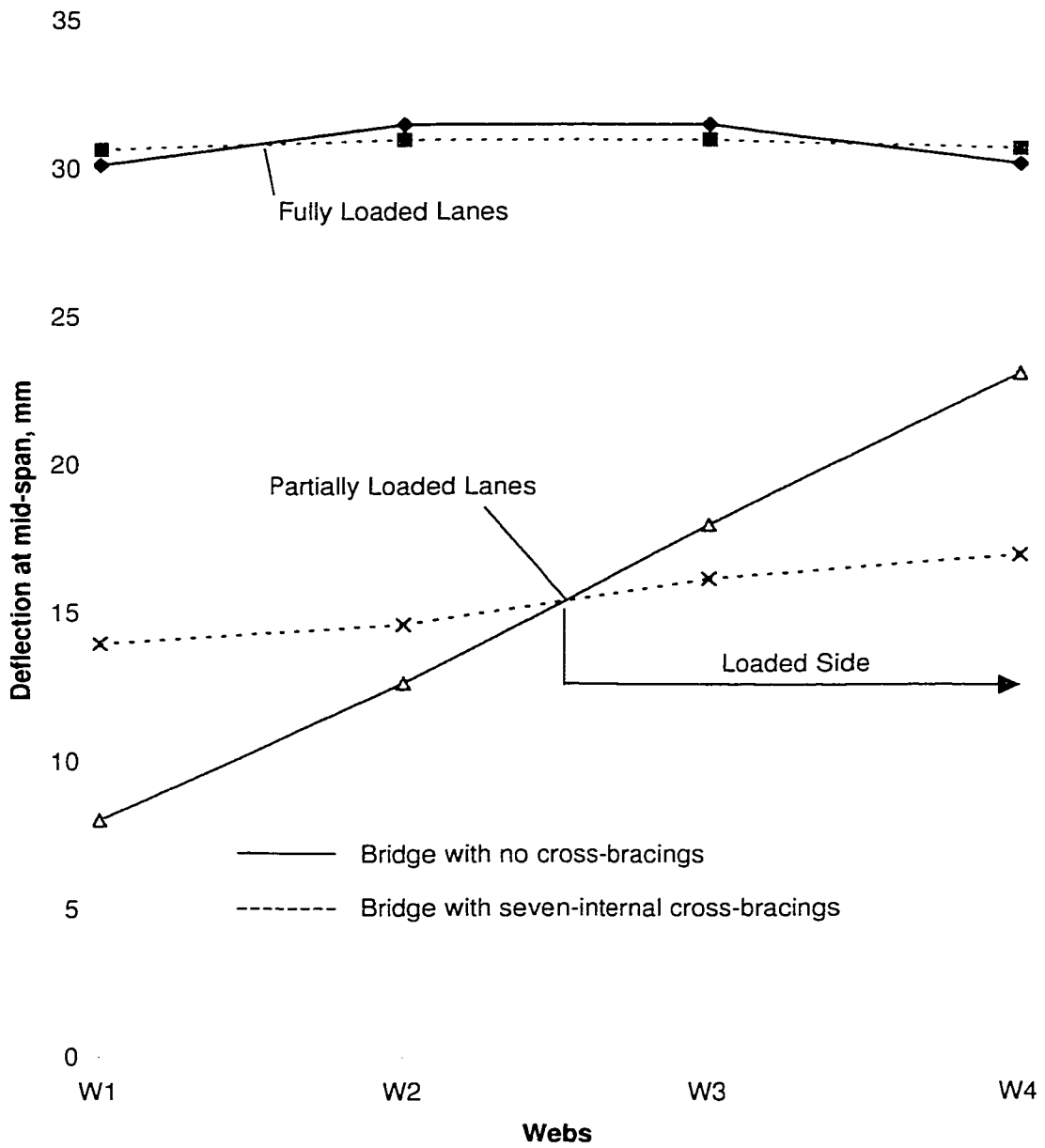


Fig.5.14. Effect of Number of Cross-bracings on mid-span web deflection of straight two-lane, two-box bridges of 60 m span

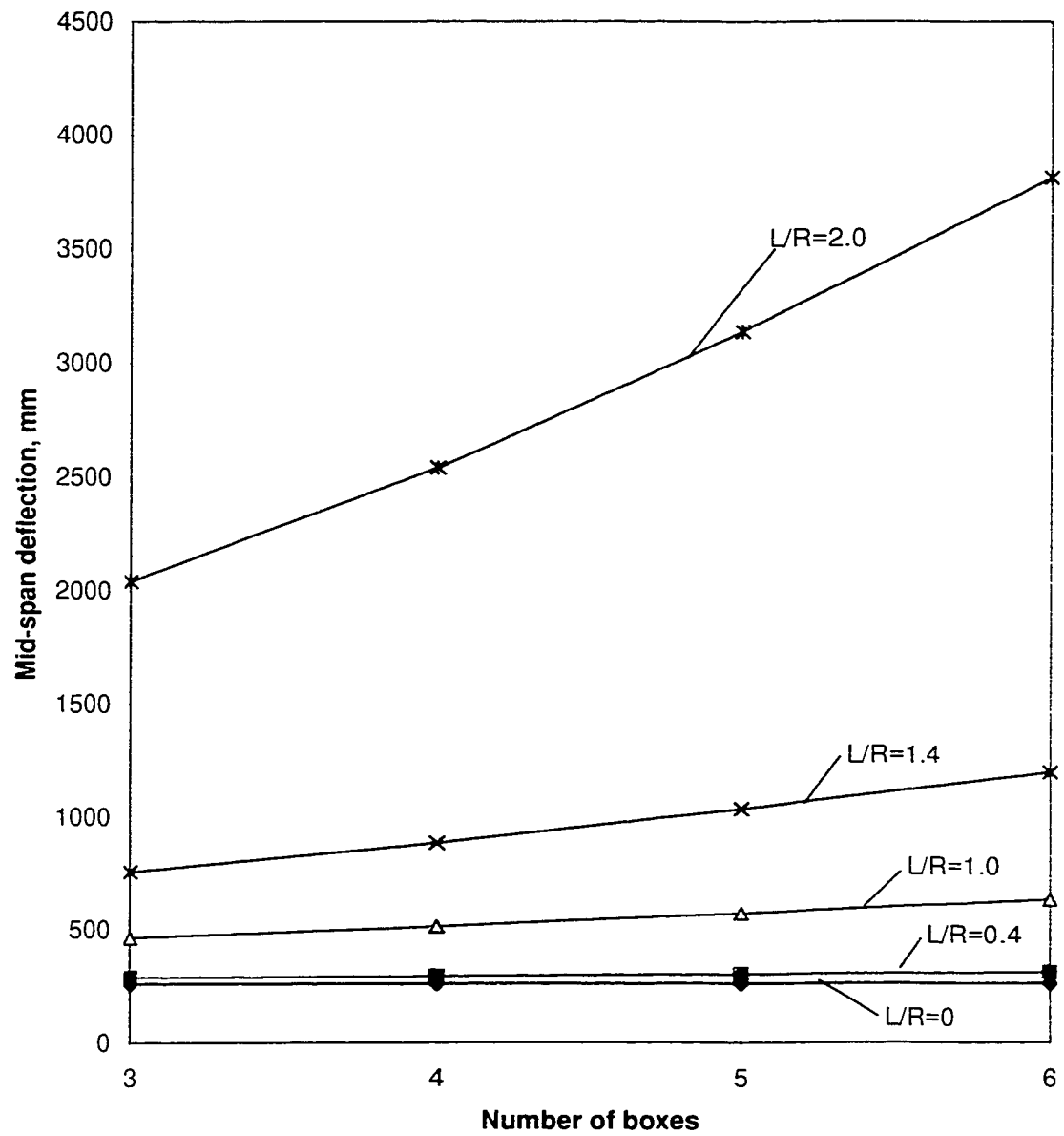


Fig.5.15. Effect of Number of boxes on the average mid-span deflection of four-lane bridges of 100 m span under dead load

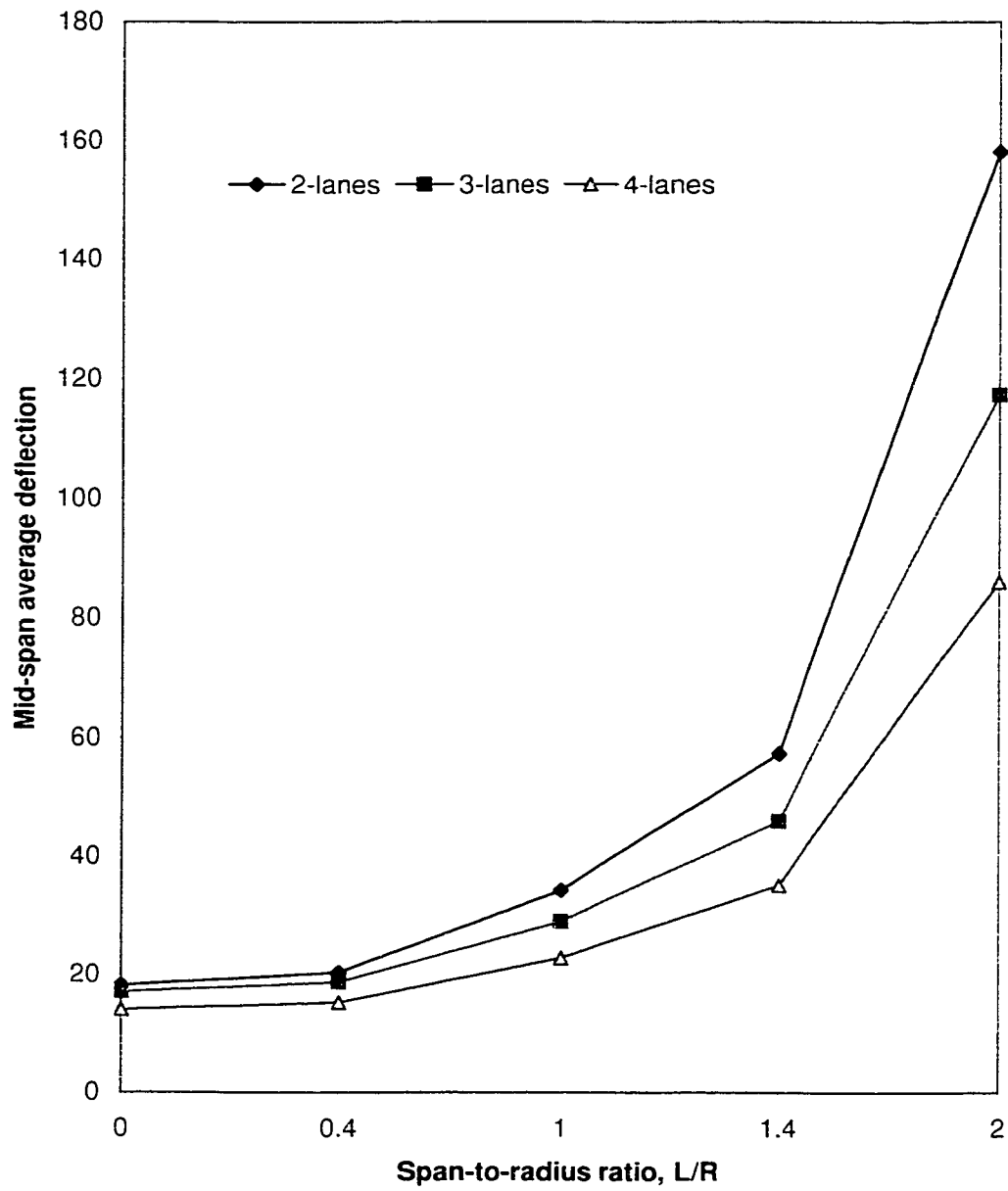


Fig. 5.16. Effect of Number of traffic lanes on the average mid-span deflection for four-box bridges of 40 m span under full AASHTO truck loading

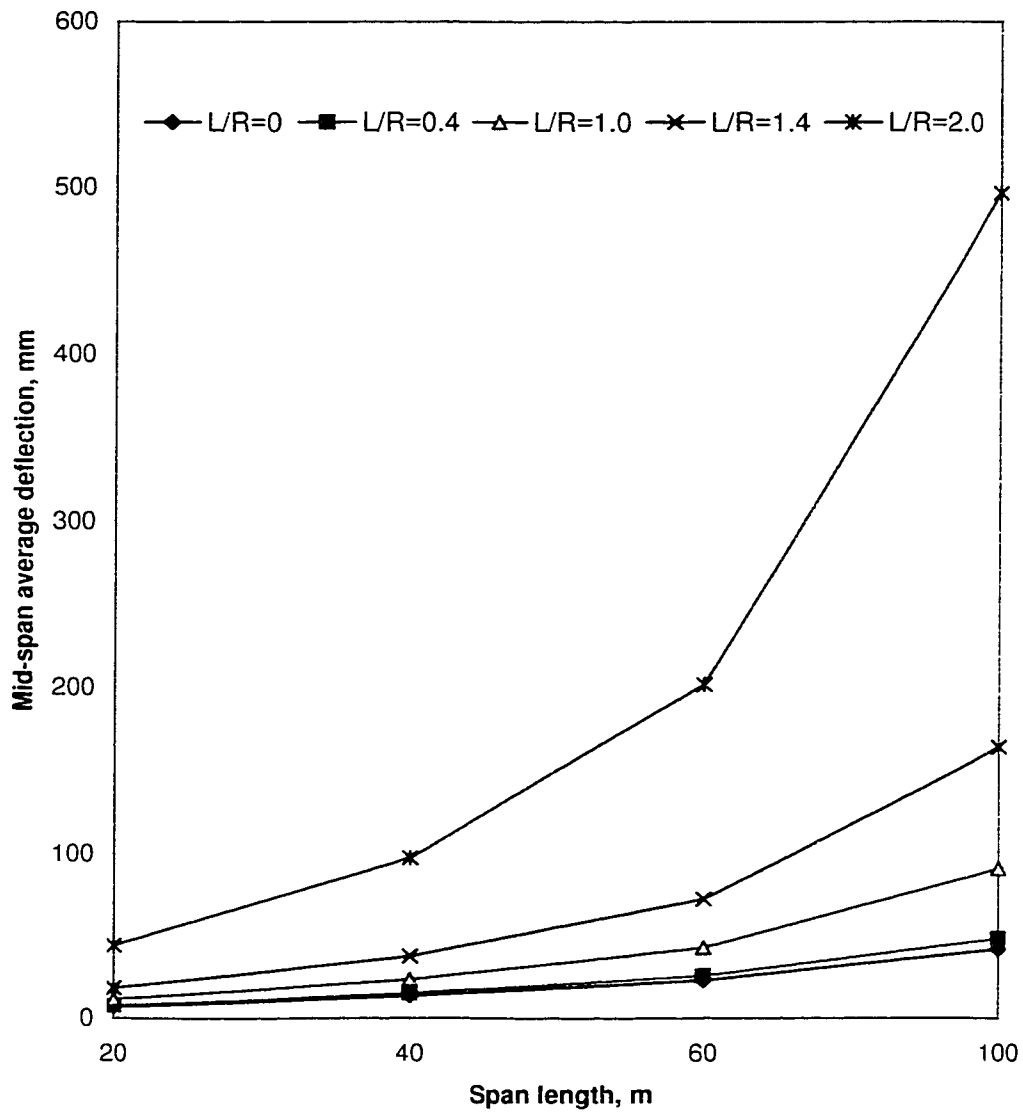
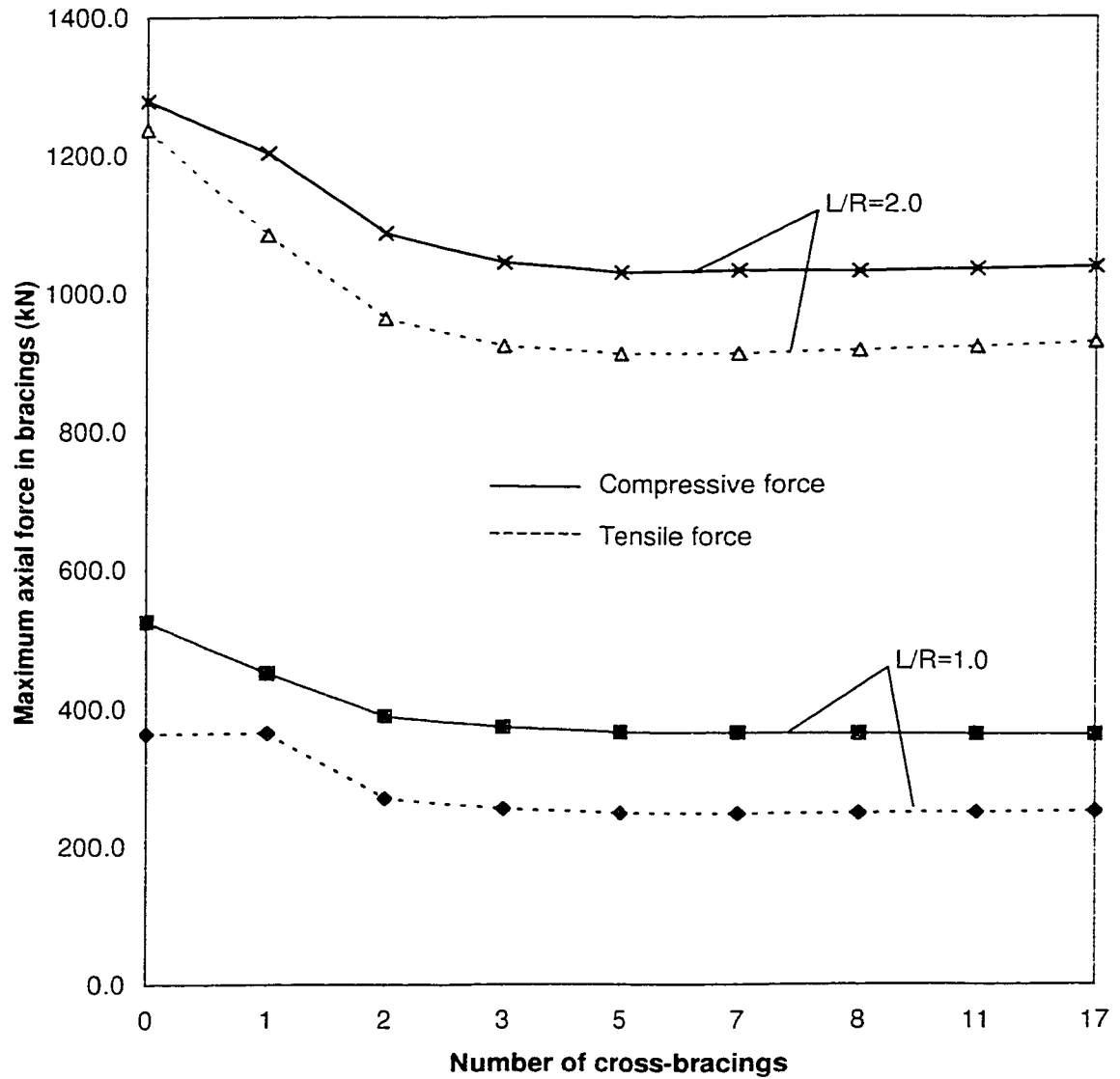


Fig.5.17. Effect of span length on the mid-span average deflection of four-lane, five-box bridges under full AASHTO truck loading



5.18. Effect of the number of cross-bracing systems on the maximum axial force in bracings of two-lane, two-box bridges of 60 m span under full AASHTO truck loading

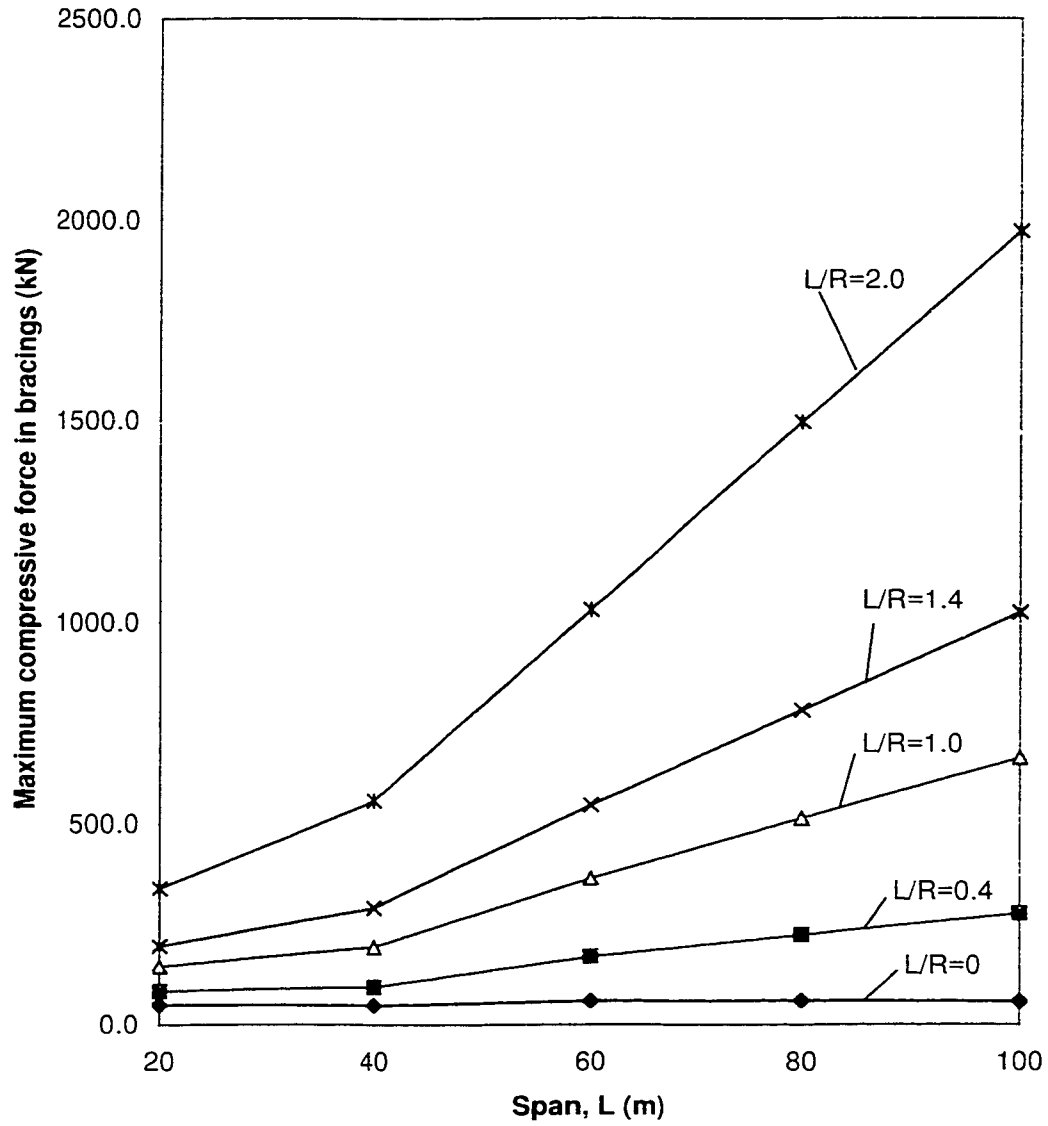


Fig.5.19. Effect of span on the maximum compressive force in bracings of two-lane, two-box bridges under full AASHTO truck loading

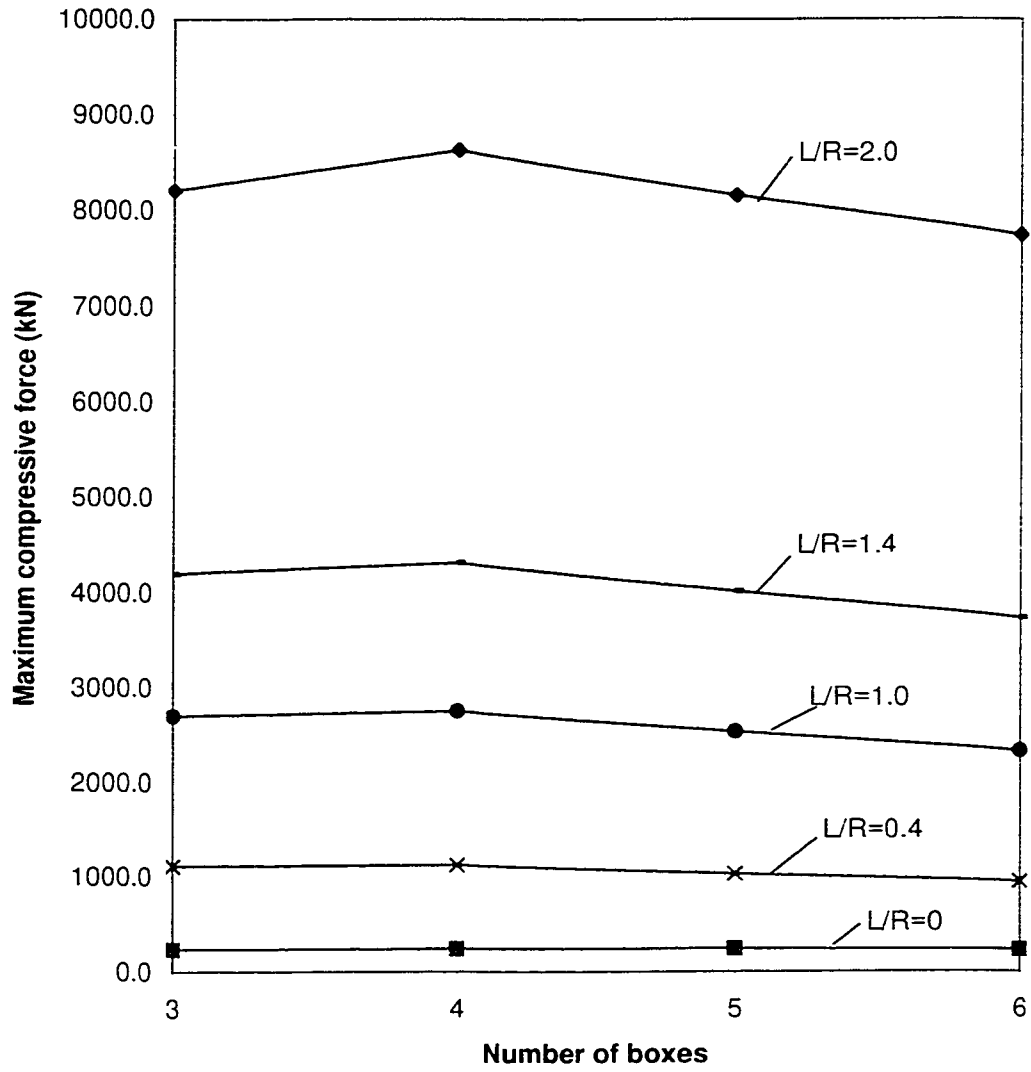


Fig.5.20. Effect of number of boxes on maximum compressive force in bracings of four-lane bridges of 100 m span under dead load

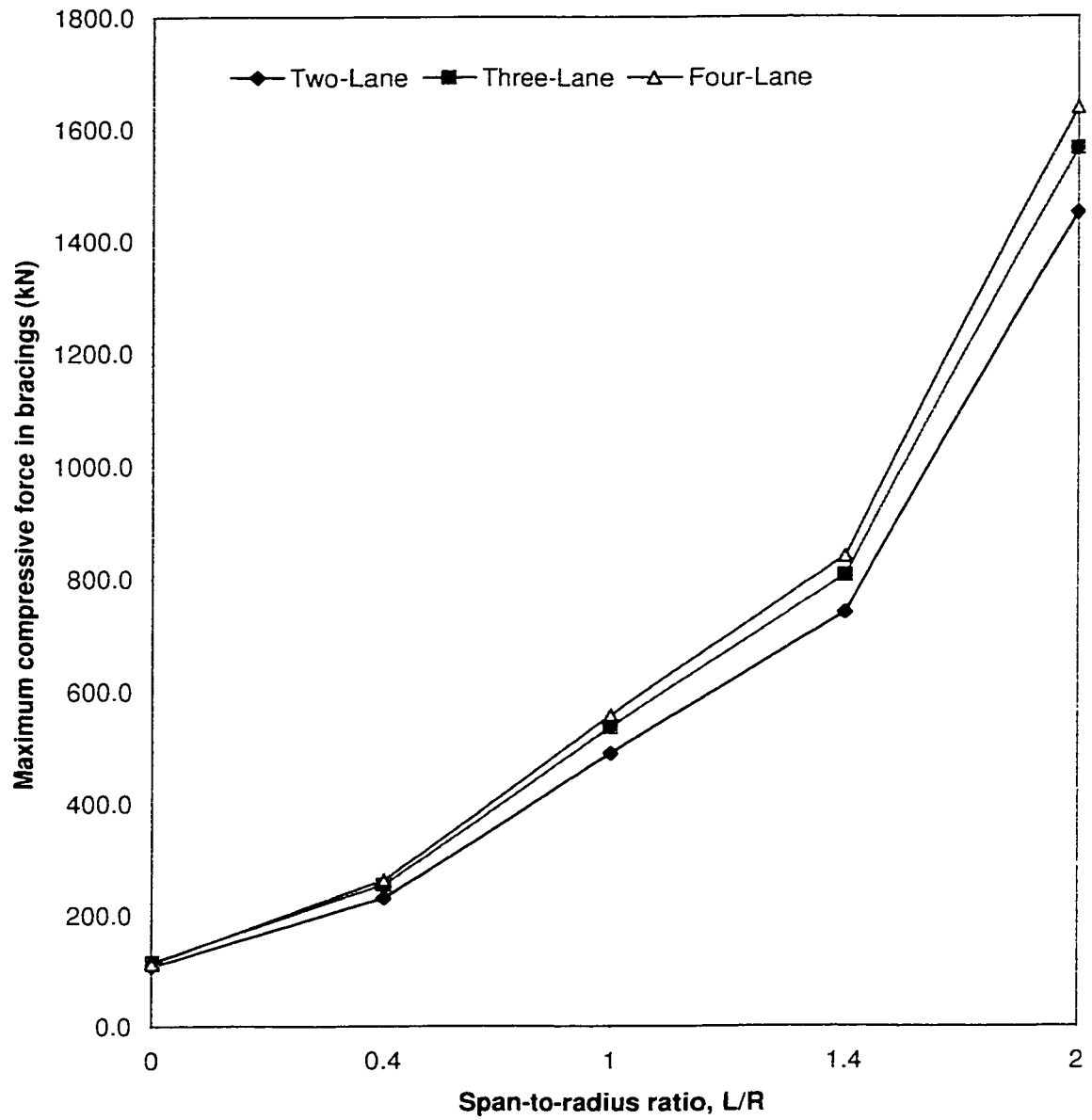


Fig.5.21. Effect of Number of traffic lanes on maximum compressive force in bracings of four-box bridges of 40 m span under dead load

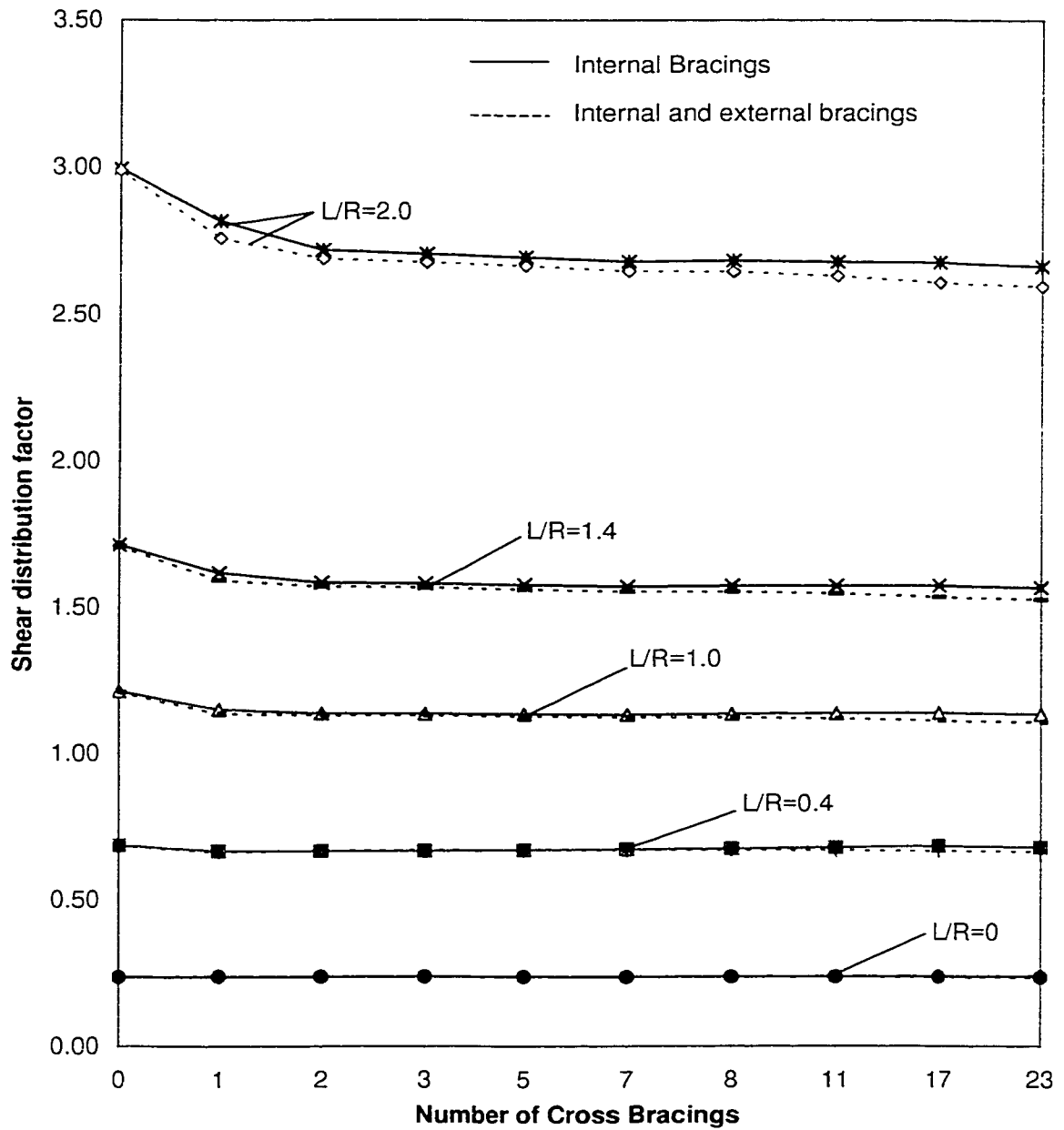


Fig.5.22. Effect of Number of Cross Bracings on shear forces carried by outer web of two-lane,two-box, 60 m bridges , under dead load condition

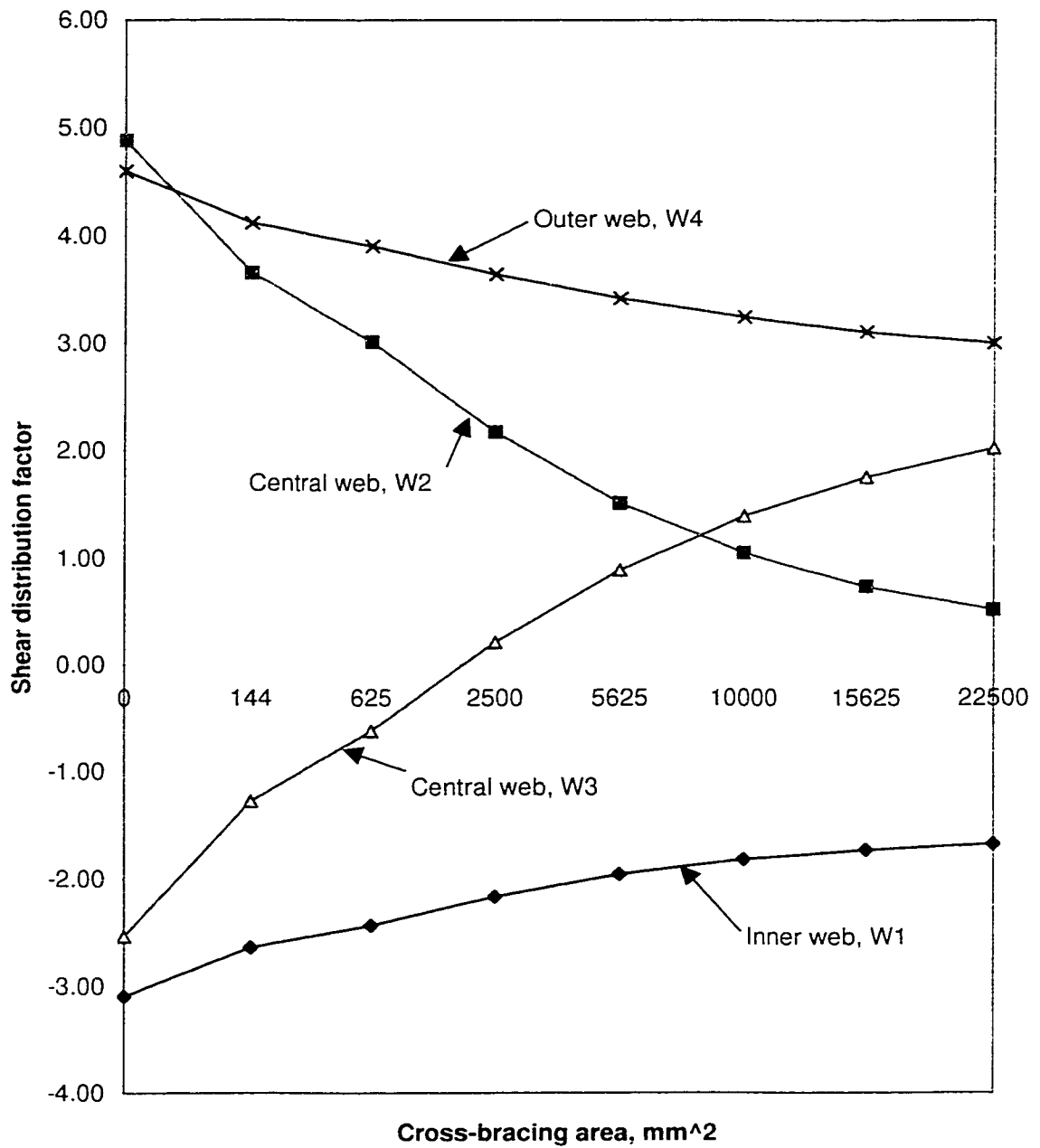


Fig.5.23. Effect of cross-bracing area on the shear force carried by the webs of two-lane, two-box curved bridges of 60 m and L/R=1 under full AASHTO truck loading

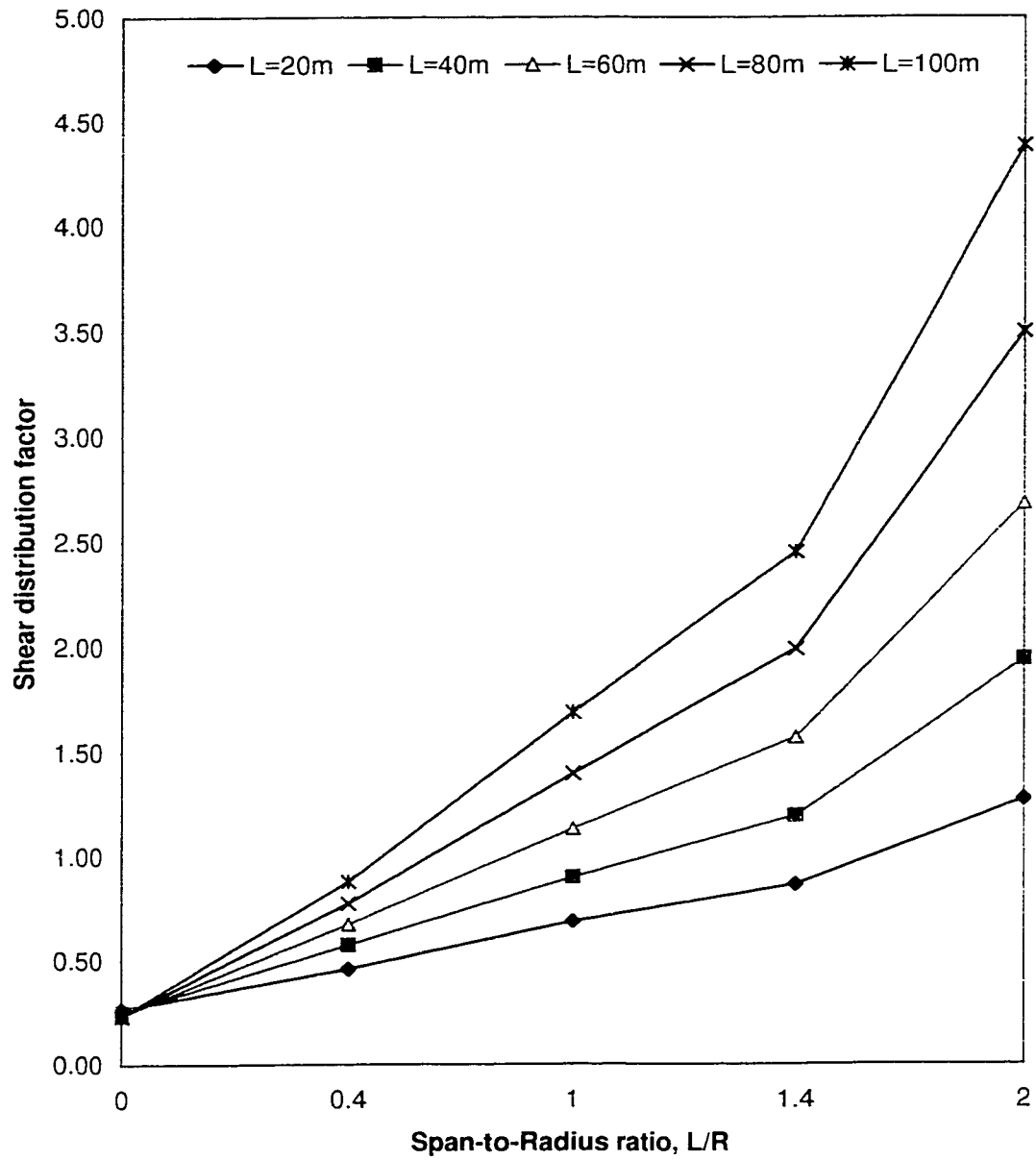


Fig.5.24. Effect of curvature on shear distribution factor for the outer web of two-lane, two-box bridges due to dead load

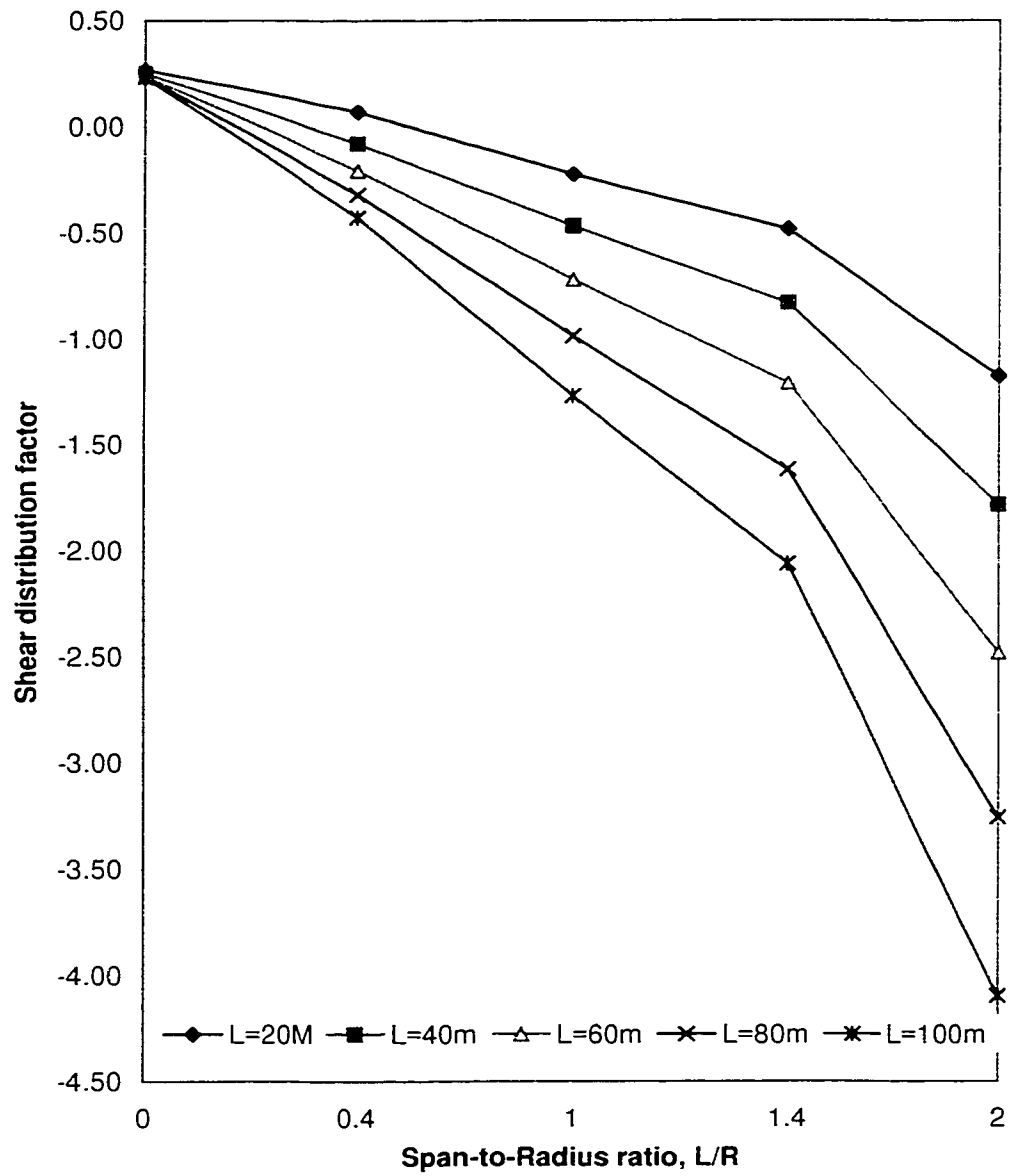


Fig.5.25. Effect of curvature on shear distribution factor for the inner web of two-lane, two-box bridges due to dead load

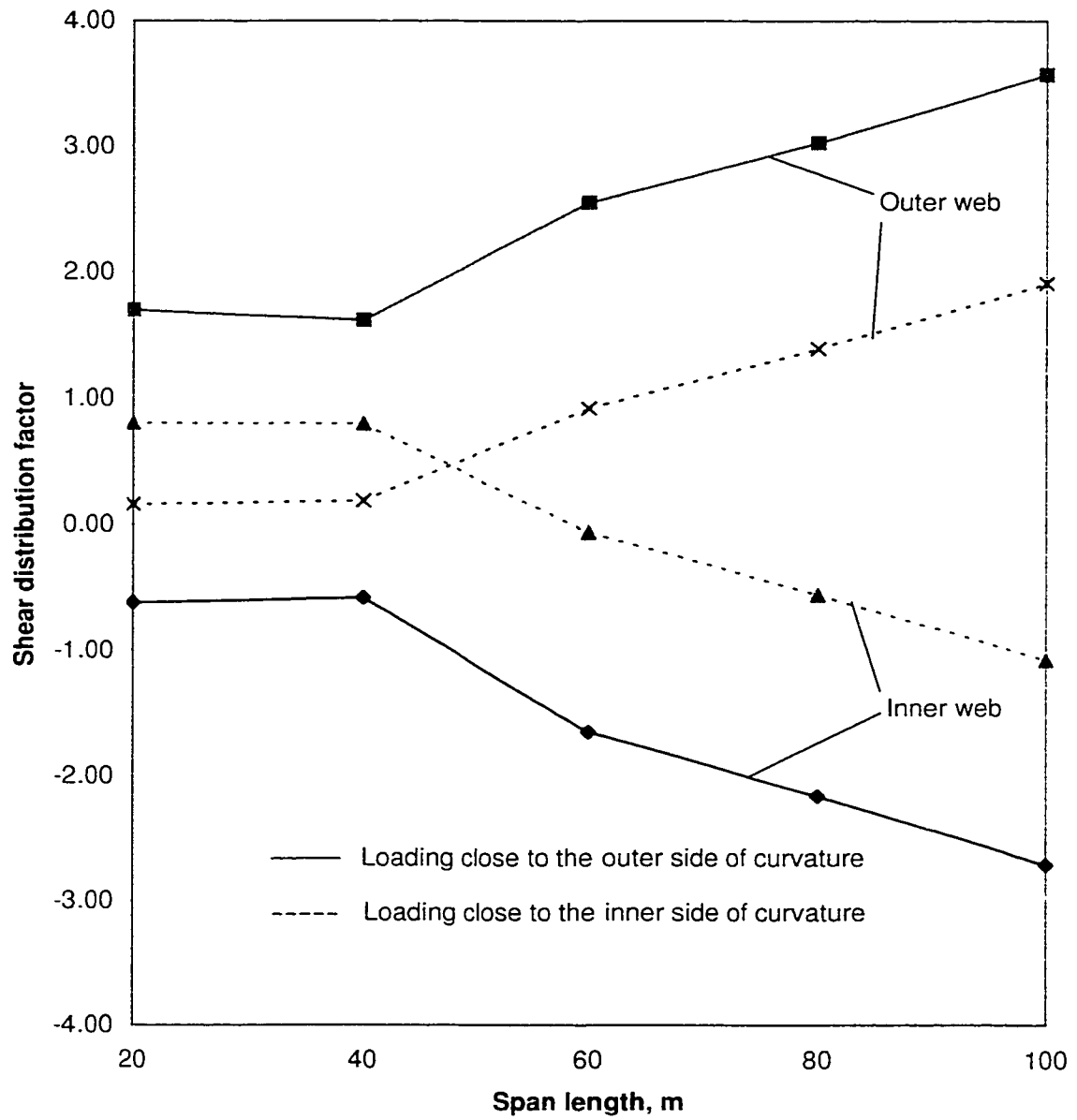


Fig.5.26. Effect of span length on shear distribution of two-lane, two-box curved bridge, with $L/R=1.0$, under partial AASHTO truck loading

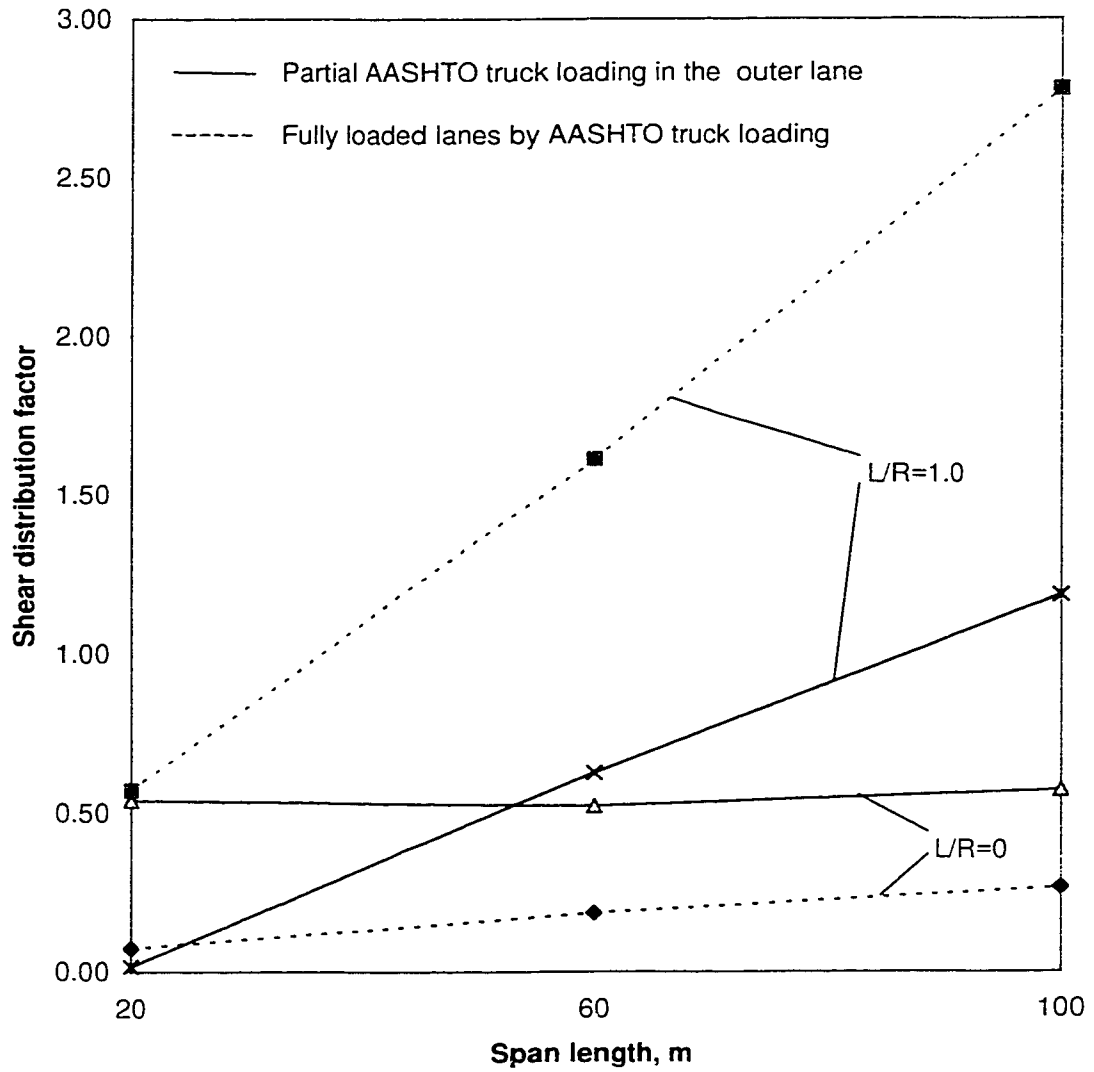


Fig.5.27. Effect of span length on shear distribution for the outer web of two-lane, four-box bridges under AASHTO truck loading

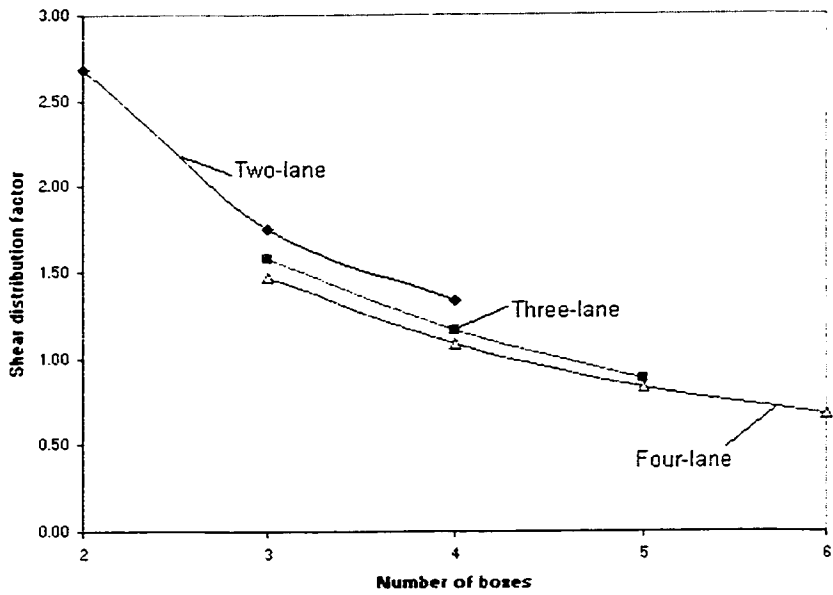


Fig.5.28. Effect of number of boxes on the shear distribution factor for the outer web of curved bridges of 60 m span , with L/R = 2, under dead load

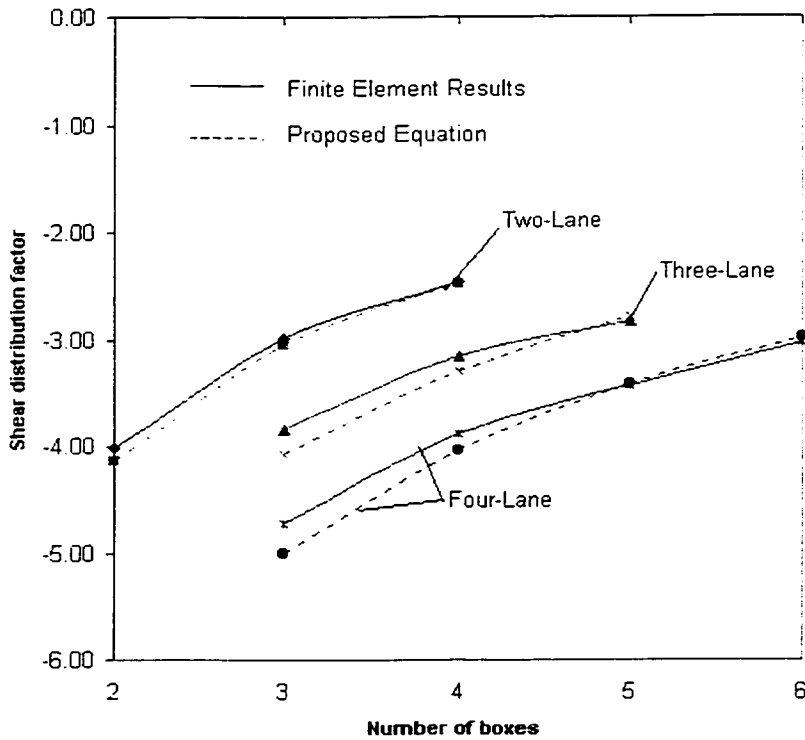


Fig.5.29. Effect of number of boxes on shear distribution factor of the inner web in curved bridges of 100 m span, with L/R=1, due to full AASHTO truck loading

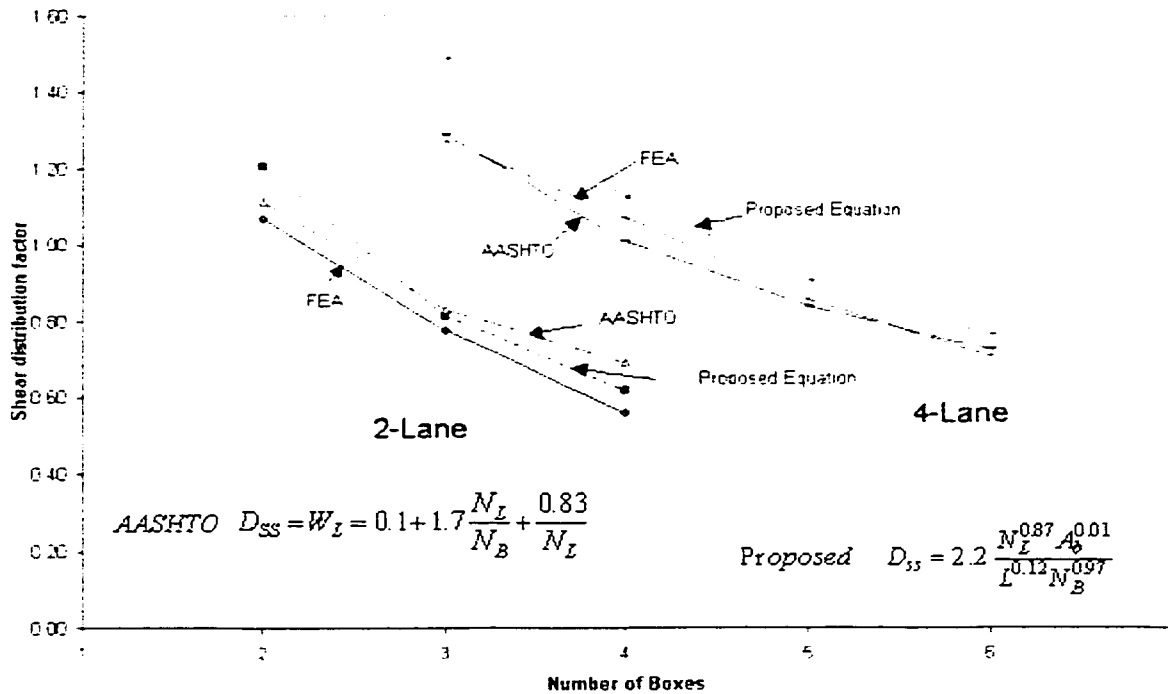


Fig.5.30. Effect of number of boxes on shear force carried by the central webs of straight bridges of 60 m with 100 mm X 100 cross-bracings due to full AASHTO loading: AASHTO formula versus Proposed equation

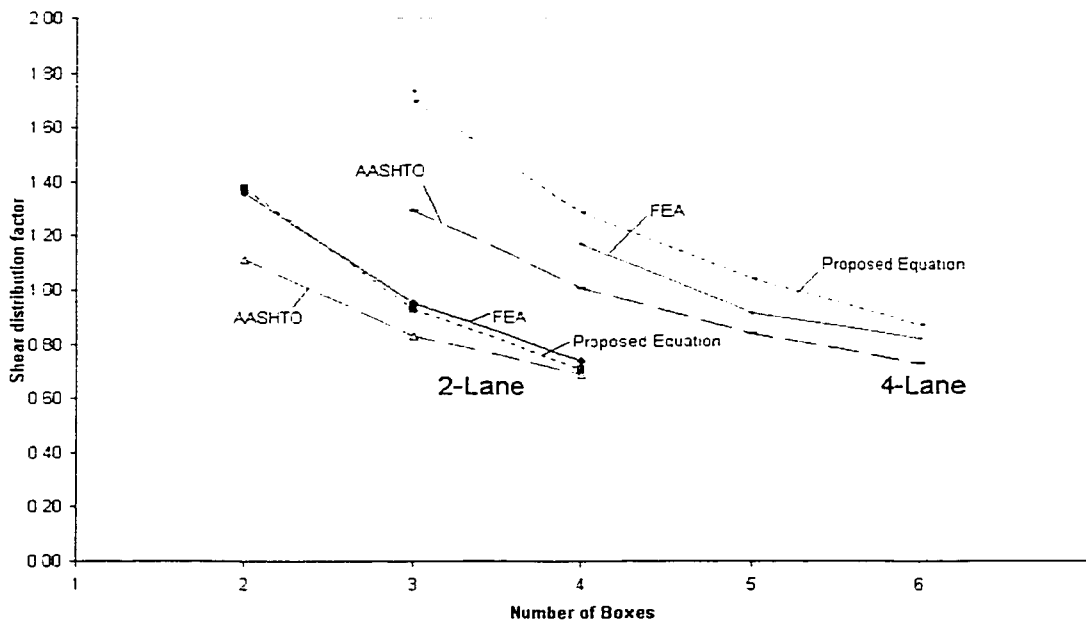


Fig.5.30. Effect of number of boxes on shear force carried by the central webs of straight bridges of 20 m with 100 mm X 100 cross-bracings due to full AASHTO loading: AASHTO formula versus Proposed equation

APPENDIX A.1

Geometries of the Bridge Prototypes Used in the Parametric Study

Table A.1.1. Geometries of bridge prototypes of 20 m span

Span. m	No. of lanes	No. of boxes	Cross-sectional dimensions, mm								
			A	B	C	D	F	t ₁	t ₂	t ₃	t ₄
20	2	2	9300	2325	300	800	1025	16	10	15	225
20	2	3	9300	1550	300	800	1025	11	8	15	225
20	2	4	9300	1160	300	800	1025	10	8	14	225
20	3	3	13050	2175	300	800	1025	16	10	17	225
20	3	4	13050	1630	300	800	1025	12	8	16	225
20	3	5	13050	1305	300	800	1025	10	8	16	225
20	4	3	16800	2800	300	800	1025	21	14	17	225
20	4	4	16800	2100	300	800	1025	16	10	18	225
20	4	5	16800	1680	300	800	1025	13	10	18	225
20	4	6	16800	1400	300	800	1025	11	10	18	225

Table A.1.2. Geometries of bridge prototypes of 40 m span

Span. m	No. of lanes	No. of boxes	Cross-sectional dimensions, mm								
			A	B	C	D	F	t ₁	t ₂	t ₃	t ₄
40	2	2	9300	2325	375	1600	1825	28	14	18	225
40	2	3	9300	1550	375	1600	1825	19	10	18	225
40	2	4	9300	1160	375	1600	1825	14	8	18	225
40	3	3	13050	2175	375	1600	1825	28	14	20	225
40	3	4	13050	1630	375	1600	1825	21	11	19	225
40	3	5	13050	1305	375	1600	1825	17	10	18	225
40	4	3	16800	2800	375	1600	1825	37	19	22	225
40	4	4	16800	2100	375	1600	1825	28	14	21	225
40	4	5	16800	1680	375	1600	1825	22	11	22	225
40	4	6	16800	1400	375	1600	1825	19	9	22	225

Table A.1.3. Geometries of bridge prototypes of 60 m span

Span. m	No. of lanes	No. of boxes	Cross-sectional dimensions, mm								
			A	B	C	D	F	t ₁	t ₂	t ₃	t ₄
60	2	2	9300	2325	450	2400	2625	40	18	23	225
60	2	3	9300	1550	450	2400	2625	27	12	22	225
60	2	4	9300	1160	450	2400	2625	20	10	21	225
60	3	3	13050	2175	450	2400	2625	40	18	25	225
60	3	4	13050	1630	450	2400	2625	30	14	25	225
60	3	5	13050	1305	450	2400	2625	24	10	25	225
60	4	3	16800	2800	450	2400	2625	53	24	27	225
60	4	4	16800	2100	450	2400	2625	40	18	26	225
60	4	5	16800	1680	450	2400	2625	32	14	27	225
60	4	6	16800	1400	450	2400	2625	30	12	27	225

Table A.1.4. Geometries of bridge prototypes of 80 m span

Span. m	No. of lanes	No. of boxes	Cross-sectional dimensions, mm								
			A	B	C	D	F	t ₁	t ₂	t ₃	t ₄
80	2	2	9300	2325	530	3200	3425	52	22	26	225
80	2	3	9300	1550	530	3200	3425	35	15	25	225
80	2	4	9300	1160	530	3200	3425	26	11	25	225
80	3	3	13050	2175	530	3200	3425	52	22	28	225
80	3	4	13050	1630	530	3200	3425	40	17	28	225
80	3	5	13050	1305	530	3200	3425	31	13	29	225
80	4	3	16800	2800	530	3200	3425	69	29	30	225
80	4	4	16800	2100	530	3200	3425	52	22	30	225
80	4	5	16800	1680	530	3200	3425	42	18	29	225
80	4	6	16800	1400	530	3200	3425	38	16	29	225

Table A.1.5. Geometries of bridge prototypes of 100 m span

Span. m	No. of lanes	No. of boxes	Cross-sectional dimensions, mm								
			A	B	C	D	F	t ₁	t ₂	t ₃	t ₄
100	2	2	9300	2325	600	4000	4225	64	26	30	225
100	2	3	9300	1550	600	4000	4225	43	18	30	225
100	2	4	9300	1160	600	4000	4225	32	13	30	225
100	3	3	13050	2175	600	4000	4225	64	26	33	225
100	3	4	13050	1630	600	4000	4225	48	20	33	225
100	3	5	13050	1305	600	4000	4225	38	16	34	225
100	4	3	16800	2800	600	4000	4225	85	35	35	225
100	4	4	16800	2100	600	4000	4225	64	26	35	225
100	4	5	16800	1680	600	4000	4225	51	21	34	225
100	4	6	16800	1400	600	4000	4225	42	18	34	225

APPENDIX A.2

“ABAQUS” Input Data

A.2.1 Input Data Deck for the Linear Response of a 4-lane, 3box, 100 m span curved bridge with a radius of 100 m

```
*HEADING
3BOX CURVED SIMPLY SUPPORTED LINEAR CASE
**DATA CHECK
*PREPRINT,ECHO=YES,MODEL=NO,HISTORY=NO
*Restart,write
*****REFERENCE NODE COORDINATES 4l3b100sc*****
*NODE
1,0,0,0
8001,0,0,-0.15500
56001,0,0,-4.09500
2,-43.91538,80.38656,0.00000
50,-51.96973,95.12995,0.00000
7202,43.91538,80.38656,0.00000
7250,51.96973,95.12995,0.00000
8006,-44.58658,81.61518,-0.15500
56006,-44.58658,81.61518,-4.09500
15206,44.58658,81.61518,-0.15500
63206,44.58658,81.61518,-4.09500
8046,-51.29853,93.90133,-0.15500
56046,-51.29853,93.90133,-4.09500
15246,51.29853,93.90133,-0.15500
63246,51.29853,93.90133,-4.09500
** ***** NODE GEN. FOR END DIAPHRAGM *****
*NGEN,NSET=ORIGIN
8001,56001,8000
*NGEN,NSET=NEND
***left end***
2,50,2
8006,56006,8000
8046,56046,8000
8006,8046,2
16006,16046,2
24006,24046,2
```



```
32006,32046,2
40006,40046,2
48006,48046,2
56006,56046,2
***right end***
7202,7250,2
15206,63206,8000
15246,63246,8000
15206,15246,2
23206,23246,2
31206,31246,2
39206,39246,2
47206,47246,2
55206,55246,2
63206,63246,2
** *****
*NSET,NSET=LEFT6
56006,56014,56022,56030,56038,56046
*NSET,NSET=RIGHT6
63206,63214,63222,63230,63238,63246
*NSET,NSET=REACT
LEFT6,RIGHT6
** *****NODE GEN. FOR TOP SLAB *****
*NGEN,NSET=NPLATET,LINE=C
2,7202,100,1
4,7204,100,1
6,7206,100,1
8,7208,100,1
10,7210,100,1
12,7212,100,1
14,7214,100,1
16,7216,100,1
18,7218,100,1
20,7220,100,1
22,7222,100,1
24,7224,100,1
26,7226,100,1
28,7228,100,1
30,7230,100,1
32,7232,100,1
34,7234,100,1
36,7236,100,1
38,7238,100,1
40,7240,100,1
42,7242,100,1
```

```

44,7244,100,1
46,7246,100,1
48,7248,100,1
50,7250,100,1
** *****NODE GEN. FOR TOP FLANGE *****
*NGEN,NSET=NTOPFLNG,LINE=C
8006,15206,100,8001
8014,15214,100,8001
8022,15222,100,8001
8030,15230,100,8001
8038,15238,100,8001
8046,15246,100,8001
** ***** NODE GEN. FOR WEBS *****
*NGEN,NSET=NWEB,LINE=C
16006,23206,100,16001
16014,23214,100,16001
16022,23222,100,16001
16030,23230,100,16001
16038,23238,100,16001
16046,23246,100,16001
24006,31206,100,24001
24014,31214,100,24001
24022,31222,100,24001
24030,31230,100,24001
24038,31238,100,24001
24046,31246,100,24001
32006,39206,100,32001
32014,39214,100,32001
32022,39222,100,32001
32030,39230,100,32001
32038,39238,100,32001
32046,39246,100,32001
40006,47206,100,40001
40014,47214,100,40001
40022,47222,100,40001
40030,47230,100,40001
40038,47238,100,40001
40046,47246,100,40001
48006,55206,100,48001
48014,55214,100,48001
48022,55222,100,48001
48030,55230,100,48001
48038,55238,100,48001
48046,55246,100,48001
56006,63206,100,56001

```

```

56014,63214,100,56001
56022,63222,100,56001
56030,63230,100,56001
56038,63238,100,56001
56046,63246,100,56001
** ***** NODE GEN FOR BOTTOM FLANGE
*****
*NGEN,NSET=NPLATEB,LINE=C
56008,63208,100,56001
56010,63210,100,56001
56012,63212,100,56001
56014,63214,100,56001
56016,63216,100,56001
56018,63218,100,56001
56020,63220,100,56001
56022,63222,100,56001
56024,63224,100,56001
56026,63226,100,56001
56028,63228,100,56001
56030,63230,100,56001
56032,63232,100,56001
56034,63234,100,56001
56036,63236,100,56001
56038,63238,100,56001
56040,63240,100,56001
56042,63242,100,56001
56044,63244,100,56001
56046,63246,100,56001
** ***** ELEMENT GEN. FOR TOP SLAB
*****
*ELEMENT,TYPE=S4R
1,2,102,104,4
*ELGEN,ELSET=ESLABT
1,72,100,24,24,2,1
** *****
*ELSET,ELSET=LANE,GEN
1,1705,24
2,1706,24
3,1707,24
4,1708,24
5,1709,24
6,1710,24
7,1711,24
8,1712,24
9,1713,24

```

10,1714,24
11,1715,24
12,1716,24
13,1717,24
14,1718,24
15,1719,24
16,1720,24
17,1721,24
18,1722,24
19,1723,24
20,1724,24
21,1725,24
22,1726,24
23,1727,24
24,1728,24

** ***** ELEMENT GEN. FOR BOTTOM FLANGE

*ELEMENT,TYPE=S4R

1729,56006,56106,56108,56008

2017,56022,56122,56124,56024

2305,56038,56138,56140,56040

*ELGEN,ELSET=ESLABB

1729,72,100,4,4,2,1

2017,72,100,4,4,2,1

2305,72,100,4,4,2,1

** ***** ELEMENT GEN. FOR TOP FLANGE *****

*ELEMENT,TYPE=B31H

2593,8006,8106

2665,8014,8114

2737,8022,8122

2809,8030,8130

2881,8038,8138

2953,8046,8146

*ELGEN,ELSET=TOPFL

2593,72,100,1

2665,72,100,1

2737,72,100,1

2809,72,100,1

2881,72,100,1

2953,72,100,1

** ***** ELEMENT GEN. FOR WEBS *****

*ELEMENT,TYPE=S4R

3025,16006,16106,8106,8006

3457,16014,16114,8114,8014

3889,16022,16122,8122,8022

```

4321,16030,16130,8130,8030
4753,16038,16138,8138,8038
5185,16046,16146,8146,8046
*ELGEN,ELSET=WEB
3025,72,100,6,6,8000,1
3457,72,100,6,6,8000,1
3889,72,100,6,6,8000,1
4321,72,100,6,6,8000,1
4753,72,100,6,6,8000,1
5185,72,100,6,6,8000,1
** ***** ELEMENT GN. FOR END DIAPHRAGM
*****
*ELEMENT,TYPE=S4R
5617,16006,16008,8008,8006
5641,16022,16024,8024,8022
5665,16038,16040,8040,8038
5689,23206,23208,15208,15206
5713,23222,23224,15224,15222
5737,23238,23240,15240,15238
*ELGEN,ELSET=DIAPH
5617,4,2,6,6,8000,1
5641,4,2,6,6,8000,1
5665,4,2,6,6,8000,1
5689,4,2,6,6,8000,1
5713,4,2,6,6,8000,1
5737,4,2,6,6,8000,1
***** END FLANGE ELEMENTS *****
*ELEMENT,TYPE=B31H
5761,8006,8008
5765,8022,8024
5769,8038,8040
5773,15206,15208
5777,15222,15224
5781,15238,15240
*ELGEN,ELSET=ENDFL
5761,4,2,1,1,1,1
5765,4,2,1,1,1,1
5769,4,2,1,1,1,1
5773,4,2,1,1,1,1
5777,4,2,1,1,1,1
5781,4,2,1,1,1,1
** ***** ELEMENT GEN FOR TRUSS ELEMENTS *****
*NGEN,NSET=XBP,LINE=C
32010,39210,200,32001
32018,39218,200,32001

```

```

32026,39226,200,32001
32034,39234,200,32001
32042,39242,200,32001
*****
*ELEMENT,TYPE=B31H
5785,8406,8414
5786,8406,32410
5787,32410,56414
5788,8414,32410
5789,32410,56406
*ELGEN,ELSET=XBRAC
5785,17,400,30,3,16,12
5786,17,400,30,3,16,12
5787,17,400,30,3,16,12
5788,17,400,30,3,16,12
5789,17,400,30,3,16,12
*****ELEMENT GEN. FOR END TRUSS ELEMENTS BETWEEN BOXES***
*ELEMENT,TYPE=B31H
20001,8014,8022
20002,8014,32018
20003,32018,56022
20004,8022,32018
20005,32018,56014
20006,56014,56022
*ELGEN,ELSET=XBRAC
20001,2,7200,12,2,16,6
20002,2,7200,12,2,16,6
20003,2,7200,12,2,16,6
20004,2,7200,12,2,16,6
20005,2,7200,12,2,16,6
20006,2,7200,12,2,16,6
*****
*NSET,NSET=REACT
LEFT6,RIGHT6
*TRANSFORM,NSET=REACT,TYPE=C
0,0,-10,0,0,10
***** MATERIAL PROPERTIES
*****
*BEAM SECTION,SECTION=RECT,ELSET=XBRAC,MATERIAL=STEEL
.1,.1
5,5
*SHELL SECTION,ELSET=WEB,MATERIAL=STEEL
.035,5
*BEAM SECTION,SECTION=RECT,ELSET=TOPFL,MATERIAL=STEEL
.085,.6

```

```

5,5
*BEAM SECTION,SECTION=RECT,ELSET=ENDFL,MATERIAL=STEEL
.085,.6
5,5
*****
*SHELL SECTION,ELSET=DIAPH,MATERIAL=STEEL
.035,5
*SHELL SECTION,ELSET=ESLABB,MATERIAL=STEEL
.035,5
*MATERIAL,NAME=STEEL
*DENSITY
7800
*ELASTIC
200000E6,.3
*SHELL SECTION,ELSET=ESLABT,MATERIAL=CON
.225,5
*MATERIAL,NAME=CON
*DENSITY
2400
*ELASTIC
27000E6,.20
** ***** MULTI POINT CONSTRAINT
*****
*NGEN,NSET=BOT21,LINE=C
6,7206,100,1
*NGEN,NSET=BOT22,LINE=C
8006,15206,100,8001
*NGEN,NSET=BOT11,LINE=C
14,7214,100,1
*NGEN,NSET=BOT12,LINE=C
8014,15214,100,8001
*NGEN,NSET=TOP11,LINE=C
22,7222,100,1
*NGEN,NSET=TOP12,LINE=C
8022,15222,100,8001
*NGEN,NSET=TOP21,LINE=C
30,7230,100,1
*NGEN,NSET=TOP22,LINE=C
8030,15230,100,8001
*NGEN,NSET=TOP31,LINE=C
38,7238,100,1
*NGEN,NSET=TOP32,LINE=C
8038,15238,100,8001
*NGEN,NSET=TOP41,LINE=C
46,7246,100,1

```

```

*NGEN,NSET=TOP42,LINE=C
8046,15246,100,8001
*NSET,NSET=T1
8,10,12,24,26,28,40,42,44
*NSET,NSET=B1
8008,8010,8012,8024,8026,8028,8040,8042,8044
*NSET,NSET=T2
7208,7210,7212,7224,7226,7228,7240,7242,7244
*NSET,NSET=B2
15208,15210,15212,15224,15226,15228,15240,15242,15244
*MPC
BEAM,BOT21,BOT22
BEAM,BOT11,BOT12
BEAM,TOP11,TOP12
BEAM,TOP21,TOP22
BEAM,TOP31,TOP32
BEAM,TOP41,TOP42
BEAM,T1,B1
BEAM,T2,B2
** *****
*BOUNDARY
LEFT6,1,3
RIGHT6,1
RIGHT6,3
** *****
*STEP
*STATIC
** *****
*DLOAD
LANE,GRAV,9.81,0,0,-1
ESLABB,GRAV,9.81,0,0,-1
TOPFL,GRAV,9.81,0,0,-1
WEB,GRAV,9.81,0,0,-1
*****
*elset,elset=eslabt1,gen
841,888
*elset,elset=eslabbl,gen
1869,1876
2157,2164
2445,2452
*ELSET,ELSET=WEB1,gen
3235,3246
3667,3678
4099,4110
4531,4542

```



```

4963,4974
5395,5406
*ELSET,ELSET=TOPFL1
2628,2629,2700,2701,2772,2773,2844,2845,2916,2917,2988,2989
*ELPRINT,POSITION=AVERAGED AT NODES,ELSET=ESLABBI
S11
*ELPRINT,ELSET=XBRAC
SF1
*NGEN,NSET=MID
59606,59646,8
*NODEPRINT,NSET=MID
U3
*****
*ENDSTEP
*STEP
*STATIC
** *****
*****CONCENTRIC TRUCK LOADING*****
*ELSET,ELSET=CTRUCK,GEN
4,1708,24
5,1709,24
6,1710,24
7,1711,24
8,1712,24
9,1713,24
10,1714,24
11,1715,24
12,1716,24
13,1717,24
14,1718,24
15,1719,24
16,1720,24
17,1721,24
18,1722,24
19,1723,24
20,1724,24
21,1725,24
*DLOAD,OP=NEW
CTRUCK,P,-2224
*NSET,NSET=C2TRUCK,GEN
3610,3642,2
*CLOAD,OP=NEW
C2TRUCK,3,-13334
3608,3,-6667
3644,3,-6667

```

```

*****
*elset,elset=eslabt1,gen
841,888
*elset,elset=eslabb1,gen
1869,1876
2157,2164
2445,2452
*ELSET,ELSET=WEB1,gen
3235,3246
3667,3678
4099,4110
4531,4542
4963,4974
5395,5406
*ELSET,ELSET=TOPFL1
2628,2629,2700,2701,2772,2773,2844,2845,2916,2917,2988,2989
*ELPRINT,POSITION=AVERAGED AT NODES,ELSET=ESLABB1
S11
*ELPRINT,ELSET=XBRAC
SF1
*NGEN,NSET=MID
59606,59646,8
*NODEPRINT,NSET=MID
U3
*****
*ENDSTEP
*STEP
*STATIC
** *****
***OUTER TRUCK LOADING***
*ELSET,ELSET=OTRUCK,GEN
14,1718,24
15,1719,24
16,1720,24
17,1721,24
18,1722,24
19,1723,24
20,1724,24
21,1725,24
22,1726,24
*DLOAD,OP=NEW
OTRUCK,P,-2965
*NSET,NSET=O2TRUCK,GEN
3630,3644,2
*CLOAD,OP=NEW

```

```
O2TRUCK,3,-1778
3628,3,-8889
3646,3,-8889
*****
*elset,elset=eslabt1,gen
841,888
*elset,elset=eslabb1,gen
1869,1876
2157,2164
2445,2452
*ELSET,ELSET=WEB1,gen
3235,3246
3667,3678
4099,4110
4531,4542
4963,4974
5395,5406
*ELSET,ELSET=TOPFL1
2628,2629,2700,2701,2772,2773,2844,2845,2916,2917,2988,2989
*ELPRINT,POSITION=AVERAGED AT NODES,ELSET=ESLABB1
S11
*ELPRINT,ELSET=XBRAC
SF1
*NGEN,NSET=MID
59606,59646,8
*NODEPRINT,NSET=MID
U3
*****
*ENDSTEP
```

VITA AUCTORIS

Said Ibrahim Nour

- 1968 Born on the 27th of July in Djibouti, Djibouti.
- 1992 Graduated with High School Diploma from Ecole Secondaire Etienne-Brule.
Toronto, Ontario, Canada.
- 1998 Graduated with Bachelor of Engineering in Civil Engineering from Ryerson
Polytechnic University, Toronto, Ontario, Canada.
- 1999 Enrolled as Master of Engineering student (Structural Engineering) in the
University of Toronto, Toronto, Ontario, Canada.
- 2000 Appointed as a Teaching and Research Assistant in the Civil and Environmental
Engineering Program, University of Windsor, Windsor, Ontario, Canada.